

AN ABSTRACT OF THE THESIS OF

Mikhail L. Orlov for the degree of Doctor of Philosophy in Chemistry presented on December 17, 1997. Title : Vibration-Rotational Studies of Isotopic Variants of Diatomic Molecules.

Redacted for Privacy

Abstract approved:


Joseph W. Nibler

An optical method for high resolution (0.001 cm^{-1}) CARS measurements of diatomic molecules excited in a glow discharge was developed. The influence of various discharge parameters on the excitation efficiency of different vibrational levels of nitrogen was investigated. It was shown that the use of a minimal gas flow of 0.4 - 0.6 L/min can enhance the excitation efficiency by a factor of 150. A novel cycling system for optical measurements in a glow discharge at low gas pressures (below 100 Torr) was designed to make economical use of precious gases.

The method was applied to measure CARS spectra of excited $^{14}\text{N}_2$ and $^{15}\text{N}_2$ in the electronic ground state $X^1\Sigma_g^+$, specifically Q branches of bands $\Delta v=1$ up to $v'=8$ for $^{14}\text{N}_2$ and $v'=7$ for $^{15}\text{N}_2$, and O and S branches of the fundamental band of $^{15}\text{N}_2$. Account was taken of small wavenumber shifts due to pressure, AC Stark, and $|\chi|^2$ interference effects. The measurement accuracy of reported wavenumbers is 0.004 cm^{-1} . Separate fits of the Q-branch data of each isotopic variant, augmented with selected data from the literature, yielded sets of term coefficients Y_{kl} for $^{14}\text{N}_2$ and $^{15}\text{N}_2$. Analysis of combined data for these

two isotopes resulted in new values of mass-independent coefficients U_{kl} and Δ_{kl} , which can be used to calculate vibration-rotational energy levels of any isotopic variant of nitrogen. Coefficients Δ_{kl} are a measure of total extramechanical corrections to these energy levels arising from incomplete separation of electronic and nuclear motion assumed in the Born-Oppenheimer approximation. A further distinction between specific types of these effects, adiabatic and nonadiabatic, did not prove possible.

A similar analysis was applied to literature data for all six dihydrogen isotopic combinations, for which accurate and reliable spectral information is available mainly for purely rotational transitions with $v''=0$ and for vibration-rotational transitions with $v''=0, 1$. This analysis gave standard errors of fits which were uncomfortably large and yielded values for the total extramechanical effects which are about half of those predicted by theory. It was concluded that, for quantitative evaluation of such effects, more accurate spectral measurements for hydrogen are required.

Vibration-Rotational Studies of Isotopic Variants of Diatomic Molecules

by

Mikhail L. Orlov

A THESIS

submitted to

Oregon State University

in partial fulfillment of
the requirements for the
degree of

Doctor of Philosophy

Presented December 17, 1997

Commencement June 1998

Doctor of Philosophy thesis of Mikhail L. Orlov presented on December 17, 1997

APPROVED:

Redacted for Privacy

Major Professor, representing Chemistry

Redacted for Privacy

Chair of Department of Chemistry

Redacted for Privacy

Dean of Graduate School

I understand that my thesis will become part of the permanent collection of Oregon State University libraries. My signature below authorizes release of my thesis to any reader upon request.

Redacted for Privacy

Mikhail L. Orlov, Author

ACKNOWLEDGMENTS

First and foremost I would like to thank my destiny for a chance to work in the wonderful environment of Dr. Nibler's group. Students of Dr. Joe Nibler enjoy a unique combination of friendly guidance and freedom. They gain a lot from his wide and yet deep knowledge of science, which goes far beyond the field of his expertise, spectroscopy. Interacting with Dr. Nibler, a person of such extraordinary analytical abilities, students develop good problem solving skills. Dr. Nibler is a mentor for his graduates not only academically but socially as well. His wonderful personality became for me an example to follow, as, I think, for all of his numerous students. There is one more thing to add. In spite of the fact that in graduate school one has a luxury to choose which twenty hours of a day to work, we always managed to find some moments for fun and quality time with our favorite professor, Joe Nibler. Without any exaggeration I can say that I spent the best years of my life working in this group.

My thanks also go to Dr. John Ogilvie. I acquired a lot of knowledge from him during our diverse conversations about science, languages, history, politics etc. They were always interesting, instructive and fun.

I would like to thank all my professors at OSU. It was challenging and exciting at the same time to take their courses. Their classes gave me a better comprehension of different areas of science and broadened my erudition.

I would like to thank my parents. I owe them a good start in my life. Without their care, love, patience, guidance, education, and support I would not have been able to reach this point of my career.

I would like to express my gratitude to my wife, Nadja, and my daughter, Sveta, for being so understanding and sustaining through all these long years. It is very important to feel reliable support when pursuing demanding goals. These years in graduate school were not easy for Nadja, since she also was a graduate student, and I highly appreciate her help.

I also would like to thank all my fellow graduate students with whom we have been through all the hardship and excitement of learning, research and life.

TABLE OF CONTENTS

	<u>Page</u>
1. INTRODUCTION.....	1
2. THEORETICAL BACKGROUND	4
2.1. Raman spectroscopy	4
2.1.1. Historical overview	4
2.1.2. Oscillating induced dipole moment	7
2.1.3. Origin of the Raman effect.....	9
2.1.4. Coherent Anti-Stokes Raman Scattering (CARS)	13
2.2. Vibration-rotational states in diatomic molecules.....	18
2.2.1. The Born-Oppenheimer approximation.....	19
2.2.2. Dunham model of energy levels in diatomic molecules.....	21
2.2.3. Extramechanical effects	23
2.3. Electrical discharge in gases	29
2.3.1. Types of discharge	29
2.3.2. Non-self-sustaining discharges.....	31
2.3.3. Glow discharge	34
3. DEVELOPMENT OF OPTICAL METHOD FOR STUDY OF DIATOMIC MOLECULES EXCITED IN A GLOW DISCHARGE	41
3.1. Introduction.....	41
3.2. Optimization of discharge parameters.....	42
3.2.1. Experimental apparatus used for optimization.....	42
3.2.2. Discharge cell and electrode configuration.....	52
3.2.3. Gas pressure.....	55
3.2.4. Discharge current	56
3.2.5. Position of the probing point	59
3.2.6. Flow rate of the gas.....	61
3.3. Cycling system.....	63

TABLE OF CONTENTS (Continued)

	<u>Page</u>
4. HIGH-RESOLUTION COHERENT RAMAN SPECTRA OF VIBRATIONALLY EXCITED $^{14}\text{N}_2$ AND $^{15}\text{N}_2^*$	67
4.1. Introduction	67
4.2. Experimental procedure	70
4.2.1. Apparatus.....	70
4.2.2. Measurements	73
4.2.3. Precision and accuracy	76
4.2.4. Additional sources of uncertainty.....	78
4.3. Analysis of spectra	81
4.3.1. Interference effects.....	81
4.3.2. Parameters in analysis of spectral results.....	87
4.4. Results.....	89
4.4.1. Weighting of data.....	92
4.4.2. Coefficients Y_{kl} and U_{kl}	93
4.4.3. Potential-energy function.....	99
4.5. Discussion	99
4.6. Summary	104
5. HYDROGEN SPECTRAL DATA.....	105
5.1. Introduction.....	105
5.2. Literature overview.....	106
5.3. Analysis of the experimental literature data.....	117
5.3.1. Determination of coefficients Y_{kl} for each isotope.....	117
5.3.2. Determination of coefficients U_{kl} and Δ_{kl}	122
5.3.3. Determination of coefficients c , u , t , s	123
5.3.4. Results of theoretical studies of extramechanical effects.....	125
5.4. Summary	129
6. CONCLUSIONS.....	131
BIBLIOGRAPHY	134
APPENDICES	142

LIST OF FIGURES

<u>Figure</u>	<u>Page</u>
2-1 Energy diagram for CARS	15
2-2 Normalized plot of the phase-matching function.....	17
2-3 Current-voltage characteristics of a gas in pre-spark regions	30
2-4 The first Townsend coefficient α as a function of electric field	34
2-5 Typical volt-ampere characteristics of various discharges in gas	35
2-6 The structure of a low pressure glow discharge.....	36
3-1 Schematic diagram of the medium resolution apparatus.....	43
3-2 Gain curve of the Hyperdye-500 dye laser for the R610/SR640 dye mixture.....	44
3-3 Geometrical interpretation of the phase-matching condition in "BOXCARS" (a) and folded BOXCARS (b) configurations	47
3-4 Spatial arrangement of beams in the folded "BOXCARS" configuration.....	48
3-5 Electrical diagram of the discharge apparatus.....	53
3-6 Schematic of the discharge cell for optimization experiments	53
3-7 Vibration-rotational excitation of molecules by a glow discharge.....	54
3-8 Influence of the discharge current on vibrational excitation	57
3-9 Optimal discharge current I_{opt} as a function of quantum number v''	58
3-10 Influence of the probing point position on the CARS signal.....	60
3-11 Influence of the gas flow on the CARS signal.....	62
3-12 The cycling system for optical measurements in a glow discharge.....	64
3-13 Vacuum characteristic of the cycling system.....	66
3-14 Comparison of cycling and regular flow regimes	66

LIST OF FIGURES (Continued)

<u>Figure</u>	<u>Page</u>
4-1 Schematic diagram of the high-resolution apparatus.....	72
4-2 Representative CARS spectra of nitrogen	74
4-3 Time drift characteristic of the high-resolution apparatus	75
4-4 Precision of the dye laser wavemeter.....	77
4-5 Influence of the laser power on the position of the line Q ₁ (10) of ¹⁴ N ₂	80
4-6 The real and imaginary parts of the third-order electric susceptibility.....	83
4-7 Displacement of the CARS peak position from the actual transition due to interference effects.....	86
4-8 Differences between calculated and experimental wavenumbers of Q branches of ¹⁴ N ₂ from various sources.....	95
4-9 Differences between calculated and experimental wavenumbers of Q branches of ¹⁵ N ₂ from various sources.....	97
4-10 Potential energy curve for dinitrogen	102
5-1 Born-Oppenheimer potential-energy curve for ¹ H ₂ molecule and adiabatic and relativistic corrections to it.....	126
5-2 Influence of adiabatic and nonadiabatic corrections on energy of vibrational levels of ¹ H ₂ molecule.....	128

LIST OF TABLES

<u>Table</u>	<u>Page</u>
4-1 Measured wavenumbers (cm^{-1}) of lines in Q branches of $^{14}\text{N}_2$	90
4-2 Measured wavenumbers (cm^{-1}) of lines in Q branches of $^{15}\text{N}_2$	91
4-3 Measured wavenumbers (cm^{-1}) of lines in O and S branches of $^{15}\text{N}_2$	92
4-4 Parameters Y_{kl} and U_{kl} for $^{14}\text{N}_2$ and $^{15}\text{N}_2$	94
4-5 Parameters for $^{14}\text{N}_2$ and $^{15}\text{N}_2$	100
5-1 Wavenumbers (cm^{-1}) of lines in Q branches of $^1\text{H}_2$ from the literature.....	108
5-2 Wavenumbers (cm^{-1}) of lines in S and O branches of $^1\text{H}_2$ from the literature.....	109
5-3 Wavenumbers (cm^{-1}) of lines in Q, S and O branches of $^2\text{H}_2$ from the literature ..	111
5-4 Wavenumbers (cm^{-1}) of lines in Q, S, R and P branches of $^1\text{H}^2\text{H}$ from the literature.....	113
5-5 Wavenumbers (cm^{-1}) of lines in Q and S branches of $^3\text{H}_2$ and $^2\text{H}^3\text{H}$ from the literature.....	115
5-6 Wavenumbers (cm^{-1}) of lines in Q, S, R and P branches of $^1\text{H}^3\text{H}$ from the literature.....	116
5-7 Parameters Y_{kl} (cm^{-1}) for $^1\text{H}_2$, $^1\text{H}^2\text{H}$ and $^2\text{H}_2$	118
5-8 Parameters Y_{kl} (cm^{-1}) for $^3\text{H}_2$ and $^2\text{H}^3\text{H}$	119
5-9 Parameters U_{kl} ($\text{cm}^{-1}\text{u}^{k/2+1}$) for hydrogen isotopes	124

LIST OF APPENDICES

	<u>Page</u>
APPENDIX A. EXPRESSIONS FOR SOME COEFFICIENTS Y_{kl} AND Z_{kl}	143
APPENDIX B. VISUAL BASIC PROGRAM FOR SPECTRAL DATA ACQUISITION	145
APPENDIX C. MULTIPLE LINEAR REGRESSION ANALYSIS USING MICROSOFT EXCEL.....	187
C.1. Introduction	187
C.2. Classification of regression models	187
C.3. Main objectives of multiple linear regression analysis.....	188
C.4. ANOVA output and its analysis.....	188
C.4.1. Coefficients	188
C.4.2. Sum of squares.....	190
C.4.3. Mean square (variance) and degrees of freedom.....	192
C.4.4. Tests of significance and F-numbers.....	193
C.4.5. Confidence interval.....	196
C.5. Regression statistics output	197
C.6. References.....	199

LIST OF APPENDIX TABLES

<u>Table</u>	<u>Page</u>
C-1 MS Excel ANOVA output (part I).....	189
C-2 MS Excel ANOVA output (part II)	189
C-3 Regression statistics output of MS Excel	198

VIBRATION-ROTATIONAL STUDIES OF ISOTOPIC VARIANTS OF DIATOMIC MOLECULES

1. INTRODUCTION

There is no doubt that modern spectroscopy is a powerful tool, which can provide different kinds of information about atoms and molecules. In this study we will use spectroscopy to investigate one of the principal cases, that of diatomic molecules.

The interest in diatomic molecules is based on the fact that these are fundamental molecular systems and new knowledge about them is invaluable by itself. In addition spectral information of diatomic molecules is also used in practical applications: e.g. diagnostics of glow discharge plasmas¹⁻⁴, concentration and temperature measurements in flames⁵⁻⁷, astrophysical studies of galactic evolution and dynamics of various phenomena in the universe⁸⁻¹⁰. There is also a great theoretical interest in experimental data for diatomic molecules to test and develop modern quantum mechanical theories and to give them quantitative analysis. For example, there exists a contemporary analytical treatment which allows one to calculate so called extramechanical effects in diatomic molecules¹¹. These effects are a measure of deviations of real systems from the Born-Oppenheimer approximation (discussed later in section 2.2.3) and are of considerable interest.

The treatment requires spectral data of **high absolute accuracy for isotopic variants** of a molecule in many vibrationally excited states. A literature search shows that such high quality information is very much limited even for basic diatomic molecules like nitrogen and hydrogen, especially for higher vibrational levels. This determined the choice

of the systems to investigate. Because of its long vibrational lifetime (of the order of 1 s at one atm)¹², nitrogen proved to be a very good molecule for efficient excitation and study of higher vibrational states. Hydrogen was also considered interesting since it is the lightest diatomic molecule and should have pronounced extramechanical effects. However, the vibrational lifetime of hydrogen is about four orders of magnitude lower than that of nitrogen¹³. This imposed significant experimental problems for measurement of higher vibrational levels of the molecule, which we were not able to resolve within this work.

It is well known that according to the Boltzmann distribution at room temperature almost all molecules are in their vibrational ground state. In order to obtain a reasonable population of higher vibrational levels (e.g. $v=8$), one needs to heat molecules such as N_2 or H_2 up to 5000 - 6000 K. It is obvious that such an approach is not realistic. However, there are at least two ways to vibrationally excite molecules at moderate temperatures: a glow discharge plasma^{3,4} and a chemical reaction¹⁴. The former was chosen in the present work.

Although modern infrared spectroscopy can provide high accuracy measurements of wavenumbers of vibration-rotational transitions in polar diatomic molecules, such is not the case for non-polar diatomics like nitrogen and hydrogen. These are IR inactive symmetric molecules (symmetry group $D_{\infty h}$). On the other hand, they are Raman active and this is the reason why Raman spectroscopy was chosen as the optical technique for our study. Since the linear Raman effect is weak, in our work we used one of the more sensitive non-linear Raman techniques: Coherent Anti-Stokes Raman Scattering (CARS). Besides its higher sensitivity, CARS, unlike regular Raman spectroscopy, can provide a

point probing feature, which is very useful for measurements in a glow discharge plasma, as we will see later in the discussion of the experimental apparatus and procedure.

The above considerations led us to the following main goals of our work. First of these was to develop in our laboratory an optical method for the study of higher vibrational levels of diatomic molecules based on the combination of CARS spectroscopy and excitation in a glow discharge plasma. The second goal was to apply this method to isotopic variants of specific molecules (e.g. nitrogen) to obtain new and/or significantly improved (in terms of absolute accuracy) spectral information about them. The final goal was to use such information to calculate extramechanical effects in these molecules.

In the following chapters we will provide some theoretical background relevant to this work, describe the development and parameters of the experimental set-up, and will present experimental results for nitrogen isotopes and their analysis. In addition we will analyze literature spectral data for hydrogen isotopic variants, for which experimental measurements were beyond the scope of this work, and summarize the outcome of our study.

2. THEORETICAL BACKGROUND

In the following chapter a discussion of the principal theoretical concepts related to our study are presented. It covers the Raman effect (linear and CARS), adiabatic and non-adiabatic effects in diatomic molecular systems, and phenomena in electric discharges in gases.

2.1. Raman spectroscopy

Both linear and non-linear Raman effects have been comprehensively described in the literature in great detail¹⁵⁻¹⁹. We give here just a short overview of the subject to facilitate understanding of the material presented in this work.

2.1.1. Historical overview

The Raman effect is the scattering of radiation with a change of frequency. It was first observed in liquids by Indian scientists C. V. Raman and K. S. Krishnan in 1928²⁰ after the effect had been predicted on theoretical grounds in 1923 by A. Smekal²¹. Only three months later Landsberg and Mandelstam²² in Russia reported the observation of light scattering with change of frequency in quartz. It is interesting to mention that in Russia the phenomenon is usually called Combination Scattering instead of Raman Scattering. By the end of 1928 some 60 papers had been published on the Raman effect.

Raman scattering has important practical advantages as a method of probing rotational and vibrational energy levels. It allows one to study all rotational and nearly all vibrational transitions using visible radiation. Consequently, Raman spectroscopy involves relatively simple optical systems and instrumentation. This is in marked contrast to the observation of rotational and vibrational wavenumbers in direct absorption, where a variety of different techniques and appropriate cell materials must be used to cover the microwave and infrared regions of the spectrum in which these absorptions occur.

In 1928, at the time of the discovery of the Raman effect, the observation of infrared absorption was difficult and tedious, and was restricted to wavenumbers greater than 650 cm^{-1} . On the other hand the new Raman scattering yielded information over the whole range of molecular wavenumbers and required only readily available equipment. In addition to that, the Raman effect made it possible to observe dipole forbidden transitions, which are inaccessible by normal linear absorption or emission spectroscopy. Not surprisingly, there was an immediate rise of interest in this new form of spectroscopy.

However, by the early fifties experimental techniques in infrared spectroscopy underwent progressive development. The wavenumber region below 650 cm^{-1} has become more and more readily available. By the late fifties microwave spectroscopy had also been highly developed although this still remained a specialized and relatively expensive experimental technique.

The experimental development in Raman spectroscopy did not keep pace with that in infrared spectroscopy. The mercury arc was almost the only practicable source of monochromatic radiation. Because of the relative weakness of Raman scattering, it was necessary therefore to use larger samples and to collect as much as possible of the

scattered radiation, which involved the use of complicated collection optics. These facts explain why in the fifties and early sixties Raman spectroscopy was far less widely used than infrared spectroscopy.

The situation dramatically changed as a result of the availability of lasers in the late sixties and early seventies. At the focus of a gas laser the power per unit area can be many orders of magnitude greater than that of a mercury arc. The output from a laser is a highly collimated and polarized beam, so that the study of polarization is greatly facilitated. The bandwidth of conventional lasers is much narrower than for a mercury arc, which significantly minimizes linewidth restrictions in the study of Raman spectra. There also have been substantial developments in the dispersing and detection systems for Raman spectroscopy.

Creation of Q-switched giant pulse lasers made it possible to obtain power up to several megawatts at the beam focus. This opened the era of non-linear Raman spectroscopy based on phenomena such as Stimulated Raman Scattering (SRS) and Coherent Anti-Stokes Raman Scattering (CARS), which has a number of advantages with respect to regular Raman (discussed later in this chapter in section 2.1.4). Pioneers of the field were Woodbury and Ng²³, who in 1962 discovered SRS, followed by Yajima and Takatsuji²⁴, and Maker and Terhune²⁵, who in 1964-65 published the first articles on CARS.

Nowadays, with the significant experimental progress made, Raman spectroscopy has become a powerful tool for the study of matter and serves as the important complement to infrared spectroscopy.

2.1.2. Oscillating induced dipole moment

We begin our theoretical discussion with the oscillating dipole moment of a molecule induced by an incident light beam because this fluctuating charge constitutes the origin of Raman as well as Rayleigh scattering. According to classical physics, any oscillating dipole moment is a source of electromagnetic radiation. The amplitudes of the electric field E and magnetic field H at an arbitrary point of observation are given by¹⁷

$$E = \frac{-\omega^2 P \sin \theta}{4\pi\epsilon_0 c^2 r}, \quad (2.1)$$

$$H = \frac{-\omega^2 P \sin \theta}{4\pi c r}, \quad (2.2)$$

in which ω is the circular frequency of the oscillating dipole moment P placed at the origin of a polar coordinate system; ϵ_0 , c and r are the permittivity of vacuum, speed of light, and the distance between the dipole and the point of observation, respectively. The angle θ is the angle between the dipole moment vector and the radius vector of the point of observation. Radiation intensity can be characterized by the so called Poynting vector T . Its amplitude is equal to energy flow per unit time, per unit area, in the direction of propagation of light. The magnitude of the Poynting vector thus corresponds to the irradiance and has SI units of $[\text{W}/\text{cm}^2]$. The vector itself is given by the cross-product of the electric and magnetic field vectors:

$$\mathbf{T} = \mathbf{E} \times \mathbf{H}. \quad (2.3)$$

From equations (2.1), (2.2), (2.3) and the fact that E and H are perpendicular to each other, we readily obtain the expression for the intensity of light generated by an oscillating induced dipole moment at any point of observation:

$$T = \frac{\omega^4 P^2 \sin^2 \theta}{16\pi^2 \epsilon_0 c^3 r^2}. \quad (2.4)$$

From this equation it follows that the intensity of light emitted is proportional to the square of the magnitude of the induced dipole moment vector P , which is related to the electric field vector E of the incident radiation by the power series²⁶

$$P = P^{(1)} + P^{(2)} + P^{(3)} + \dots, \quad (2.5)$$

in which

$$P^{(1)} = \alpha \cdot E, \quad (2.6)$$

$$P^{(2)} = \frac{1}{2!} \beta : EE, \quad (2.7)$$

$$P^{(3)} = \frac{1}{3!} \gamma : EEE. \quad (2.8)$$

In these equations, P and E have units of C·m and V/m, respectively; α , β and γ , which relate P and E , are tensors since, in general, the direction of the induced dipole is not the same as that of the electric field producing it.

The tensor α is termed the polarizability tensor and is a second-rank tensor whose components have units of (C·m²)/V; β is the hyperpolarizability tensor and is a third-rank tensor whose components have units of (C·m³)/V²; γ is referred to as the second hyperpolarizability tensor and is a fourth-rank tensor whose components have units of

$(\text{C}\cdot\text{m}^4)/\text{V}^3$. Typical orders of magnitude for components of α , β and γ in the corresponding units mentioned above are 10^{-40} , 10^{-50} and 10^{-61} , respectively.

In the literature¹⁶ one also encounters the so called electrical susceptibility tensors $\chi^{(n)}$ of order n and rank $n+1$. These are related to the tensors α , β and γ in the following simple way:

$$\chi^{(1)} = \alpha, \quad (2.9)$$

$$\chi^{(2)} = \frac{1}{2!}\beta, \quad (2.10)$$

$$\chi^{(3)} = \frac{1}{3!}\gamma. \quad (2.11)$$

The first-order susceptibility is responsible for linear Raman and Rayleigh scattering as we will see shortly. The second-order susceptibility is zero for isotropic materials such as gases and liquids and is omitted from our discussion. The third-order susceptibility is the material property responsible for generation of sum and difference frequencies when more than one light frequency is incident on the sample, e.g. CARS spectroscopy. In subsequent sections of this chapter first we consider principal concepts of the linear Raman scattering using linear case for illustration and then later discuss the main aspects of the CARS method.

2.1.3. Origin of the Raman effect

In this section we will use a classical treatment of vibrational Raman scattering to explain the origin of the Raman effect. If we neglect higher order terms in equation (2.5) the expression for the induced dipole moment simplifies to

$$\mathbf{P} = \mathbf{P}^{(1)} = \boldsymbol{\alpha} \cdot \mathbf{E}, \quad (2.12)$$

in which $\mathbf{P}^{(1)}$ is referred to as the linear induced dipole moment. This equation implies that the magnitudes of the components of \mathbf{P} are related to the magnitudes of \mathbf{E} by the following three linear equations:

$$\begin{aligned} P_x &= \alpha_{xx}E_x + \alpha_{xy}E_y + \alpha_{xz}E_z \\ P_y &= \alpha_{yx}E_x + \alpha_{yy}E_y + \alpha_{yz}E_z \\ P_z &= \alpha_{zx}E_x + \alpha_{zy}E_y + \alpha_{zz}E_z \end{aligned} \quad (2.13)$$

Let us consider a space-fixed single vibrating diatomic molecule exposed to the harmonically oscillating electric field associated with electromagnetic radiation (light) of circular frequency ω_0 . It is to be expected that the polarizability of the molecule will be a function of the nuclear coordinates. The variation of the polarizability with vibrations of the molecule can be expressed by expanding each component α_{ij} of the polarizability tensor in a Taylor series with respect to the normal coordinate Q around the equilibrium position:

$$\alpha_{ij} = (\alpha_{ij})_0 + \sum_{n=1} \frac{1}{n!} \left(\frac{\partial^n \alpha_{ij}}{\partial Q^n} \right)_0 Q^n, \quad (2.14)$$

in which n is an integer and $i, j = x, y, z$. As a good approximation, we can neglect higher order terms ($n \geq 2$) and the equation simplifies to

$$\alpha_{ij} = (\alpha_{ij})_0 + (\alpha'_{ij})Q, \quad (2.15)$$

where we introduced the following definition of (α'_{ij}) :

$$(\alpha'_{ij}) = \left(\frac{\partial \alpha_{ij}}{\partial Q} \right)_0. \quad (2.16)$$

The (α_{ij}') elements are components of a new tensor α' which is termed the polarizability derivative tensor. If we define α and α_0 to be tensors with components (α_{ij}) and $(\alpha_{ij})_0$, respectively, then equation (2.15) becomes

$$\alpha = \alpha_0 + \alpha'Q. \quad (2.17)$$

Assuming mechanical harmonicity of vibrations, the time dependence of Q is given by

$$Q = Q_0 \cos(\omega t + \delta), \quad (2.18)$$

in which Q_0 is the normal coordinate amplitude and δ is a phase factor. Inserting equation (2.18) into equation (2.17) gives us the time dependence of the polarizability tensor resulting from the molecular vibration:

$$\alpha = \alpha_0 + \alpha'Q_0 \cos(\omega t + \delta). \quad (2.19)$$

Since for the radiation of the circular frequency ω_0 the variation of the electric field vector E with time is given by

$$E = E_0 \cos \omega_0 t, \quad (2.20)$$

taking into account equations (2.12) and (2.19), we can obtain an expression for the linear induced dipole moment $P^{(1)}$:

$$P^{(1)} = \alpha_0 \cdot E_0 \cos \omega_0 t + \alpha' \cdot E_0 Q_0 \cos \omega_0 t \cos(\omega t + \delta). \quad (2.21)$$

Using the trigonometric identity

$$\cos A \cos B = \frac{1}{2} \{ \cos(A + B) + \cos(A - B) \} \quad (2.22)$$

the second term in equation (2.21) can be reformulated and we may then rewrite $P^{(1)}$:

$$\begin{aligned} P^{(1)} = & P_0^{(1)}(\omega_0) \{ \cos \omega_0 t \} + \\ & + P_0^{(1)}(\omega_0 - \omega) \{ \cos((\omega_0 - \omega)t - \delta) \} + \\ & + P_0^{(1)}(\omega_0 + \omega) \{ \cos((\omega_0 + \omega)t + \delta) \} \end{aligned} \quad (2.23)$$

in which the following identities have been used:

$$P_0^{(1)}(\omega_0) \equiv \alpha_0 \cdot E_0, \quad (2.24)$$

$$P_0^{(1)}(\omega_0 - \omega) \equiv \frac{1}{2} Q_0 \alpha' \cdot E_0, \quad (2.25)$$

$$P_0^{(1)}(\omega_0 + \omega) \equiv \frac{1}{2} Q_0 \alpha' \cdot E_0. \quad (2.26)$$

Quantities $P_0^{(1)}(\omega_0)$, $P_0^{(1)}(\omega_0 - \omega)$ and $P_0^{(1)}(\omega_0 + \omega)$ can be interpreted as magnitudes of three different oscillating dipole moments:

$$P^{(1)}(\omega_0) \equiv P_0^{(1)}(\omega_0) \{ \cos \omega_0 t \}, \quad (2.27)$$

$$P^{(1)}(\omega_0 - \omega) \equiv P_0^{(1)}(\omega_0 - \omega) \{ \cos((\omega_0 - \omega)t - \delta) \}, \quad (2.28)$$

$$P^{(1)}(\omega_0 + \omega) \equiv P_0^{(1)}(\omega_0 + \omega) \{ \cos((\omega_0 + \omega)t + \delta) \}. \quad (2.29)$$

The total linear induced dipole moment is just the sum of them:

$$P^{(1)} = P^{(1)}(\omega_0) + P^{(1)}(\omega_0 - \omega) + P^{(1)}(\omega_0 + \omega). \quad (2.30)$$

From these equations we conclude that the linear induced dipole moment has three distinct frequency components which give rise to radiation at three different frequencies ω_0 , $\omega_0 - \omega$ and $\omega_0 + \omega$.

The mechanism of Rayleigh and Raman scattering in terms of classical radiation theory can be described as follows. Rayleigh scattering arises from the dipole oscillating at ω_0 induced in the molecule by the electric field of the incident radiation, which itself oscillates at ω_0 . Raman scattering arises from dipole moments oscillating at $\omega_0 \pm \omega$, which are produced when the dipole oscillating at ω_0 is modulated by the molecule oscillating at frequency ω . Alternatively, we can say that the frequencies observed in Raman scattering

are beat frequencies between the radiation frequency ω_0 and the molecular frequency ω . Scattered radiation at $\omega_0 - \omega$ and $\omega_0 + \omega$ is termed Raman Stokes and Raman anti-Stokes scattering, respectively.

2.1.4. Coherent Anti-Stokes Raman Scattering (CARS)

As mentioned at the end of section 2.1.2 the property responsible for CARS is the third-order electric susceptibility $\chi^{(3)}$. To simplify notation in further discussion we will omit the superscript in “chi-three” and use the symbol χ instead.

In principle, to obtain the frequency dependence of the light scattering processes based on the third-order electric susceptibility one needs to go through a procedure similar to that discussed for linear scattering in the previous section (2.1.3). In the CARS case, however, the third-order term $P^{(3)}$ from equation (2.5) is to be considered:

$$P^{(3)} = \chi : EEE . \quad (2.31)$$

Since “chi-three” is a fourth rank tensor, it permits the mixing of three independent electric fields with frequencies ω_1 , ω_2 and ω_3 in matter. Such a mixing leads to the generation of a fourth field with frequency ω_4 which carries information regarding the matter itself. It can be shown that the generated field has a number of frequencies equal to any additive combination of ω_1 , ω_2 and ω_3 , e.g. $\omega_4 = \omega_1 + \omega_2 + \omega_3$, $\omega_4 = \omega_1 + \omega_2 - \omega_3$, $\omega_4 = \omega_1 - \omega_2 - \omega_3$, etc. Thus the third-order electric susceptibility is the origin of a number of different nonlinear effects, and CARS is only one of those. In the case of CARS, the generated radiation has the frequency given by the expression:

$$\omega_4 = \omega_1 - \omega_2 + \omega_3. \quad (2.32)$$

It is typical for CARS experiments that two out of three beams of incident radiation have the same frequency $\omega_1 = \omega_3$ and these are referred to as “pump beams”; the third incident beam of frequency ω_2 is termed the “Stokes beam”; the generated beam ω_4 is called the “anti-Stokes beam”. Introducing identities $\omega_p \equiv \omega_1 = \omega_3$, $\omega_s \equiv \omega_2$ and $\omega_{CARS} \equiv \omega_4$ equation (2.32) can be rewritten as

$$\omega_{CARS} = 2\omega_p - \omega_s. \quad (2.33)$$

The energy diagram for CARS is shown in Figure 2-1. Dashed and solid lines represent virtual and real states, respectively. Frequency ω_p is normally kept constant as the Stokes frequency ω_s is being changed. At resonance, the difference between the frequencies of pump and Stokes beams $\omega_p - \omega_s$ is equal to a transition frequency ω_{mn} of a molecule, and the CARS signal beam of frequency ω_{CARS} has the maximum intensity. The reason for that will become clear shortly. Thus, scanning the frequency of the Stokes beam and monitoring the intensity of the CARS signal provides information about energy levels of a molecule.

The time averaged intensity of the CARS signal I_{CARS} is proportional to a number of parameters, as given by the following equation²⁷:

$$I_{CARS} \propto \omega_{CARS}^2 |\chi|^2 I_p^2 I_s \left(\frac{\sin(\Delta k / 2)}{\Delta k / 2} \right)^2, \quad (2.34)$$

in which I_p , I_s are intensities of incident pump and Stokes beams, respectively; Δk is the absolute value of the phase mismatch vector $\Delta \mathbf{k}$:

$$\Delta \mathbf{k} = 2\mathbf{k}_p - \mathbf{k}_s - \mathbf{k}_{CARS}, \quad (2.35)$$

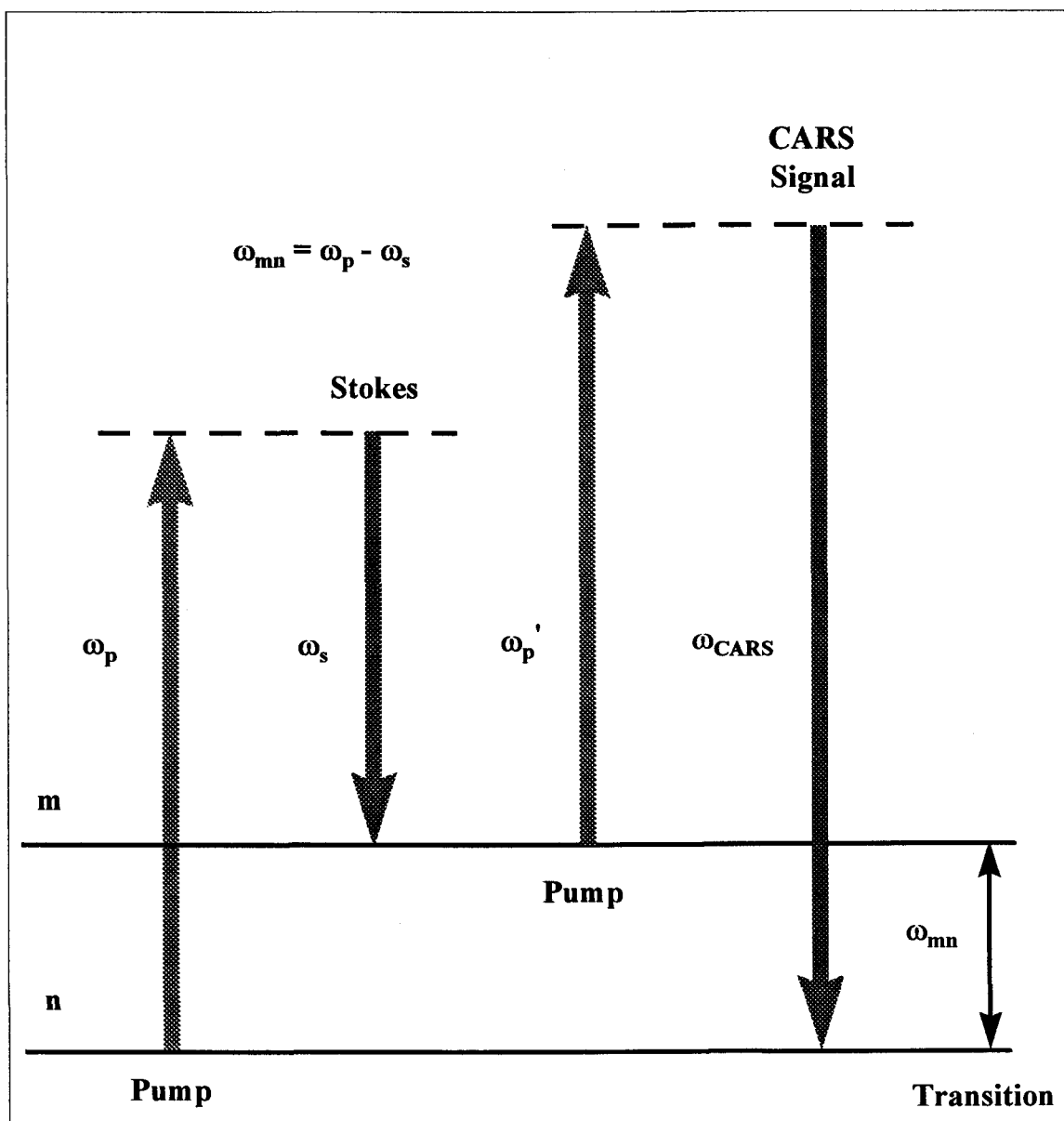


Figure 2-1. Energy diagram for CARS. Dashed and solid lines represent virtual and real states, respectively. Frequency ω_p is normally kept constant as the Stokes frequency ω_s is being changed. At resonance, the difference between frequencies of pump and Stokes beams $\omega_p - \omega_s$ equals a transition frequency of a molecule ω_{mn} , and the CARS signal beam has the maximum intensity. In this way scanning the frequency of the Stokes beam and monitoring the intensity of the CARS signal provides information about the energy levels of a molecule.

in which \mathbf{k}_p , \mathbf{k}_s and \mathbf{k}_{CARS} are the wave vectors of the pump, Stokes and CARS signal beams, respectively. A wave vector has the same direction as light and its absolute value is $k=(2\pi\omega)/n$, where ω and n are wavenumber of a lightwave and index of refraction, respectively. The frequency dependence of χ is given by

$$\chi \propto \frac{N_n - N_m}{\omega_{mn} - (\omega_p - \omega_s) - i\Gamma_{mn}}, \quad (2.36)$$

where $N_n - N_m$ is the population difference between lower and upper states of transition; ω_{mn} and Γ_{mn} are the frequency and the damping constant of the corresponding transition, respectively. It is obvious that the maximum value of χ is achieved when

$$\begin{aligned} \delta\omega &\equiv \omega_{mn} - (\omega_p - \omega_s) = 0 \\ &\text{or} \\ \omega_{mn} &= \omega_p - \omega_s \end{aligned} \quad (2.37)$$

Since, according to equation (2.34), the intensity of CARS is proportional to $|\chi|^2$, this is the condition for the maximum CARS signal as well. The damping constant Γ_{mn} determines the line shape of a transition, which will be discussed later in a section on analysis of experimental spectra in Chapter 4 (section 4.3.1 on p. 81).

The intensity of the CARS signal also depends on the absolute value of the phase mismatch Δk . The behavior of the "sinc" function squared $\left(\frac{\sin(\Delta k / 2)}{\Delta k / 2}\right)^2$ from the intensity expression (2.34) is shown in Figure 2-2. It is apparent that the phase-matching of incident beams diminishes quite dramatically for $\Delta k \neq 0$. The consequence of this is that only certain geometrical arrangements of three incident beams will provide the optimal CARS signal. To fulfill phase-matching condition these beams should be either collinear

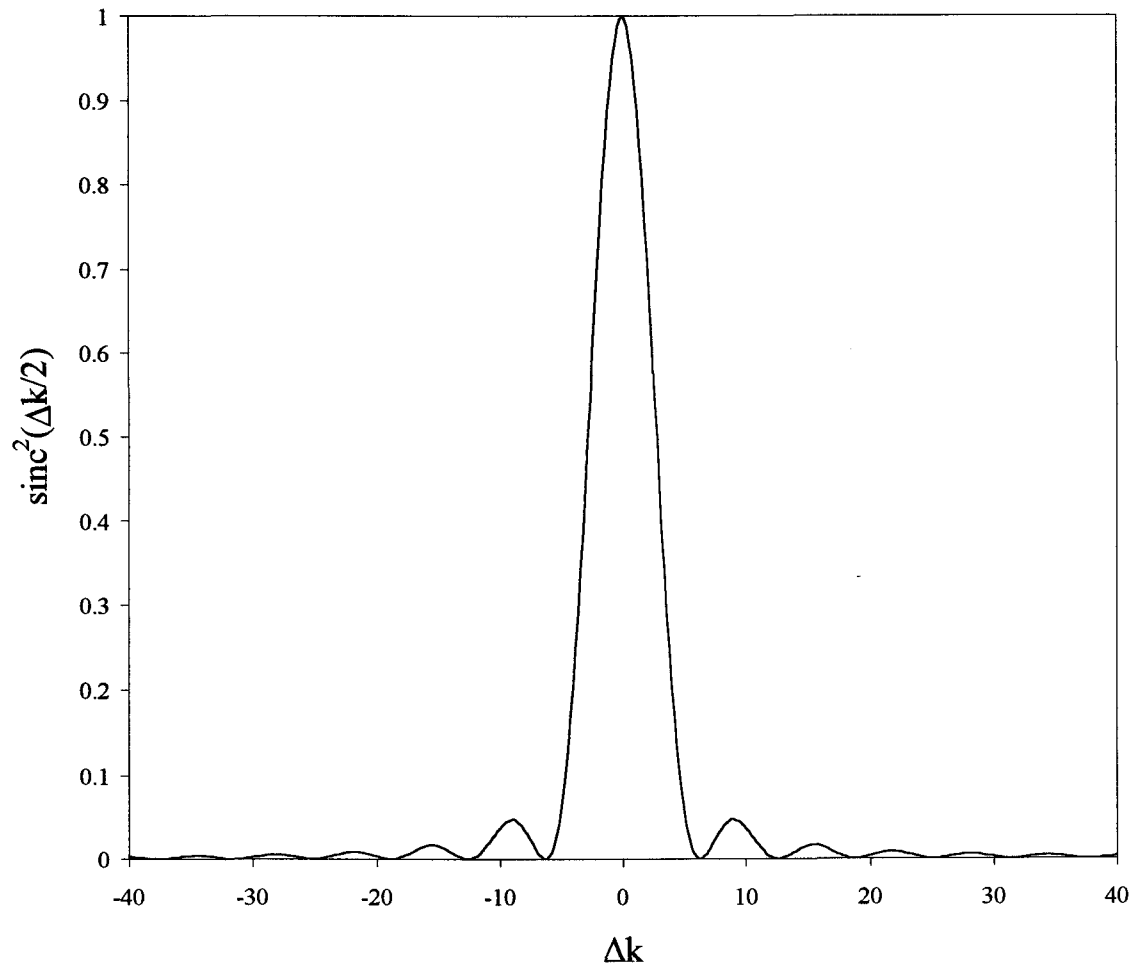


Figure 2-2. Normalized plot of the phase-matching function squared versus the phase-mismatch magnitude Δk .

or crossed at one point at a certain angle. Our choice for such a geometrical configuration and the motivation for it will be described later in the experimental part (Chapter 3; p. 45).

Concluding this section we would like to summarize some of the attractive features of the CARS method. As for any Raman scattering process, it permits observation of IR forbidden transitions, but it is much more sensitive than the usual linear Raman technique. The signal is emitted in a well-collimated laser-like beam, which makes discrimination against stray light much easier. It has point probing capability, which makes the technique an excellent diagnostic tool. It allows one to achieve resolution much higher than in the regular Raman method because this is limited by the linewidth of the input laser beams rather than by the resolution of a monochromator. The spectral position of the signal, to the anti-Stokes side of the pump frequency ω_p , also makes it easier to reject fluorescence interference, which usually lies to the Stokes side of ω_p .

A further, more detailed, discussion of different coherent Raman techniques, including CARS, and other nonlinear optical effects can be found in a number of the literature sources.²⁶⁻³⁶

2.2. Vibration-rotational states in diatomic molecules

The traditional approach to molecular vibrations and rotations is based on separate treatment of nuclear and electronic motions, first introduced into quantum mechanics by Born and Oppenheimer³⁷. The basic assumption is that electronic configuration of a molecule momentarily adjusts to any given nuclear position as a molecule undergoes its internal motions. However, in the real situation electrons do not follow the nuclei

perfectly. Electrons lead or lag the nuclei as the molecule rotates and vibrates. This gives rise to so-called **nonadiabatic rotational** and **nonadiabatic vibrational** corrections. In addition, the internuclear potential energy depends not only on internuclear distance, as follows from the Born-Oppenheimer approximation, but also on the relative nuclear momenta, hence on individual nuclear masses. This generates so called **adiabatic** corrections.

Quantum-mechanically, adiabatic effects are related to expectation values of certain operators within one electronic state, generally the ground state; nonadiabatic effects are formally attributed to interactions between the electronic state of interest and other electronic states of the molecular system (see discussion on p. 24).

In the following sections of this chapter we provide a short outline of the Born-Oppenheimer approximation and its specific application for diatomic systems (Dunham theory); then we discuss adiabatic and nonadiabatic corrections to it.

2.2.1. The Born-Oppenheimer approximation

The total Schrodinger's equation for a diatomic molecular system with N electrons is given by

$$\left[-\sum_{k=1}^2 \frac{\hbar^2}{2m_k} \nabla_k^2 - \sum_{j=1}^N \frac{\hbar^2}{2m_e} \nabla_j^2 + V_c(R) \right] \Psi(r, R) = E \Psi(r, R), \quad (2.38)$$

in which m_k and m_e are the mass of a nucleus and the mass of the electron, E denotes the total energy, $V_c(R)$ is the Coulombic potential, k and j are nuclear and electron indices.

The total wavefunction is written as a product of a nuclear term $\chi(R)$, which depends

only on internuclear separation R , and an electronic term $\psi(r;R)$, which is an explicit function of electron radial coordinate r and parametrically depends on internuclear separation R :

$$\Psi(r,R) = \chi(R)\psi(r;R). \quad (2.39)$$

Applying nuclear and electronic Laplacian operators (∇_k^2 and ∇_j^2) in equation (2.38) to this function we obtain:

$$-\sum_{k=1}^2 \frac{\hbar^2}{2m_k} \left[\psi \nabla_k^2 \chi + \chi \nabla_k^2 \psi + 2\nabla_k \chi \nabla_k \psi \right] - \sum_{j=1}^N \frac{\hbar^2}{2m_e} \chi \nabla_j^2 \psi + V_c(R) \chi \psi = E \chi \psi \quad (2.40)$$

The separation of nuclear and electronic coordinates can be achieved if we neglect the latter two terms in the bracket on the left-hand side of equation (2.40),

$$\chi \nabla_k^2 \psi + 2\nabla_k \chi \nabla_k \psi, \quad (2.41)$$

divide both sides by $\chi \psi$, and re-arrange the equation:

$$-\sum_{j=1}^N \frac{\hbar^2}{2m_e} \frac{\nabla_j^2 \psi(r;R)}{\psi(r;R)} + V_c(R) = \sum_{k=1}^2 \frac{\hbar^2}{2m_k} \frac{\nabla_k^2 \chi(R)}{\chi(R)} + E \quad (2.42)$$

Since the left-hand side of equation (2.42) depends on R only parametrically, and the right-hand side does not depend on r , we can set both sides separately equal to a quantity $V^{BO}(R)$, which has dimensions of energy:

$$-\sum_{j=1}^N \frac{\hbar^2}{2m_e} \frac{\nabla_j^2 \psi(r;R)}{\psi(r;R)} + V_c(R) = V^{BO}(R) \quad (2.43)$$

$$\sum_{k=1}^2 \frac{\hbar^2}{2m_k} \frac{\nabla_k^2 \chi(R)}{\chi(R)} + E = V^{BO}(R) \quad (2.44)$$

These equations can be rewritten as:

$$-\sum_{j=1}^N \frac{\hbar^2}{2m_e} \nabla_j^2 \psi(r; R) + V_c(R) \psi(r; R) = V^{BO}(R) \psi(r; R) \quad (2.45)$$

$$-\sum_{k=1}^2 \frac{\hbar^2}{2m_k} \nabla_k^2 \chi(R) + V^{BO}(R) \chi(R) = E \chi(R) \quad (2.46)$$

In equation (2.45), the total electron energy $V^{BO}(R)$ (including internuclear repulsion), with internuclear separation fixed at R , becomes a potential energy for nuclear motions according to expression (2.46). The procedure just described is the Born-Oppenheimer approach, which is also referred to as the clamped nuclei approximation.

2.2.2. Dunham model of energy levels in diatomic molecules

In 1932 J. L. Dunham developed a mechanical model based on the Born-Oppenheimer approximation to describe diatomic systems^{38,39}. He used the semi-classical Wentzel⁴⁰-Brillouin⁴¹-Kramers⁴² (WBK) method to obtain an expression for energy eigenvalues without solving explicitly Schrodinger's equation for wavefunctions. For a vibrating rotor, Schrodinger's equation is

$$\frac{d^2 \psi_{vJ}(x)}{dx^2} + \frac{2\mu R_e^2}{\hbar^2} \left[E(v, J) - V(x) - \frac{\hbar^2 J(J+1)}{2\mu R_e^2 (1+x)^2} \right] \psi_{vJ}(x) = 0, \quad (2.47)$$

in which, besides common notation for the equation, μ is the reduced nuclear mass, R_e , v , J are equilibrium internuclear separation, vibrational and rotational quantum numbers, respectively; x is the reduced internuclear distance:

$$x = \frac{R - R_e}{R_e}, \quad (2.48)$$

where R is the regular internuclear distance. The last term in the bracket in equation (2.47) is due to the centrifugal force of rotation.

Since it is difficult to incorporate the effect of rotation into conventional potential functions V , such as the Morse potential, the following power series expansion of V around the point $x=0$ was used instead:

$$V(x) = a_0 x^2 \left(1 + \sum_{j=1} a_j x^j\right), \quad (2.49)$$

where a_0 is given in terms of molecular vibrational and rotational constants ω_e and B_e as

$$a_0 = \frac{\omega_e^2}{4B_e} \quad (2.50)$$

and the a_j constants are to be determined. Using this form for the potential function V , Dunham showed that a WBK treatment yields the following expression for the energy levels in diatomic molecules:

$$E(v, J) = \sum_{k=0} \sum_{l=0} Y_{kl} \left(v + \frac{1}{2}\right)^k [J(J+1)]^l, \quad (2.51)$$

in which coefficients Y_{kl} are referred to as Dunham coefficients and are functions of ω_e , B_e and a_i coefficients from equation (2.49). There exists an approximate correspondence between conventional molecular constants and Dunham coefficients. For example,

$$Y_{1,0} \approx \omega_e, \quad (2.52)$$

$$Y_{0,1} \approx B_e, \quad (2.53)$$

$$Y_{2,0} \approx -\omega_e x_e, \quad (2.54)$$

$$Y_{0,2} \approx -D_e, \text{ etc.} \quad (2.55)$$

The difference between molecular constants and Dunham coefficients is proportional to term B_e^2/ω_e^2 , which for most molecules is a very small quantity. It is important to notice that there is certain interdependence between different Dunham coefficients, e.g.

$$Y_{0,2} = -\frac{4Y_{0,1}^3}{Y_{1,0}^2}. \quad (2.56)$$

In principle, from a solution of equations (2.47) and (2.49) one can obtain not only molecular eigenenergies, but also the vibration-rotational wavefunctions $\psi_{v,J}(x)$ as well. The appropriate method for performing this was proposed by Herman *et al.*⁴³ and extended by Tipping and Ogilvie⁴⁴.

2.2.3. Extramechanical effects

During succeeding decades after Dunham's theory was developed, it was used by spectroscopists to determine potential-energy functions for various diatomic molecules. By this method they sought to achieve a reduction of many wavenumber data to relatively few molecular parameters in the form of either coefficients in the potential-energy function, or set of Dunham coefficients from equation (2.51). These served to reproduce the observed spectroscopic data, which during the course of time became more and more precise. The spectra of isotopic variants of particular molecules have been routinely subjected to simultaneous analysis. In many circumstances, Dunham's theory was found inadequate to describe quantitatively isotopic data of the available quality¹¹. Effects beyond those taken into account by the theory appeared not only to cause deviations from

the expected mass-scaling factors relating the energies of isotopes but also to lead to systematic discrepancies in the energies of highly rotationally excited states of a single isotopic species⁴⁵. As it was mentioned at the beginning of the section, the deviations from the mechanical behavior of Dunham's theory are due to adiabatic, nonadiabatic vibrational and nonadiabatic rotational effects, which sometimes are collectively referred to as **extramechanical effects**⁴⁶.

During the several decades since the work of Born, Oppenheimer and Dunham, many researchers have considered these effects^{11,43,44,47-57}. The basic concepts related to this issue can be summarized as follows.

For nuclear motion characterized by the wavefunction $\chi_n(R)$, the exact Schrodinger's equation (2.40) can be transformed into the following form^{58,59}:

$$\left[-\frac{\hbar^2}{2\mu} \nabla_R^2 + V_n^{BO}(R) + \hat{H}'_{nn}(R) - E \right] \chi_n(R) = \sum_{m \neq n} \hat{H}'_{mn}(R) \chi_m(R), \quad (2.57)$$

where

$$\hat{H}'_{mn}(R) = -\frac{\hbar^2}{2} \int \psi_m^*(r; R) \left(\frac{\nabla_a^2}{m_a} + \frac{\nabla_b^2}{m_b} \right) \psi_n^*(r; R) dr. \quad (2.58)$$

Here ψ_m and ψ_n denote Born-Oppenheimer electronic wavefunctions for different electronic states and indices a and b refer to two different nuclei. Neglecting the right-hand side of expression (2.57), one obtains the Schrodinger's equation for the so-called adiabatic approximation:

$$\left[-\frac{\hbar^2}{2\mu} \nabla_R^2 + V_n^{BO}(R) + \hat{H}'_{nn}(R) - E \right] \chi_n(R) = 0. \quad (2.59)$$

According to expressions (2.58) and (2.59), adiabatic corrections to the Born-Oppenheimer potential are given by

$$\Delta V^{AD}(R) \equiv H'_{nn}(R) = -\frac{\hbar^2}{2} \int \psi_n(r; R) \left[\frac{\nabla_a^2}{m_a} + \frac{\nabla_b^2}{m_b} \right] \psi_n(r; R) dr, \quad (2.60)$$

and involve Born-Oppenheimer electronic wavefunctions of the same electronic state n .

Nonadiabatic corrections to the total energy are represented by

$$\Delta E^{NA} = \sum_{m \neq n} \hat{H}'_{mn}(R) \chi_m(R) \quad (2.61)$$

and mix electronic wavefunctions of different electronic states.

For a diatomic system in a $^1\Sigma$ electronic state, expression (2.57) leads to an effective Hamiltonian for vibrational and rotational motion^{11,60}:

$$H_{eff} = -\frac{\hbar^2}{2\mu} \frac{d}{dR} [1 + \beta(R)] \frac{d}{dR} + V(R) + \frac{\hbar^2}{2\mu R^2} [1 + \alpha(R)] J(J+1) \quad (2.62)$$

with the reduced nuclear mass μ given by

$$\mu = \frac{M_a M_b}{M_a + M_b}, \quad (2.63)$$

where M_a , M_b are nuclear masses. The internuclear potential $V(R)$ has two main contributors:

$$V(R) = V^{BO}(R) + V^{AD}(R), \quad (2.64)$$

in which Born-Oppenheimer potential $V^{BO}(R)$ is a part independent of nuclear mass and similar to the potential defined in equation (2.49), and adiabatic effects $V^{AD}(R)$ are mass dependent. Terms $\alpha(R)$ and $\beta(R)$ reflect specific types of nonadiabatic corrections ΔE^{NA} : rotational and vibrational, respectively. In subsequent considerations, we will use a new reduced internuclear displacement variable:

$$z = 2 \frac{(R - R_e)}{(R + R_e)} \quad (2.65)$$

that, unlike parameter x defined in equation (2.48), has the virtue of remaining finite throughout the range of molecular separations: for $0 \leq R \leq \infty$, $-2 \leq z < 2$ ^{61,62}. The potential energy $V^{BO}(R)$ in terms of z becomes

$$V^{BO}(z) = c_0 z^2 \left(1 + \sum_{j=1} c_j z^j\right). \quad (2.66)$$

Terms V^{AD} , α and β are given by the following expansions^{46,63}:

$$V^{AD}(z) = \frac{m_e}{M_a} \sum_{j=0} u_j^a z^j + \frac{m_e}{M_b} \sum_{j=0} u_j^b z^j, \quad (2.67)$$

$$\alpha(z) = \frac{m_e}{M_a} \sum_{j=0} t_j^a z^j + \frac{m_e}{M_b} \sum_{j=0} t_j^b z^j, \quad (2.68)$$

$$\beta(z) = \frac{m_e}{M_a} \sum_{j=0} s_j^a z^j + \frac{m_e}{M_b} \sum_{j=0} s_j^b z^j, \quad (2.69)$$

in which m_e is the mass of the electron and $u_j^{a,b}$, $t_j^{a,b}$, $s_j^{a,b}$ are expansion coefficients for nuclei A and B. The magnitudes of the coefficients c_j , $j > 0$ and of all $t_j^{a,b}$ and $s_j^{a,b}$ should be of the order of unity whereas the magnitudes of c_0 and of all coefficients $u_j^{a,b}$ are expected to be of order of (B_e/γ^2) ; $\gamma \equiv 2B_e/\omega_e$ has the range of values $[10^{-4}, 0.026]$ for known diatomic molecules in their ground state⁶³.

Molecular energy levels within a particular electronic state (vibration-rotational terms) can be expressed in the form of the systematic double summation^{63,64}

$$E_{vJ} = \sum_{k=0} \sum_{l=0} (Y_{kl} + Z_{kl}^{v,a} + Z_{kl}^{v,b} + Z_{kl}^{r,a} + Z_{kl}^{r,b}) \left(v + \frac{1}{2}\right)^k [J(J+1)]^l. \quad (2.70)$$

Auxiliary coefficients Z_{kl}^v , Z_{kl}^r for either nucleus represent extramechanical corrections to the Dunham model given by equation (2.51). Coefficients Z_{kl}^v include adiabatic and nonadiabatic vibrational corrections:

$$Z_{kl}^v = f(u_j, s_j, c_j, M_a, M_b), \quad (2.71)$$

and coefficients Z_{kl}^r include both nonadiabatic rotational and vibrational effects⁴⁶:

$$Z_{kl}^r = f(t_j, s_j, c_j, M_a, M_b). \quad (2.72)$$

Term coefficients Y_{kl} depend on the molecular parameters such as the harmonic force constant k_e , the equilibrium separation R_e , the potential-energy coefficients c_j , and the nuclear masses M_a and M_b , but do not depend on coefficients responsible for extramechanical effects:

$$Y_{kl} = f(k_e, R_e, c_j, M_a, M_b). \quad (2.73)$$

Concrete forms of functions (2.71), (2.72) and (2.73) are involved algebraic expressions⁶³, some of which can be found in Appendix A.

Each term coefficient Y_{kl} consists of a series of contributions⁶⁵:

$$Y_{kl} = Y_{kl}^{(0)} + Y_{kl}^{(2)} + Y_{kl}^{(4)} + \dots \quad (2.74)$$

To a very good approximation all higher order terms in the expansion can be neglected and only the leading term $Y_{kl}^{(0)}$ ⁵⁴,

$$Y_{kl}^{(0)} = U_{kl} \mu^{-\left(\frac{k+l}{2}\right)}, \quad (2.75)$$

which depends on the reduced mass, retained. Coefficients U_{kl} become independent of mass and are the same for all isotopic variants of a molecule. These coefficients also appear in a commonly used empirical relation⁶⁶

$$E_{\nu J} = \sum_{k=0} \sum_{l=0} U_{kl} \mu^{-(\frac{k}{2}+l)} \left[1 + m_e \left(\frac{\Delta_{kl}^a}{M_a} + \frac{\Delta_{kl}^b}{M_b} \right) \right] \left(\nu + \frac{1}{2} \right)^k [J(J+1)]^l. \quad (2.76)$$

Here U_{kl} is the dominant contribution to Y_{kl} , and conventional parameters Δ_{kl} absorb both extramechanical effects and mechanical effects of order greater than those signified in coefficient U_{kl} .

Introduction of mass independent coefficients U_{kl} permits analysis of isotopic spectral data in one "global" fit. From the formalism just presented the transition frequency between two energy levels n and m can be expressed in general form as

$$\omega_{mn} = E(\nu' J') - E(\nu'' J'') = f(M_a, M_b, \nu', \nu'', J', J'', U_{kl}, u_j, s_j, t_j, c_j), \quad (2.77)$$

in which vibrational and rotational quantum numbers (ν', J') and (ν'', J'') belong to the upper and the lower state of the transition, respectively. Experimental transition frequencies can be fitted using expression of type (2.77) with regression variables M_a , M_b , ν' , J' , ν'' , J'' and regression parameters U_{kl} , u_j , s_j , t_j , c_j .

We note that the extramechanical effects are quantitatively characterized by the set of coefficients u_j , s_j and t_j , which increase with decrease of an isotopic molecular mass. These coefficients are of the order of the ratio of mass of the electron to the reduced mass of a molecule. Determination of coefficients u_j , s_j and t_j was one of the objectives of the present work.

2.3. Electrical discharge in gases

As mentioned before, to prepare molecules in their vibrationally excited states an electrical discharge was used in our work. In this section we provide a brief theoretical overview of electrical phenomena in gases, understanding of which was essential for the development of the discharge apparatus employed in our experiments.

The first observations of gas discharges were made in the course of electrostatic investigations dated back to the seventeenth century. However, the detailed scientific study of the phenomenon began in the nineteenth century⁶⁷⁻⁶⁹.

The term *gas discharge* is used to describe the flow of electric current through a gaseous medium. The requirements for such a passage of current are that some of atoms or molecules of the gas should be ionized by some means, and that there should exist an electric field to drive the charged particles to produce a current.

2.3.1. Types of discharge

Gas discharges can take place over a very wide range of gas pressure, from a few Torr up to one atmosphere⁷⁰, and involve currents I ranging from fraction of microampere to 10^6 A and more⁷¹. According to the current discharges are classified into three types:

- (i) The dark discharge ($i < 10^{-6}$ A).
- (ii) The glow discharge (10^{-6} A $\leq i < 10^{-1}$ A).
- (iii) The arc discharge (10^{-1} A $\leq i$ A).

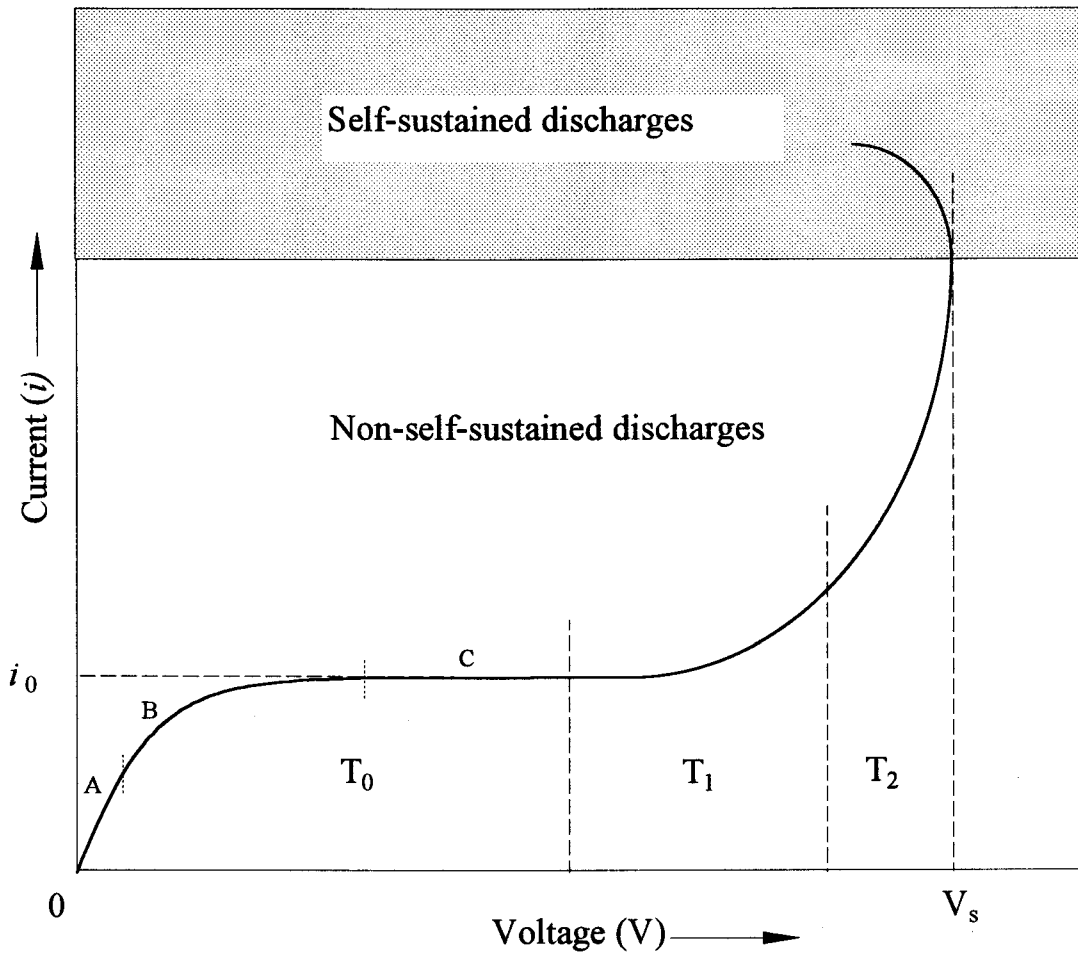


Figure 2-3. Current-voltage characteristics of a gas in pre-spark regions T_0 , T_1 , T_2 . The current i_0 is the "saturation" current of region T_0 . The discharges in regions T_1 and T_2 are referred to as Townsend discharges, after J. S. Townsend. V_s represents the breakdown voltage.

In the study of gas discharges, it is also customary to divide them in to two general kinds: those which are and those which are not self-sustaining⁷². The mechanism of breakdown of a gas, called a spark, is a transition from a non-self-sustaining discharge, which is a dark discharge, to one of the several kinds of self-sustaining discharge (e.g. glow and arc discharges).

2.3.2. Non-self-sustaining discharges

As an example of a non-self-sustaining discharge, consider a gas between two electrodes which is ionized by some means (e.g. X-rays, UV radiation). The current-voltage plot of such a system is shown in Figure 2-3. When voltage is first applied, the current through the gas increases slowly as the charged species, ions and electrons, move through the gas with an average velocity determined by their mobility for the particular value of electric field. Further increase of voltage results in "saturation". This is true for a considerable range of voltage as is indicated by the region T_0 of Figure 2-3. The current again increases with voltage, slowly at first as in region T_1 and then rapidly as in region T_2 . The discharges in regions T_1 and T_2 are called Townsend discharges, after J. S. Townsend, who conducted early and extensive investigations in this field⁷³. The current in the T_0 region and the regions of Townsend discharges T_1 and T_2 ceases as soon as the external ionizing source is removed and hence are not self-sustained.

The total current density through an ionized gas j is the sum of the electron and ion current densities j_e and j_i ⁷⁴

$$j = j_i + j_e = n_i e v_i + n_e e v_e, \quad (2.78)$$

in which n, e, v represent number density, charge of electron and velocity, respectively, for ions and electrons (subscripts i and e). Since $n_i = n_e = n$, in terms of mobility of ions and electrons (μ_i, μ_e), applied voltage V and the distance between electrodes d , the expression becomes

$$j = ne(\mu_i + \mu_e) \frac{V}{d} = ne(\mu_i + \mu_e)E. \quad (2.79)$$

This is true for small values of field strength $E=V/d$ ($\approx 1\text{V/cm}$ at several Torr of gas pressure) and explains why the discharge current first increases linearly with the voltage (part A of region T_0 in Figure 2-3). This mechanism is termed the simple collection.

As voltage V progressively increases, the charged species are eventually being drawn to the electrodes much faster than they are generated by the external ionizing source. If it is assumed that no new electrons and ions are produced by the field, there should be no further increase in current with voltage. The current achieves its saturation value i_0 since ionization becomes the rate limiting process (part C of region T_0 in Figure 2-3). Part B of T_0 region is the transition between simple collection and saturation mechanisms.

When the applied potential becomes greater than or equal to the ionization potential of a gas V_i , the primary electrons produced by the external ionization agent can acquire an energy from the electric field which is sufficient for them to ionize the molecules of the gas. The same will be true for the electrons produced as a result of such an ionization, and so on. This avalanche effect gives rise to a rapid increase in the total current and is referred to as the multiplication mechanism (Townsend discharges T_1 and T_2 in Figure 2-3).

It can be shown⁷⁵ that the total discharge current density j for the T_1 region depends on the saturation current density j_0 , distance between electrodes d and the so called first Townsend coefficient α , which is the average number of ionizing collisions of electron per unit path in the direction of the field:

$$j = j_0 \frac{\exp(\alpha d) - 1}{\alpha d}. \quad (2.80)$$

The first Townsend coefficient is related to the electric field and gas pressure by⁷³

$$\frac{\alpha}{p} = A \exp\left(-\frac{B}{(E/p)}\right) \quad (2.81)$$

in which constants A and B depend on the gas used⁷⁶. The expression is illustrated in Figure 2-4 . The experimental maxima α/p ($=A$) are of the order of $10 \text{ (Torr}\cdot\text{cm)}^{-1}$ ⁷⁴. Expressions (2.80) and (2.81) constitute the mathematical description of the multiplication mechanism in T_1 discharges.

For the voltage values V corresponding to the region of the T_2 discharge, besides the α process, new phenomena take place. For example, the positive ions formed by electron collisions begin to gain enough energy from the field to produce secondary electrons from the cathode by collisions. In turn, these secondary electrons take part in ionization, and so on. This leads to the concept of the coefficient γ , the number of secondary electrons per each bombarding positive atom. The quantity γ is expected to have the same functional form as α in equation (2.81). The current density due to the γ process is⁷¹

$$j_\gamma = j_0 \frac{\exp(\alpha d)}{1 - \gamma[\exp(\alpha d) - 1]}, \quad (2.82)$$

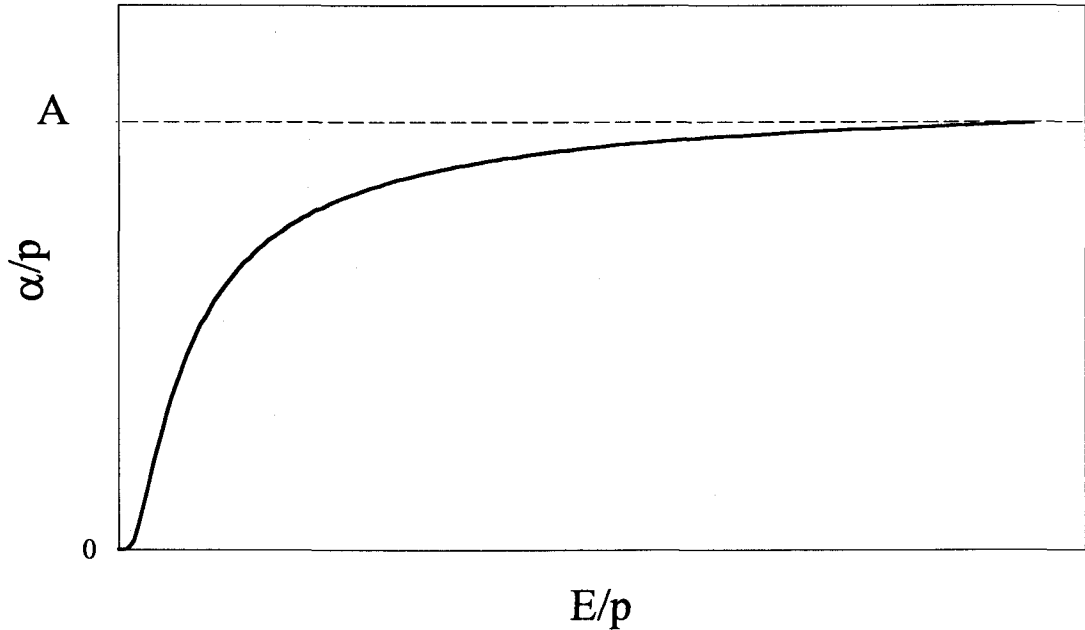


Figure 2-4. The first Townsend coefficient α as a function of electric field.

and this is mainly responsible for the T_2 region of the current-voltage characteristic of a gas in Figure 2-3. The last expression contains a breakdown condition. The current density j_γ becomes infinite if

$$\gamma[\exp(\alpha d) - 1] = 1, \quad (2.83)$$

which is termed the Townsend criterion for transfer from non-self-sustained to self-sustained discharges.

2.3.3. Glow discharge

Typical volt-ampere characteristics of self-sustained discharges are shown in Figure 2-5 (BCDEF line). These characteristics are obtained for a discharge tube in series

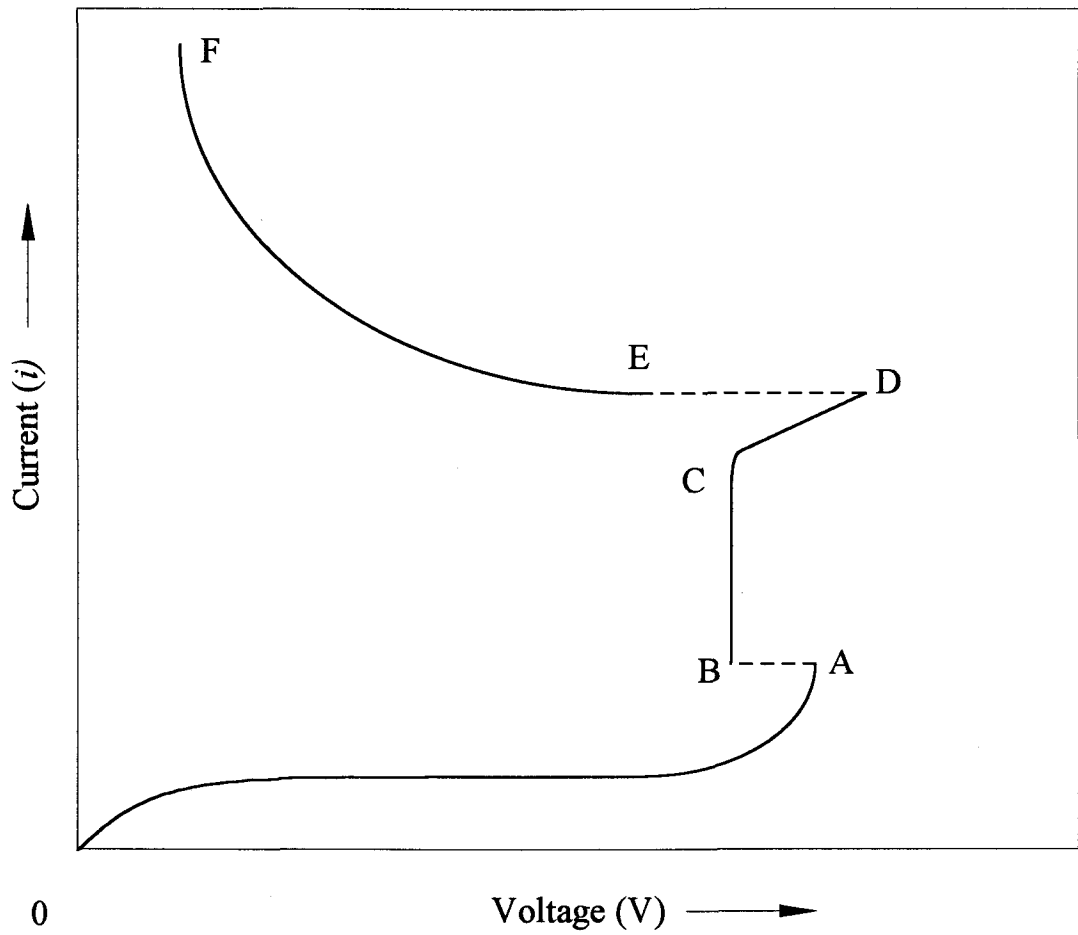


Figure 2-5. Typical volt-ampere characteristics of various discharges in gas.

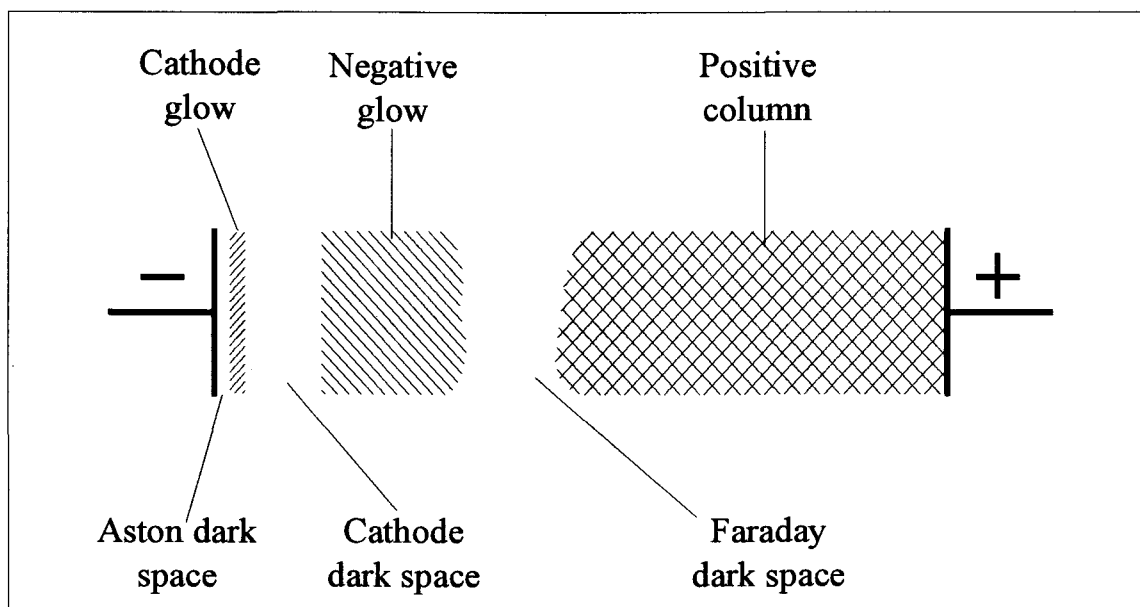


Figure 2-6. The structure of a low pressure glow discharge.

with a battery of voltage V_b and a variable resistance R^{72} . Changing resistance R effectively changes current i through the gas as well as the voltage drop V between electrodes of the tube. The OA part of the curve represents non-self-sustained discharges discussed in the previous section. The breakdown (AB) of a gas leads to the region of the glow discharge (BCD). If the current i is increased beyond point D the arc discharge takes place (EF).

We restrict our discussion to only one kind of the self-sustained discharges, the glow discharge, the low pressure glow discharge in particular, which was involved in our measurements for vibration-rotational excitation of molecules.

When the pressure of a discharge tube is reduced to a few Torr, an applied voltage can produce a uniform glow throughout the tube. The discharge is seen to consist of alternate dark and light regions⁷² as it shown in Figure 2-6. If the discharge is operating within region BC of Figure 2-5, it is found⁷² that the cathode glow covers only a part of the cathode surface, and that this part increases or decreases in the direct proportion to the discharge current. In this case the current density as well as the voltage drop across the discharge remain constant. Further, at the point C, the whole cathode is covered by the glow, and the voltage drop and the current density start increasing with the discharge current. The regions BC and CD are referred to as the normal and abnormal glow, respectively.

The effect of changing pressure is pronounced and manifests itself by the fact that the length of the cathode dark space is inversely proportional to the gas pressure⁷¹. The length of the other regions vary in roughly the same manner, except for the positive column, which tends to occupy as much of the tube space as is available to it. Extremes of pressure put limits on maintaining the glow discharge. At very low pressures the cathode dark space fills the entire tube and eventually the supply of electrons by positive-ion bombardment (see γ process in section 2.3.2, p. 33) is no longer sufficient to retain the discharge. On the other hand, as the gas pressure increases the current density j increases as well (for a few Torr, $j \propto p^2$; for higher pressure, $j \propto p^{\frac{4}{3}}$)⁷⁷ and the glow discharge readily transforms to the arc discharge.

If the gas pressure is kept constant and the distance between electrodes is reduced, it is found⁷⁴ that such a reduction first shortens the length of the positive column, while the rest of the structure remains unchanged, and the voltage drop between the electrodes falls

only slightly. This process continues until the anode is in the negative glow, at which point the voltage required to maintain the discharge begins to rise. From these observations it appears that the positive column is not characteristic of the discharge and all essential processes occur in the cathode region, which is the area stretching from the surface of the cathode to the beginning of the negative glow. The description of the processes in this cathode region as well as in other zones of a glow discharge follow⁷⁴.

In the Aston dark space, the electrons coming from the cathode do not have enough energy to ionize or to excite the gas molecules. On the other hand, the positive ions moving towards the cathode already have high enough velocity such that the probability of a radiative recombination is small. Finally, ions excited in the other regions have already had time to radiate and return to their ground state. As result of these facts, no light emission is seen in this dark space.

The cathode glow, which is sometimes referred to as the cathode sheath, will appear at the point where ions excited by electrons return to their ground level emitting radiation. In many cases the cathode glow completely masks the Aston dark space.

In the cathode (or Crookes) dark space the gas is ionized by those accelerated electrons which have not already lost much energy in exciting the gas species of the cathode glow region. As the result of ionization, multiplication of charges takes place (α process described in section 2.3.2, p. 33). However, in this region the secondary electrons do not have enough energy for the excitation of the gas species. On the other hand, the velocity of the primary electrons which gave rise to them is still high enough to prevent active radiative recombination with the positive ions. Due to this lack of excitation and recombination the region emits little light.

In the negative glow region the large number of secondary electrons liberated in the cathode dark space begin to excite and ionize the ambient gas⁷⁸. There is therefore a considerable emission of light. Since the density of positive ions is great in this region, part of radiation come from the recombination process.

At the anode end of the negative glow the electrons lose their energy and can not any longer excite or ionize the gas. At this point the so-called Faraday dark space begins. The field in this region is small and electrons can not regain much energy quickly. The current in this zone is essentially due to the drift of the charged particles.

The positive column follows the Faraday dark space and is the most luminous part of the discharge⁷⁹ after the negative glow. It starts when the electrons have gained enough energy in the Faraday dark space to excite and eventually ionize the gas species. The positive column behaves like a plasma, since the densities of positive and negative particles are equal.

In some cases, depending on pressure, distance between electrodes and their shape, discharge current, etc., two more zones might appear in the vicinity of the anode after the positive column: the anode dark space and the anode glow. However, these are very small regions and they were not observed under conditions of our experiments described later in Chapter 3.

From above discussion follows that a glow discharge contains several zones with excited ionized gas. Collisions between neutral molecules and charged species accelerated in electric field, as well as recombination of excited ions result in the production of vibrationally excited molecular states. Although the positive column is not essential for the maintenance of the glow discharge itself, it is a very important region for

such an excitation. The positive column is the most ionized part of the discharge; unlike other ionized zones its size can be easily enlarged by changing the distance between electrodes while retaining the desired gas pressure in the discharge tube, hence turning the positive column into a major excitation source without perturbing other discharge parameters. Optimization of such parameters for the maximum vibrational excitation of molecules was one of the objectives of the first stage of our project, which is discussed in the next chapter.

3. DEVELOPMENT OF OPTICAL METHOD FOR STUDY OF DIATOMIC MOLECULES EXCITED IN A GLOW DISCHARGE

3.1. Introduction

The development of the method for optical study of diatomic molecules excited by a glow discharge involved four major steps. The first of these was the construction of a discharge cell and optimization of the discharge parameters for the maximum CARS signal. The medium resolution apparatus was used for these preliminary experiments. A second step, the necessity of which became evident in the course of optimization, was the development of the cycling system for optical measurements of precious gases in a glow discharge. Third was an assessment of figures of merit of the high resolution experimental apparatus, which was used for the ultimate spectral measurements. The last part was the development of the experimental algorithm itself. Accordingly, several pilot projects were fulfilled before the main measurements to realize these steps. Commercial $^{14}\text{N}_2$ of 99.98% purity was used in all preliminary studies.

First two steps are described in the present chapter. The last two are discussed later in Chapter 4. They are an integral part of our article on high resolution CARS measurements of vibrationally excited nitrogen isotopes⁸⁰, which constitutes the body of the latter chapter.

3.2. Optimization of discharge parameters

3.2.1. Experimental apparatus used for optimization

The principle diagram for the experimental set-up used in the preliminary study on the optimization of the glow discharge parameters is shown in Figure 3-1 and described in the subsequent sections in some details.

3.2.1.1. *Light sources*

A Lightwave Electronics S-100 infrared diode laser produces a so called "seed" beam of about 2 mW which is injected in the cavity of the pulsed Nd:YAG laser (Quanta Ray DCR-1A) to obtain single mode operation at 1064 nm. The Nd:YAG laser pulses of about 8-10 ns are generated at a frequency of 10 Hz and have spectral width of about 0.003 cm^{-1} .

The original infrared 1064 nm output of the Nd:YAG laser is converted to 532 nm green radiation by a KDP doubling crystal. The green beam of energy of 90-100 mJ/pulse is divided by a beam splitter into two unequal parts: $\sim 2/3$ are used as a pump source for the tunable pulsed dye laser (Hyperdye-500) and the remaining radiation is engaged in the generation of the CARS signal in the experimental cell. The latter in turn is divided into two equal parts to obtain the pump beams needed for CARS process in the folded "BOXCARS" configuration (discussed later in section 3.2.1.2 on p. 45). The third beam, Stokes beam (see the energy diagram shown in Figure 2-1 on p. 15), originates from the Hyperdye-500 dye laser.

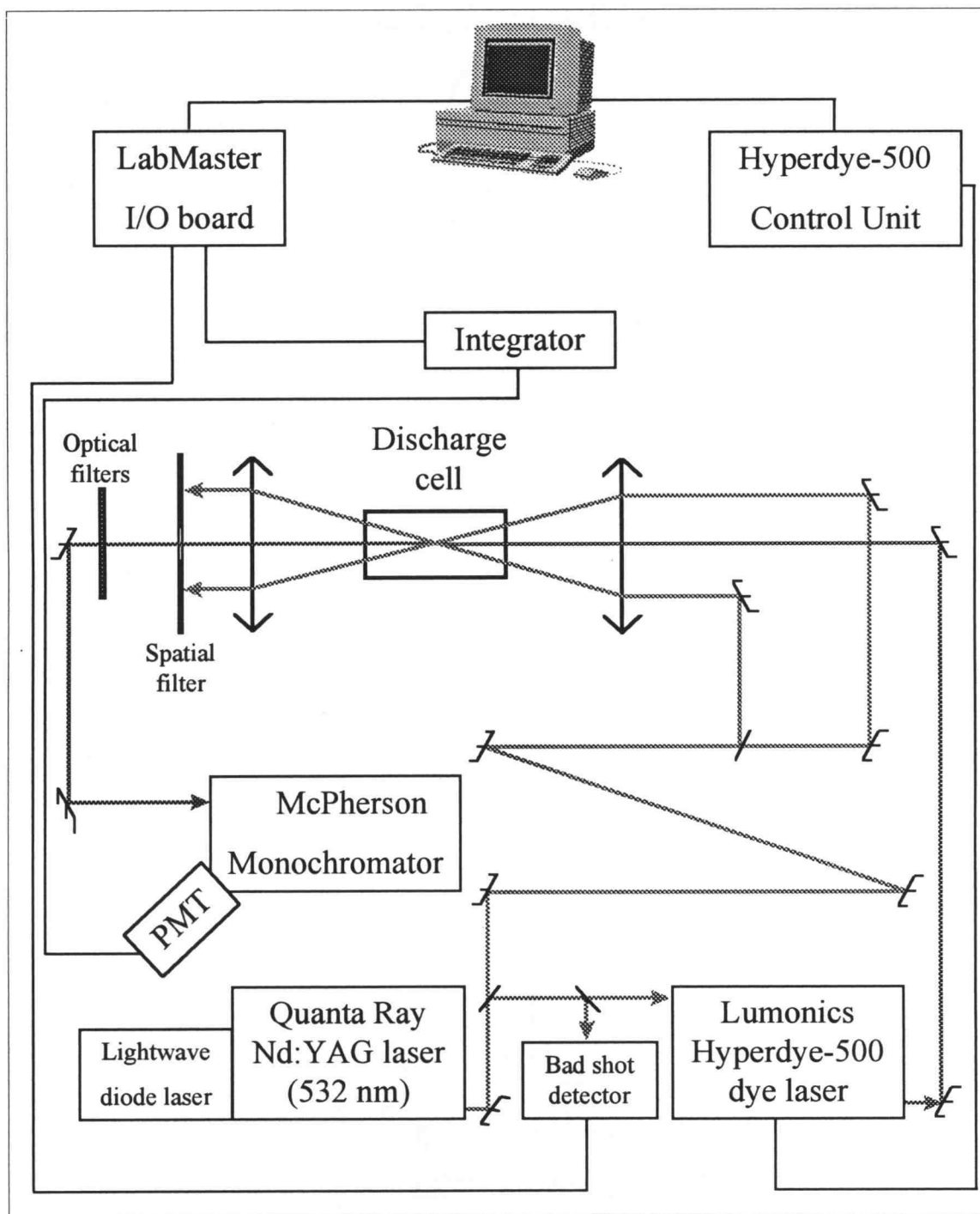


Figure 3-1. Schematic diagram of the medium resolution apparatus used in the optimization of the glow discharge parameters.

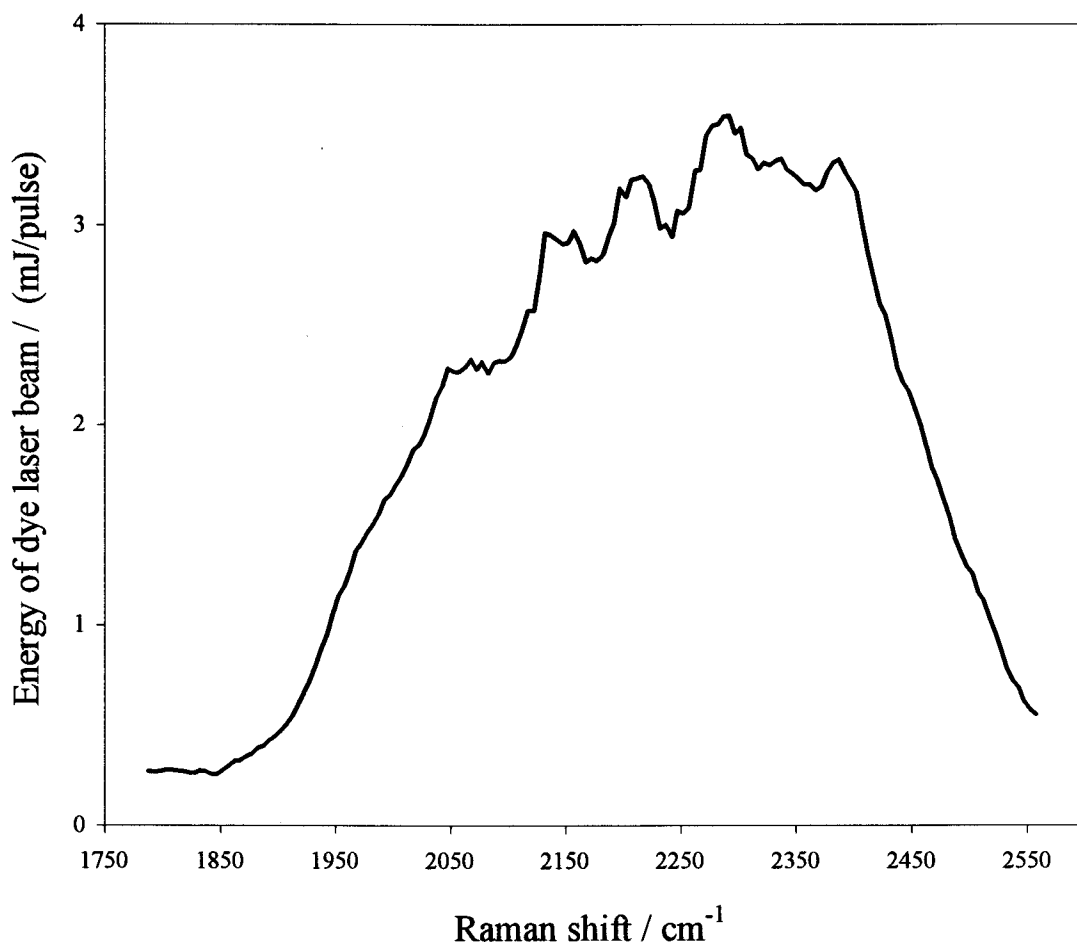


Figure 3-2. Gain curve of the Hyperdye-500 dye laser for the R610/SR640 dye mixture. The dyes were dissolved in the spectral grade methanol and had the following concentrations: R610 ($1.85 \cdot 10^{-4}$ M) and SR640 ($0.17 \cdot 10^{-4}$ M). The pump power from the Nd:YAG laser typically was about 60 mJ/pulse at 532 nm.

The Lumonics Hyperdye-500 is a tunable pulsed dye laser which consists of an oscillator and single amplifier stage, together with the necessary steering optics for the pump beam. Tuning between 320 and 730 nm is accomplished with the standard 2400 lines/mm grating in the oscillator cavity. The typical linewidth of the laser output is 0.05 cm^{-1} . The original dye laser beam produced in the oscillator is then amplified in the amplifier stage. Up to 10 mJ/pulse of output energy can be achieved in certain instances⁸¹. This value, however, greatly depends on the dye and the frequency of the laser. In our case the solution of two dyes in the spectral grade methanol was used: R610 ($1.85 \cdot 10^{-4} \text{ M}$) and SR640 ($0.17 \cdot 10^{-4} \text{ M}$). With the pump energy from Nd:YAG laser $\sim 60 \text{ mJ/pulse}$ at 532 nm the output energy of the dye laser was typically about 3-4 mJ/pulse at the maximum of the gain curve shown in Figure 3-2.

3.2.1.2. Geometrical beams configuration

There are two common geometrical beam arrangements for CARS experiments: collinear and folded "BOXCARS"^{82,83}. The collinear arrangement is the simplest one and requires only two beams (one pump beam and one Stokes beam), which follow the same path through the sample. The optical alignment is much easier than that for "BOXCARS". However, the price for the simplicity is that the probe volume is not well defined, and some CARS signal is generated in the side arms, i.e. far from the focal point. The signal beam follows the same path as the incident beams do, which makes the signal isolation more complicated, since filters and gratings are necessary to separate the weak blue anti-Stokes signal from the intense green pump and red Stokes beams. In addition, the level of

undesired non-resonant background signal (see discussion later in section 4.3.1 on p. 81) is higher for the collinear configuration. It can be produced anywhere in the overlap region of the incident beams, which is much larger in the collinear case.

The "BOXCARS" geometry requires three beams: two pump beams and one Stokes beam, which should propagate at certain angles relative to each other, so the phase-matching condition is met: i.e the phase mismatch $\Delta k=0$ (see section 2.1.4 , p. 16). Vectorially this condition is given by

$$\Delta \mathbf{k} = 2\mathbf{k}_p - \mathbf{k}_s - \mathbf{k}_{\text{CARS}} = 0. \quad (3.1)$$

Geometrical interpretation of this equation is shown in Figure 3-3. In the regular "BOXCARS" geometry displayed in Figure 3-3 (a), all the beams are in the same plane and their components along OZ axis comply with the following algebraic expression:

$$2k_p \cos \theta_p - k_s \cos \theta_s - k_{\text{CARS}} \cos \theta_{\text{CARS}} = 0 \quad (3.2)$$

or

$$\cos \theta_{\text{CARS}} = \frac{2k_p \cos \theta_p - k_s \cos \theta_s}{k_{\text{CARS}}} \quad (3.3)$$

As it was mentioned in section 2.1.4, absolute value of a wave vector \mathbf{k} is given by $k=(2\pi\omega)/n$, where ω and n are wavenumber and index of refraction, respectively. For a given gas, indices of refraction are approximately the same for all four beams involved in the CARS process therefore wave vectors \mathbf{k}_i ($i = p, s, \text{CARS}$) in equation (3.3) can be substituted by corresponding wavenumbers and the equation becomes:

$$\cos \theta_{\text{CARS}} \approx \frac{2\omega_p \cos \theta_p - \omega_s \cos \theta_s}{\omega_{\text{CARS}}}. \quad (3.4)$$

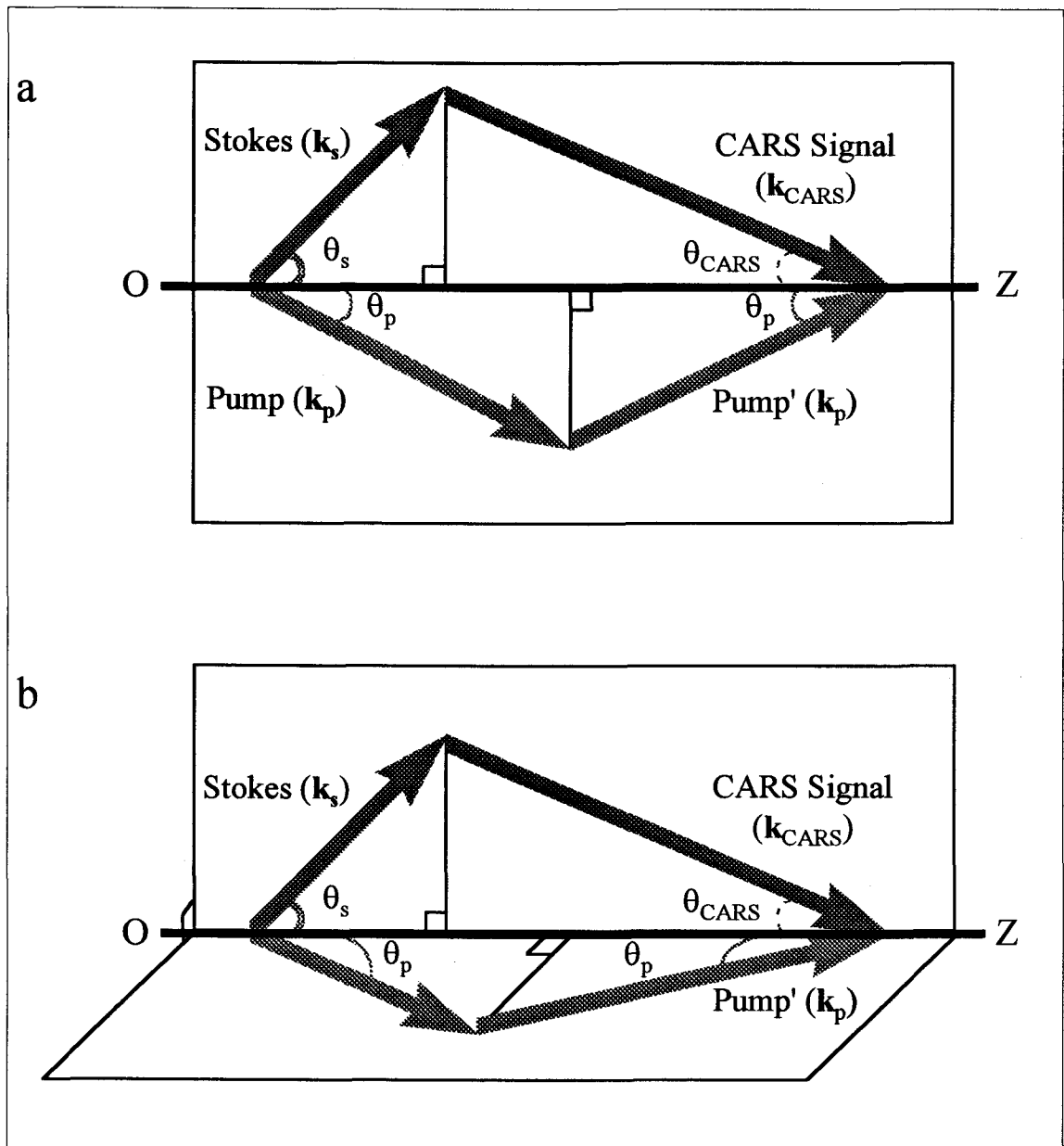


Figure 3-3. Geometrical interpretation of the phase-matching condition in "BOXCARS" (a) and folded BOXCARS (b) configurations. Vectors \mathbf{k}_i ($i = p, s, \text{CARS}$) are wave vectors of corresponding beams involved in the CARS process.

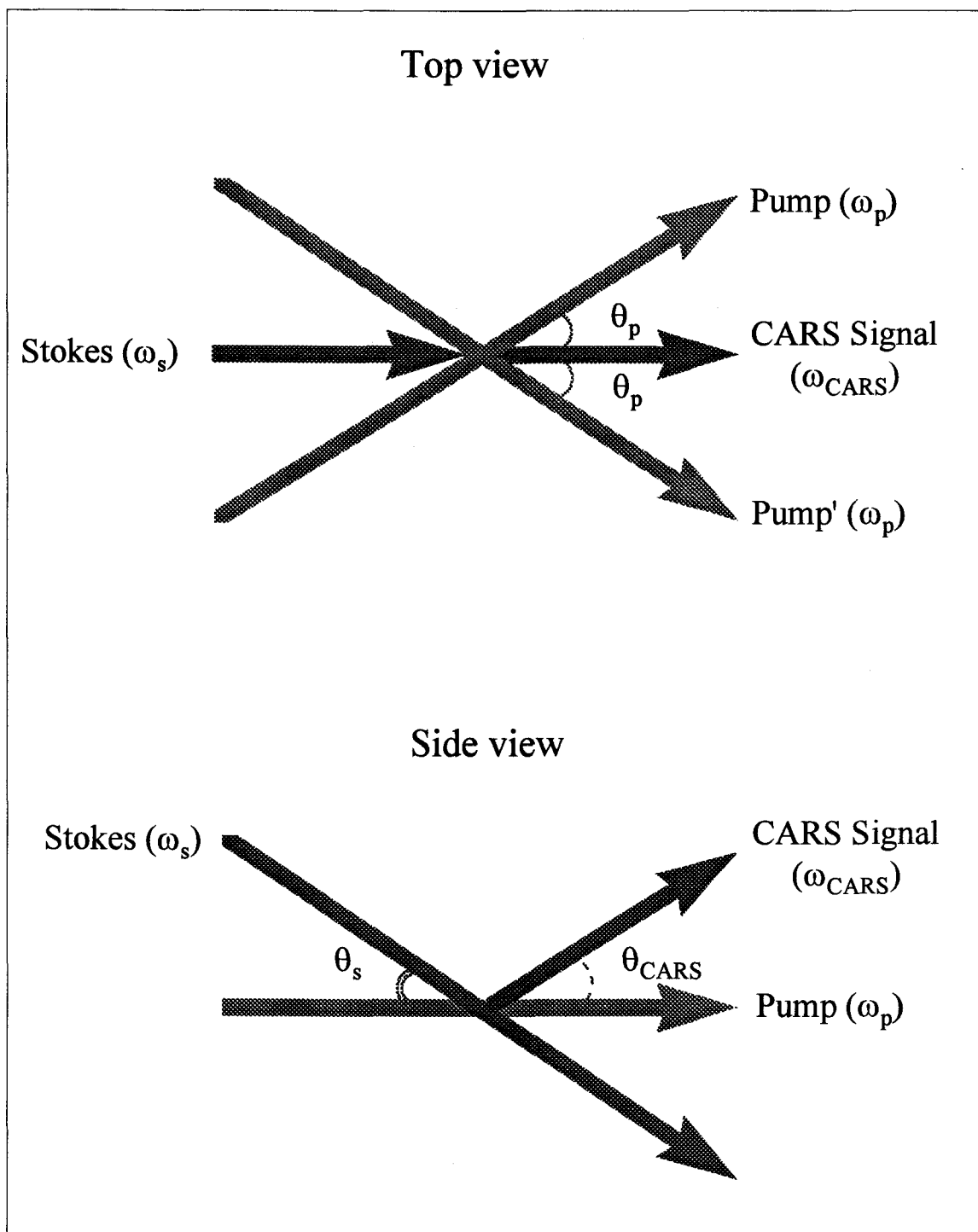


Figure 3-4. Spatial arrangement of beams in the folded "BOXCARS" configuration. See also the energy diagram in Figure 2-1 on p. 15.

Figure 3-3 (b) illustrates the folded "BOXCARS" configuration. Angles between wave vectors and OZ axis are preserved to maintain phase match, but two vectors \mathbf{k}_p lie in the plane perpendicular to that of Stokes and CARS wave vectors. Translation of three incident beams (two pump and one Stokes) in such a way that they are focused at one point gives the spatial arrangement of beams in the folded "BOXCARS" configuration as shown in Figure 3-4.

Although the folded "BOXCARS" configuration is more complicated and difficult to align, it has, on the other hand, the virtue of the point probing and lower level of non-resonant background. Besides, the CARS signal is spatially separated from the incident beams and can be easily isolated from them. For these reasons the folded "BOXCARS" arrangement was chosen for our measurements.

3.2.1.3. Signal detection and data acquisition control

The anti-Stokes beam generated in the folded "BOXCARS" configuration is directed through the aperture of a spatial filter to discriminate against the pump and Stokes beams. After that, to further reduce undesired radiation from the incident beams, it also passes two optical filters (colored Corning CS 5-57 and a 532 nm interference filter). The final isolation of the CARS signal beam is achieved by a monochromator (McPherson, model 218). Mounted on the exit slit of the monochromator, a photomultiplier (RCA 31034) operated at voltages up to 1750 V is used for the detection of the CARS signal. The PMT output is integrated with a signal averager (SRS, model SR 250) and then sent to a Scientific Solutions Lab Master I/O board (Figure 3-1).

Data acquisition and dye laser control is accomplished via computer interface based on the Lab Master board and software written by M. Orlov for Windows 3.1/Windows 95 in Visual Basic III (see Appendix B). Communication between computer and the dye laser is achieved through the computer's serial port and Control Unit of the laser in ASCII using the command language specific for the Hyperdye laser series⁸⁴. The Lab Master board is responsible for the digitizing of the analog signals in the range from 0 to +10 V generated during scans of the dye laser and the data are then stored in the computer. The digitizing is fulfilled by the board's 12-bit A/D converter and is initially triggered by the "busy" output signal of the SR 250 integrator. The integrator itself is triggered by the Q-switch synchronous output of the Nd:YAG laser. Software engages 4 out of 8 differential channels of the A/D converter. For signal acquisitions up to three channels can be simultaneously used and displayed, and one channel is reserved for the bad shot detector.

The latter is an electronic device which indicates the mode of operation of the Nd:YAG laser. The laser is tuned in such a way that the single mode doubled 532 nm output corresponds to one of the strong, sharp absorption lines of iodine. The device is supplied with a small reflection of 532 nm green light which is then split into two equal intensity beams inside the device; one of these passes through the iodine cell, the other serves as a reference. The beams are separately sensed by two photodiodes to measure their intensity difference. If the Nd:YAG laser operates in the single mode the intensity of one of the beams decreases due to absorption in the iodine cell leading to the large difference in the signals from the photodiodes. In this case the detector produces high output. In the multimode operation, some of the lasing modes do not match the iodine

absorption so that the iodine cell signal is high and the signal difference from the photodiodes is small, hence the detector has low output. During scans the software continuously monitors the output of the detector for each Nd:YAG laser pulse, omits "bad" (multimode) shots and displays a corresponding warning on the screen of the computer when it happens. The "bad" shot rejection significantly improves the signal to noise ratio.

The spectra acquisition is controlled by the software in the following way. The program takes initial and final wavenumbers along with the step size and the number of shots to average, n_s , as main scan parameters. At the beginning of each scan it positions the dye laser at the initial wavenumber, stores the current wavenumber and an average voltage value of the integrator's output from n_s shots (excluding "bad" ones), and then scans the dye laser one step size towards the final wavenumber. This procedure is repeated until the final wavenumber is reached.

The program also allows one to monitor spectra on the screen as they are scanned, to interrupt scanning, to save in ASCII format digitized spectra along with the relevant information (e.g. date, number of shots averaged, step size, dye used and any other information typed in by an operator in the two text boxes provided for these purposes). It also permits one to display previously saved spectra with the corresponding information text boxes and to print them out directly on a printer.

3.2.2. Discharge cell and electrode configuration

The principle electrical diagram of the discharge apparatus is shown in Figure 3-5. Besides the discharge cell, it involves a DC power supply (Hipotronics, model 820-50) capable of delivering currents up to 50 mA at 25 kV. An ammeter A of the power supply indicates the discharge current through the cell which is limited by an internal resistor R and controlled by variation of primary voltage V_0 . The value of the voltage drop across the electrodes of the cell is measured and displayed by an internal voltmeter V . The power supply has an automatic protection against the out-of-range current (> 50 mA).

The discharge cell used in the optimization study is shown in Figure 3-6. It is a cylindrical glass tube of 22 cm length with standard glass O-ring seals at the ends. Two optical windows (Edmund Scientific, BK-7, diameter 41 mm, thickness 2.3 mm) are sealed with viton O-rings and held in place with glass joint clips. The cell has an inlet connected to a commercial gas cylinder and an outlet attached to a rotary oil-sealed vacuum pump (VacTorr 25, Precision Scientific Company). Three tungsten wires (diameter 1.3 mm) are fed through the glass walls and serve as electrodes. During the operation both electrodes are cooled with a flow of compressed air. The incident laser beams injected in the cell through one of the windows are focused in the discharged gas sample at one point and along with the generated anti-Stokes beam leave the cell through another window.

The electrical glow discharge serves as an excitation source of higher vibration-rotational energy levels of a molecule, as illustrated by Figure 3-7. With the glow discharge, a rotationally resolved spectrum of the fifth hot band of nitrogen ($v=6\leftarrow 5$) was readily obtained. A similar scan with no discharge shows no evidence of such a spectrum.

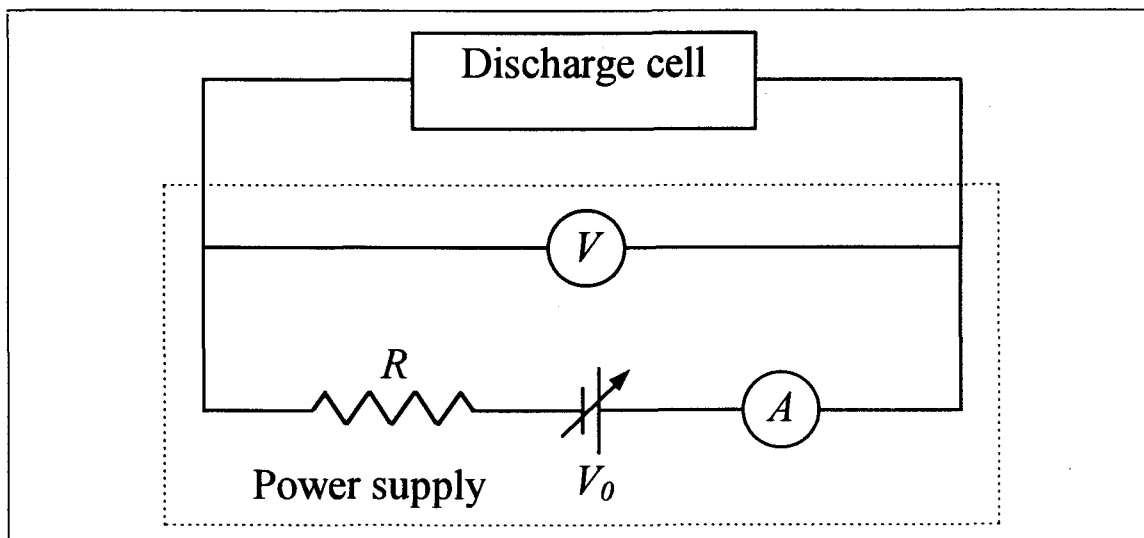


Figure 3-5. Electrical diagram of the discharge apparatus.

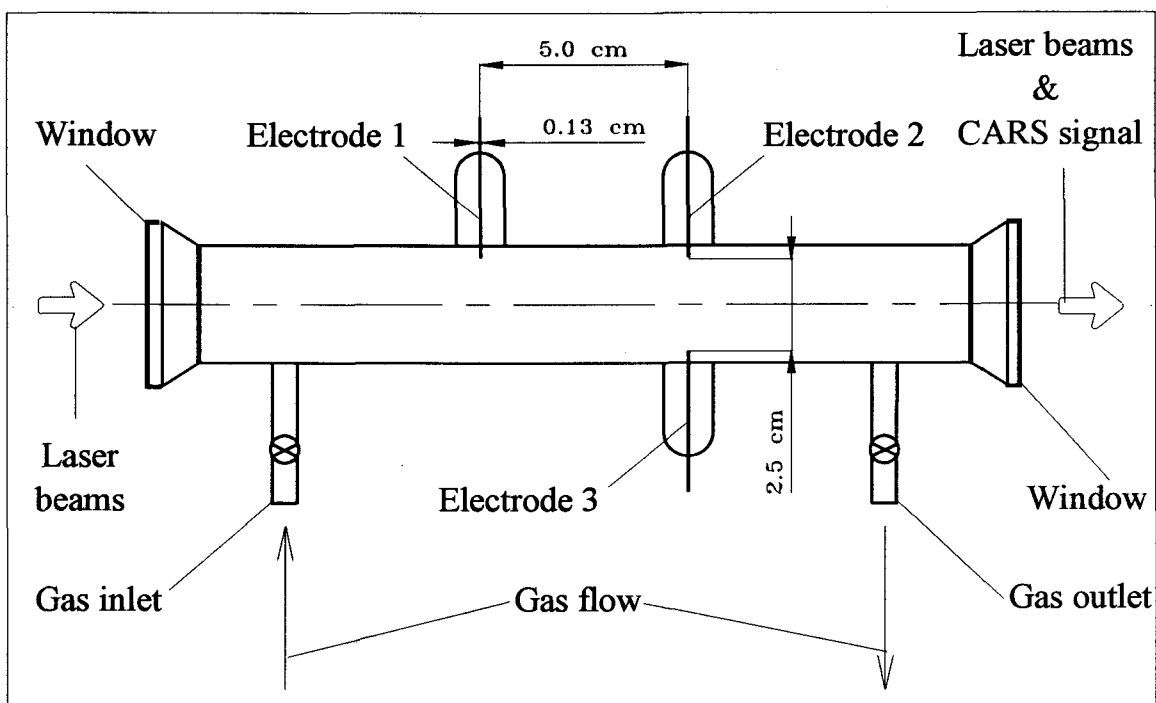


Figure 3-6. Schematic of the discharge cell for optimization experiments.

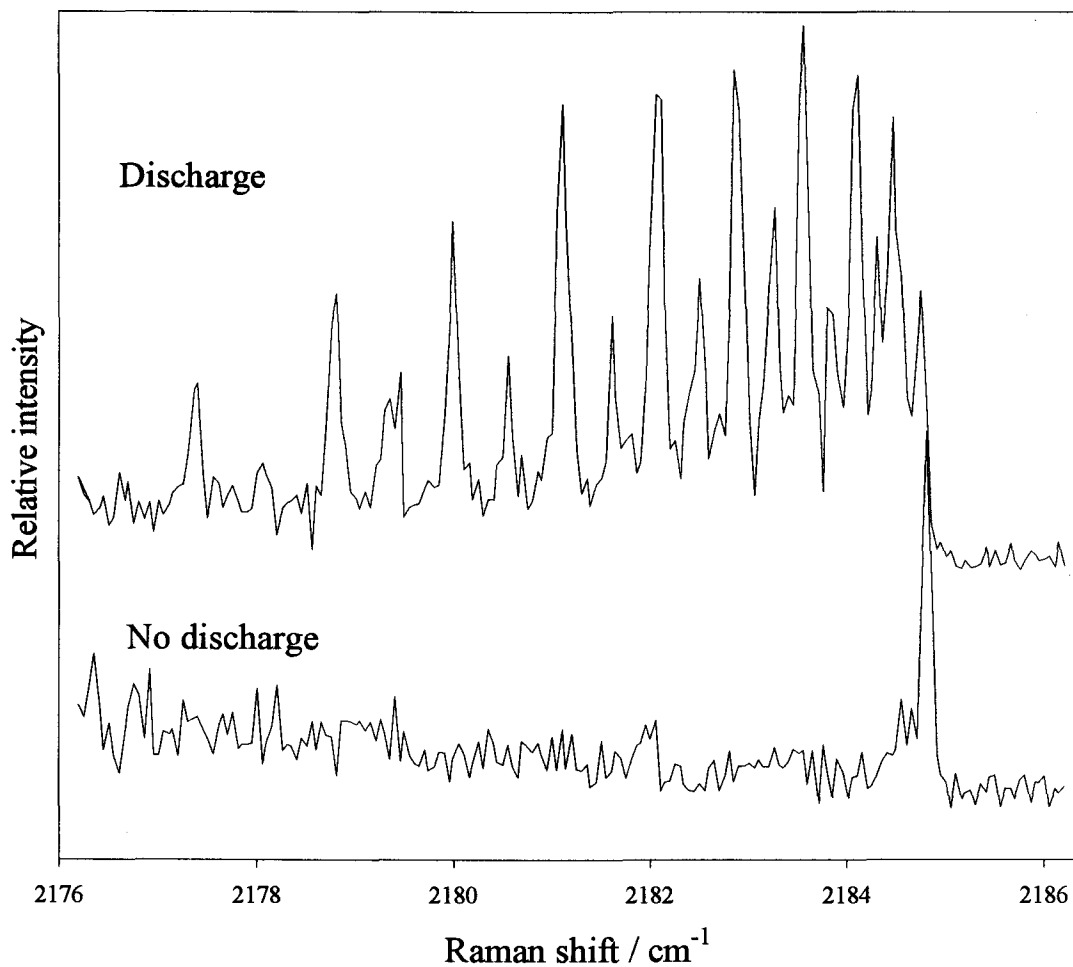


Figure 3-7. Vibration-rotational excitation of molecules by a glow discharge. The spectrum of the nitrogen hot band ($\nu=6\leftarrow 5$) with the glow discharge on is represented by the upper trace. In the absence of the discharge the spectrum is not detectable (lower trace).

Although only two electrodes were simultaneously engaged for maintenance of a glow discharge, the design allowed us to probe three different geometrical electrode configurations: transverse (electrodes 1 and 2), longitudinal (electrodes 2 and 3) and diagonal (electrodes 1 and 3). They vary from each other by the different orientation relative to the gas flow and by the distance between the electrodes. In fact several discharge cells with different sets of distances were tried. Each configuration was probed at various discharge zones as well as outside of the discharge and at different points in the cross-section of the cell. In the course of the study it was determined that the transverse configuration gave the maximum CARS signal for $^{14}\text{N}_2$ with the 2.5 cm gap between electrodes, and this arrangement was chosen for the subsequent experiments.

3.2.3. Gas pressure

As follows from equations (2.34) and (2.36) in section 2.1.4, the intensity of the CARS signal is proportional to the squared number of density of the gas sample. Hence, the pressure increase should significantly elevate signal level and improve signal to noise ratio. On the other hand, several negative effects take place with such an increase. For example, the pressure broadening of the spectral lines can cause overlap of closely spaced spectral lines and wavenumber line shifts, resulting in a reduction in the accuracy of transition frequency measurements. In addition, the glow discharge becomes less stable as the gas pressure grows, and eventually it becomes impossible to maintain it without a significant rise in the discharge voltage and current. A reasonable pressure range for our apparatus was between ~15 and 110 Torr of nitrogen. For the strong transitions (e.g. Q

branches) the lower pressure of ~30 Torr was used; for the weaker transitions (e.g. O and S branches), a pressure of 100 Torr was employed.

3.2.4. Discharge current

For the transverse electrode configuration (2.5 cm gap) and the gas pressure limits discussed in the previous sections, the apparatus shown in Figure 3-5 can maintain the glow discharge in nitrogen within the ~5 - 50 mA current range. The excitation efficiency of different vibrational levels was found to be sensitive to the value of the discharge current as it is illustrated by Figure 3-8. It is evident that for a given hot band transition there is a pronounced maximum in the CARS signal as the discharge current changes. The position of this maximum determines the optimal current value I_{opt} .

It was discovered that the latter depends significantly on the vibrational level to be excited. Figure 3-9 shows the optimal discharge current values I_{opt} as function of the lower vibrational quantum number v'' for different hot band transitions of nitrogen. It appears that the larger current values are required to excite higher molecular vibrational levels. For the regular $^{14}\text{N}_2$ isotopic form we were able to probe vibrational energy levels up to $v''=7$. The maximum current of the power supply (50 mA) established the upper limit for energy level possible to excite. Qualitatively, the described influence of the discharge current on the excitation process was insensitive to the probing point position and the flow rate of nitrogen through the cell.

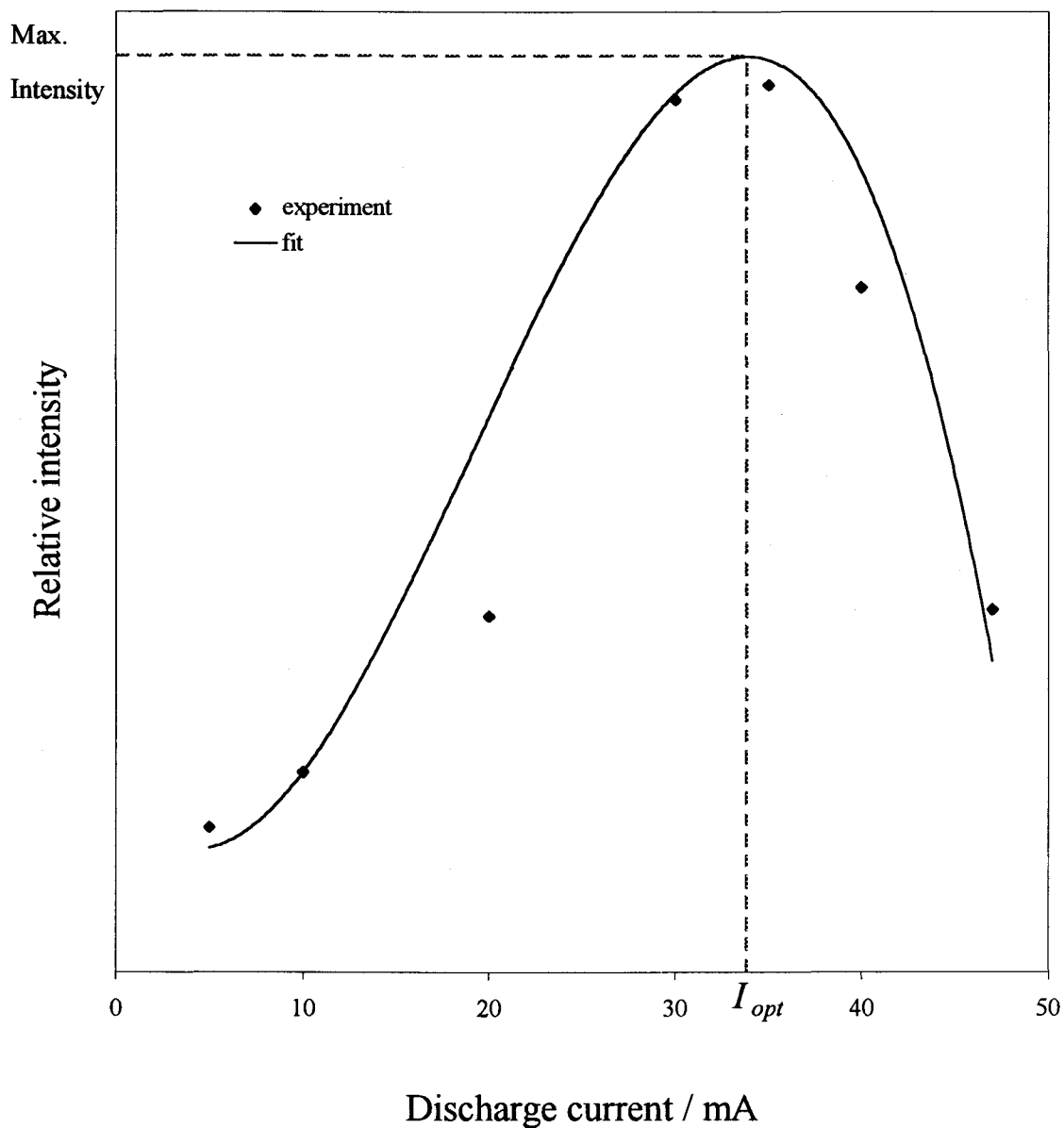


Figure 3-8. Influence of the discharge current on vibrational excitation. CARS signal for the sixth hot band ($v=7\leftarrow 6$) of nitrogen is plotted as a function of the current. The position of the maximum intensity determines the optimal current value I_{opt} .

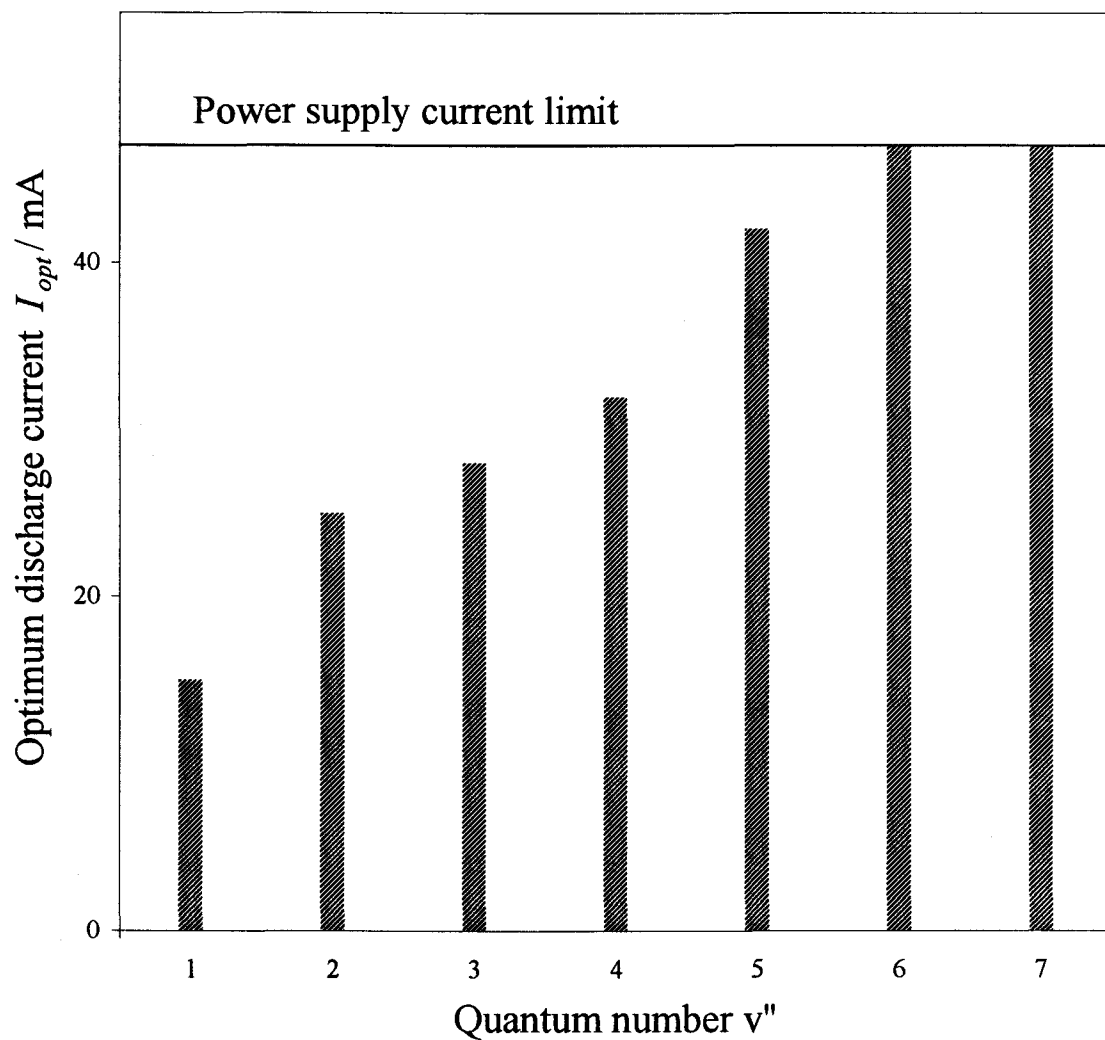


Figure 3-9. Optimal discharge current I_{opt} as a function of quantum number v'' . To excite higher vibrational levels of nitrogen larger values of the discharge current are required. The maximum current of the power supply imposes the upper limit for excitation. The transition $v=8\leftarrow 7$ was the highest it was possible to observe.

3.2.5. Position of the probing point

The position of the probing point relative to the discharge area was another optimization parameter. For each electrode configuration discussed in section 3.2.2 (p. 52) various relative positions were tried (i.e. different discharge zones and areas outside the discharge region, different points in the cross-section of the gas flow). Coupling with other system parameters (e.g. discharge current, flow rate, transition, pressure) was studied as well. Since in all instances the transverse electrode configuration consistently produced the highest CARS signal level, it was subjected to more detailed measurements.

The result of such measurements appears in Figure 3-10. It shows the level of the CARS signal for a particular hot band transition of nitrogen ($v=6\leftarrow 5$) as function of the probing point distance from the axis of the electrodes. Due to the gas flow through the cell the discharge area is significantly distorted. The shape of the discharge zone scaled to the x-axis is shown above the plot. It is evident that the maximum signal is achieved at the downstream border of the discharge. This optimal relative location of the probing point in horizontal direction remained the same for different transitions, currents and flow rates. On the other hand, the signal was not very sensitive to the vertical position, although it exhibited a broad maximum at the center of the tube's cross-section for various locations along the x-axis. Such a behavior probably results from the fact that the major part of the cross-section between electrodes is occupied by the positive column of the discharge (see section 2.3.3 on p. 34), hence conditions in the inter-electrode space are more or less uniform.

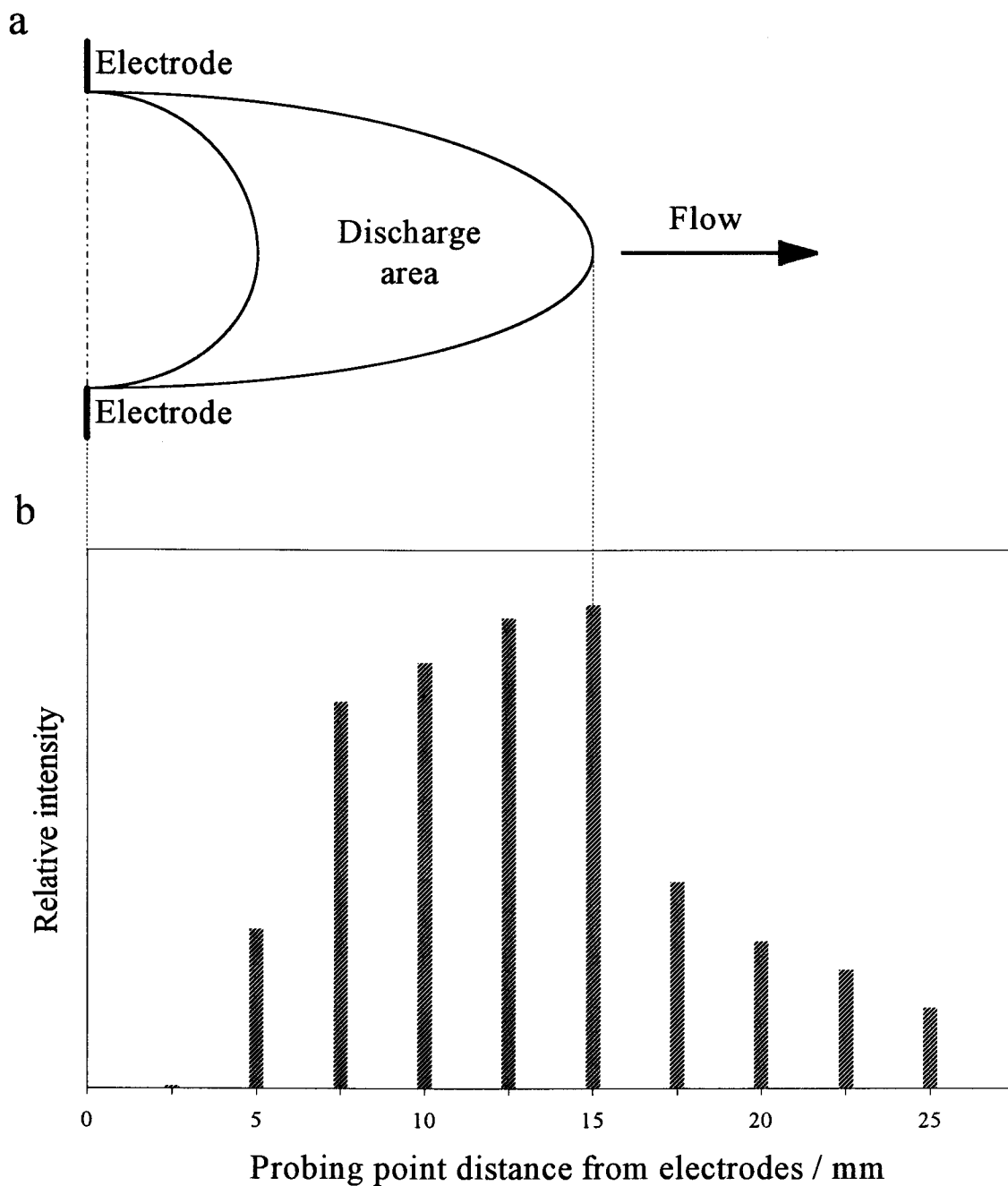


Figure 3-10. Influence of the probing point position on the CARS signal. (a) The discharge area is distorted due to the gas flow. (b) The relative signal level for the hot band transition ($v=6\leftarrow 5$) of nitrogen is a function of distance between the electrodes axis and the probing point. The maximum signal level is obtained at the downstream border of the discharge.

3.2.6. Flow rate of the gas

The gas flow rate turned out to be a very important parameter affecting the level of the signal as it shown in Figure 3-11. The CARS signal for the fifth hot band transition of nitrogen ($v=6\leftarrow 5$) is plotted as a function of the gas flow rate. Measurements were performed in the transverse electrode configuration. Other discharge parameters, discussed in the previous sections of this chapter, were kept at their optimal state for the transition.

It is obvious from the plot that the gas flow can significantly enhance the CARS signal. A minimum flow rate of about 0.4 -0.6 L/min is required to increase the signal level by a factor of ~ 150 with respect to that for the static cell. At least two reasons can be suggested to explain such a behavior. The flow leads to a decrease in the gas temperature, since new and cool portions of the gas are being continuously delivered to the discharge area. Consequently, fewer rotational levels of a given vibrational state are populated. For this reason the gas molecules are now spread among fewer states so that each has a higher population resulting in a signal increase. The flow also establishes the "preferred" direction in which charged particles are extracted by the gas stream from the discharge area for subsequent recombination to form neutral excited species. Thus, the maximum concentration of the vibration-rotationally excited nitrogen molecules is to be expected at the downstream edge of the discharge region. At this point ionized molecules become neutral, but yet do not have enough time to relax down to the vibrational ground state. This agrees perfectly with the optimal relative position of the probing point discussed in section 3.2.5.

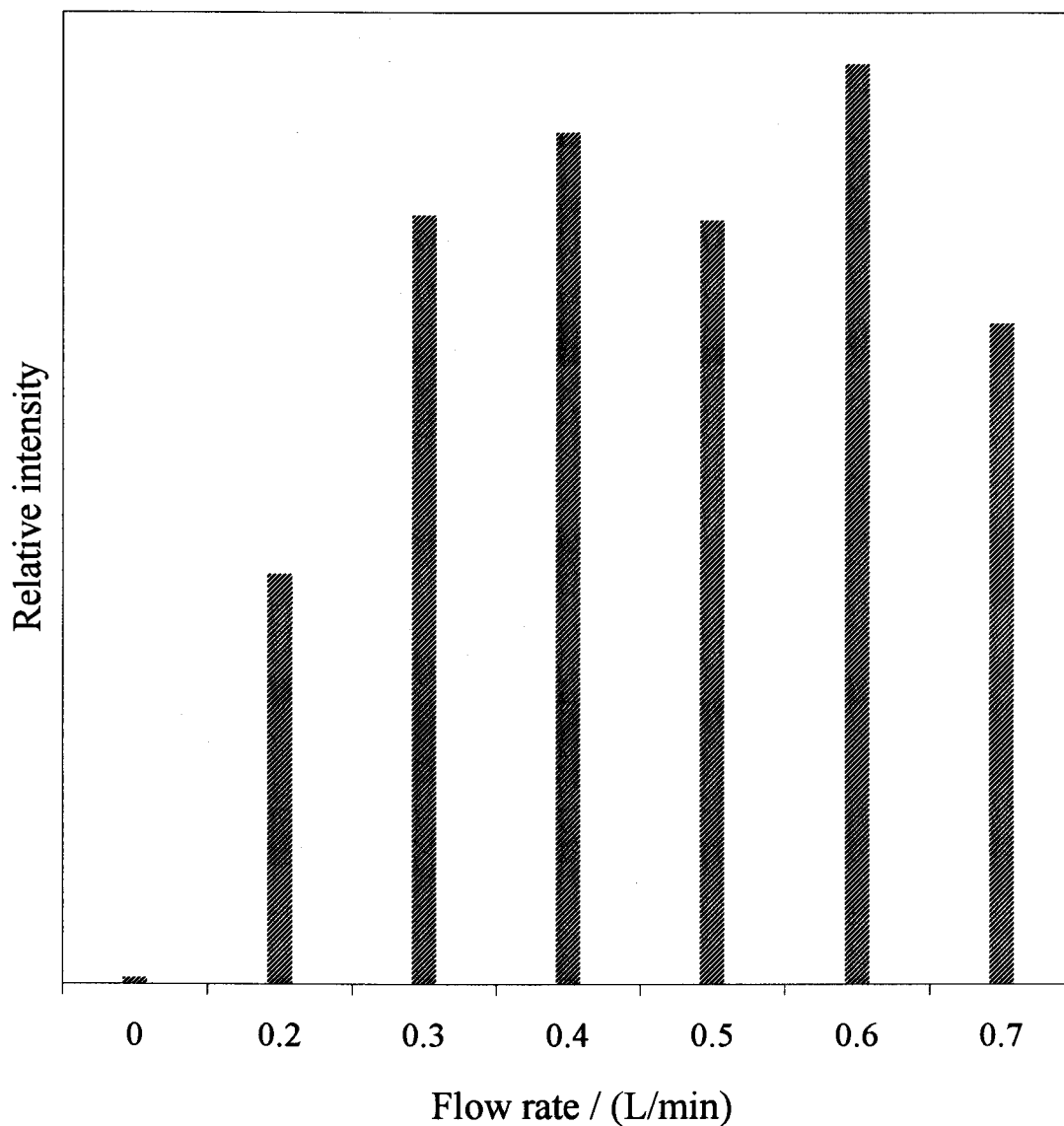


Figure 3-11. Influence of the gas flow on the CARS signal. The relative signal level for the hot band transition ($v=6\leftarrow 5$) of nitrogen is given as a function of the gas flow rate. Other discharge parameters were kept at the optimum for the transition. The rate of 0.4 - 0.6 L/min enhances the signal by a factor of about 150 with respect to that for the static cell.

3.3. Cycling system

The necessity for a gas flow through the cell imposes a significant experimental problem for the CARS measurements of precious isotopes such as $^{15}\text{N}_2$. Unlike regular nitrogen $^{14}\text{N}_2$, which was simply exhausted into the atmosphere in the course of measurements, $^{15}\text{N}_2$ had to be recycled due to its high cost. A search found no commercial cycling pumps able to deliver necessary flow rates at the very low working gas pressures required in our experiments (see section 3.2.3 on p. 55).

To solve this circulation problem a novel cycling system for optical measurements in a glow discharge was designed and built in our laboratory. The schematic diagram of the system is shown in Figure 3-12. The glass discharge cell was similar to one previously described in section 3.2.2 (p.52) but with only two electrodes in the transverse configuration. The new feature was a fan housing supported by a brass chamber. The chamber fits onto a pair of glass branches of the cell and is sealed with O-rings. In operation, the system is evacuated via the gas outlet to about 20 mTorr and tested to ensure no leak. The gas is then admitted through the inlet to the working pressure with the outlet closed. A simple electrical microfan (Elina HDF4020L-12MB, dc, 4x4x1 cm, similar to those used in computers for CPU cooling) serves as a pump for the gas recirculation.

Special care was taken to minimize any gas leakage from the atmosphere. Electrical feedthroughs for the fan were mechanically sealed with the combination of a drilled through Teflon rod and a Swagelok. To eliminate some small gas leakage through the glass/metal joints of the electrodes, they were coated with high temperature

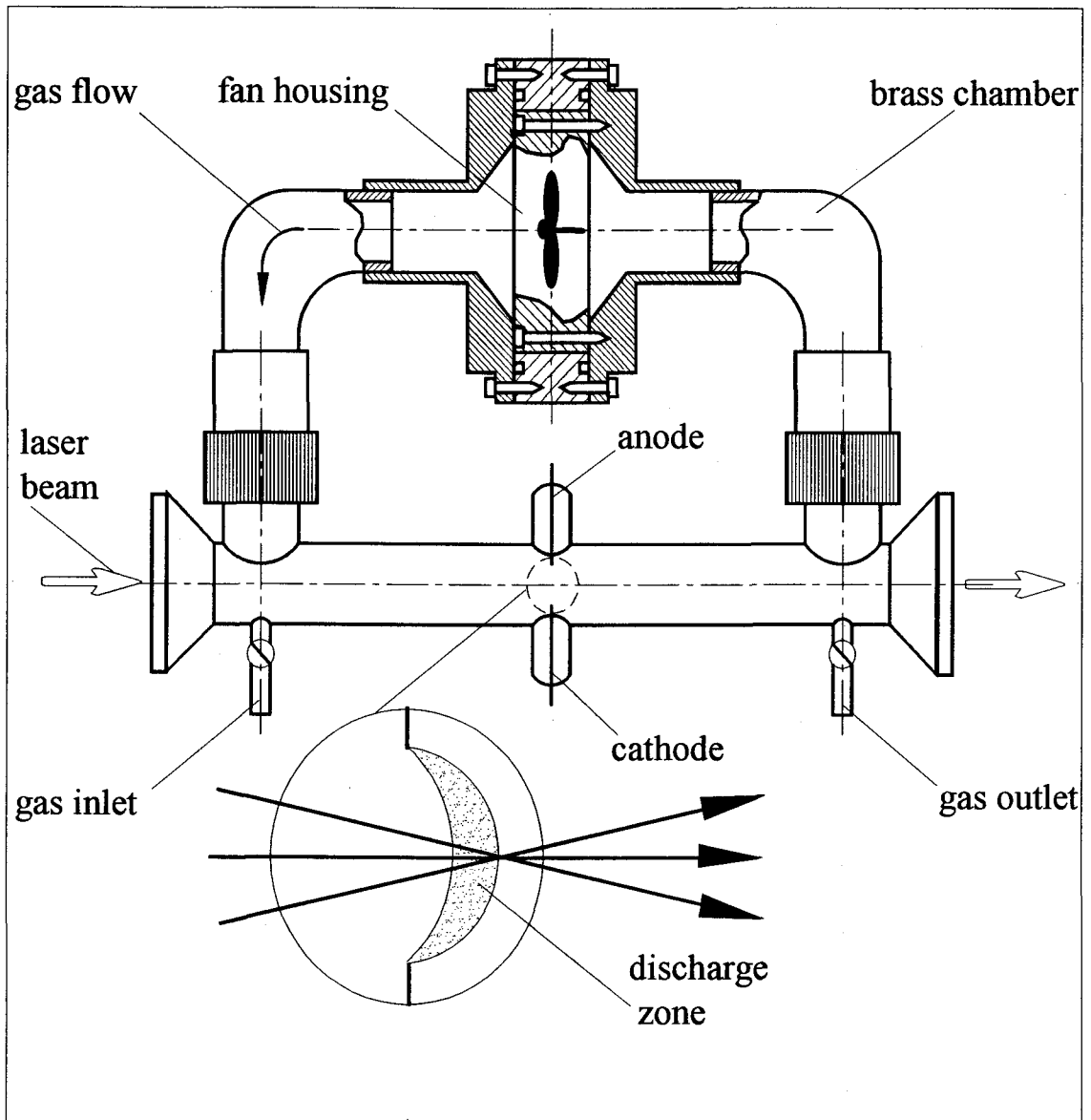


Figure 3-12. The cycling system for optical measurements in a glow discharge.

vacuum glue (High Vacuum Sealant, Physics R/D, Inc.) able to withstand temperatures up to 300 °C. These joints were also cooled by a stream of air so that their temperature never exceeded 100-110 °C.

The vacuum leakage of the system is shown in Figure 3-13. After three hours of full operation of the fan the gas pressure in the cell increased from about 10 to 300 mTorr. This is about 1% degradation of the vacuum with respect to 30 Torr - the lowest pressure used in our experiments. The actual duration of scans never exceeded 60-70 min. so leakage was not a problem in of our measurements.

The measured spectra proved to be insensitive to the mode of gas flow operation. There was virtually no difference between two spectra of the same transition of nitrogen taken in the regular and cycling flow regimes (Figure 3-14): the same signal level and signal to noise ratio was observed in both cases.

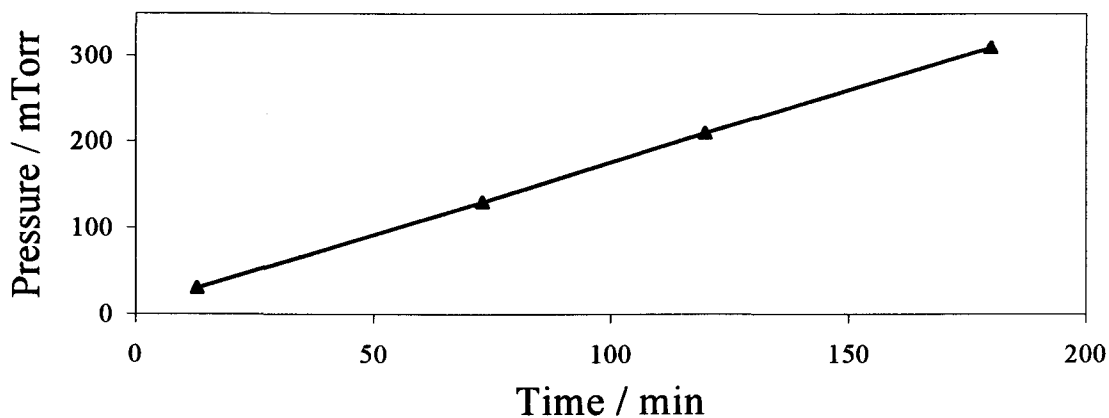


Figure 3-13. Vacuum characteristic of the cycling system.

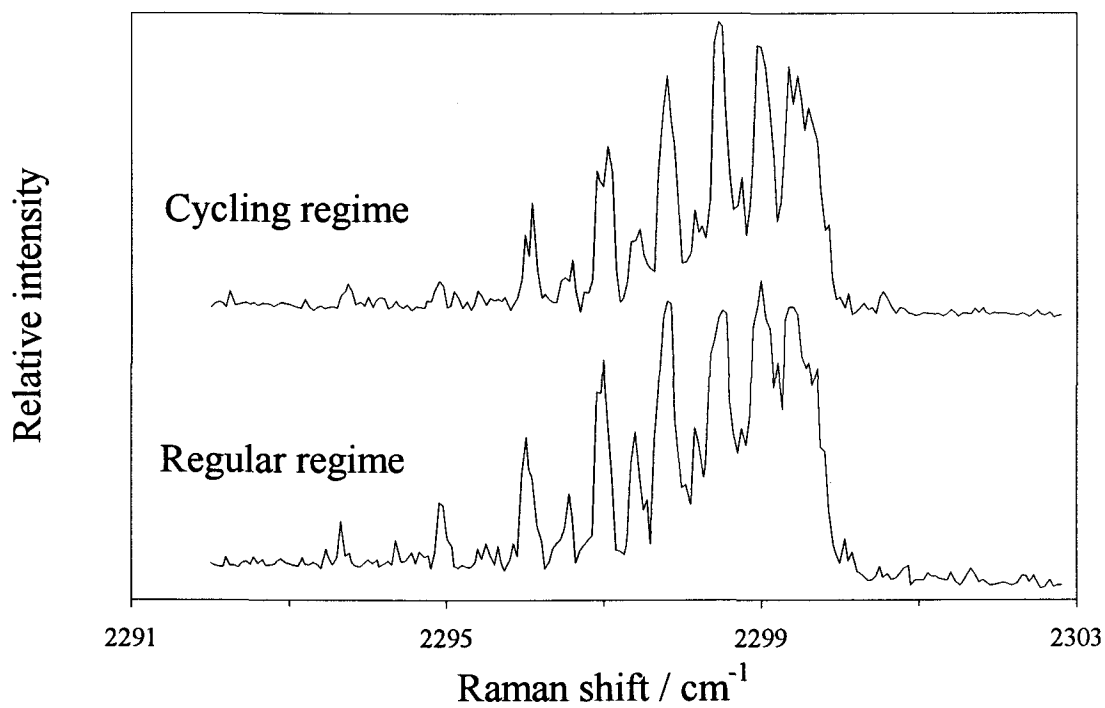


Figure 3-14. Comparison of cycling and regular flow regimes. Spectrum of the nitrogen hot band transition ($\nu=2\leftarrow 1$) exhibits comparable CARS signal level and signal to noise ratio for both regimes of operation.

4. HIGH-RESOLUTION COHERENT RAMAN SPECTRA OF VIBRATIONALLY EXCITED $^{14}\text{N}_2$ AND $^{15}\text{N}_2^*$

4.1. Introduction

Although contemporary infrared spectra of polar diatomic molecular species can yield abundant measurements of wavenumbers of vibration-rotational transitions with precision typically about 0.001 cm^{-1} , or even much better ($\sim 10^{-6}\text{ cm}^{-1}$) in exceptional cases, the corresponding transition energies of non-polar molecules are less well established. To characterize well a diatomic molecule in its ground electronic state, information about spectral parameters of many vibrationally excited states is required, but this is generally difficult to acquire. In a few cases of polar diatomic molecules that have several isotopic variants, one can deduce precise functions of potential energy and assess the importance of electronic adiabatic and non-adiabatic effects⁵⁷. An approach to acquire analogous data for non-polar species requires coherent Raman spectra of molecules excited in electric discharges, as has been already discussed in Chapter 1. We present here such results for $^{14}\text{N}_2$ and $^{15}\text{N}_2$.

Previous spectral observations on $^{14}\text{N}_2$ in its electronic ground state $X\ ^1\Sigma_g^+$ include both infrared and Raman transitions⁸⁵⁻⁹², with other information from rovibronic transitions⁹³. For infrared spectra, both a long cell in a laboratory⁸⁵ and the terrestrial atmosphere with the sun as source⁸⁶ enabled measurements of quadrupolar absorption of lines in the O and S branches of the fundamental band at resolutions $0.002 - 0.01\text{ cm}^{-1}$.

* The research presented in this chapter is published in the Journal of Molecular Spectroscopy⁸⁰. The publication, with some additions and modifications, constitutes the body of the chapter.

Spontaneous Raman spectra were reported for the purely rotational region at resolution 0.1 cm^{-1} by Butcher *et al.*⁸⁷ and at resolution 0.15 cm^{-1} by Bendtsen⁸⁸, who also measured lines in O, Q and S branches of the fundamental vibrational band. Gilson *et al.*⁸⁹ measured coherent anti-Stokes Raman scattering (CARS) spectra at resolution 0.15 cm^{-1} of Q branches in the bands $1 \leftarrow 0$ and $2 \leftarrow 1$ of $^{14}\text{N}_2$ in a vessel at 1200 K; these measurements were not calibrated absolutely but were normalized to Bendtsen's data⁸⁸. Measurements on heated $^{14}\text{N}_2$ were made also by Lavorel and coworkers^{90,91} in the form of stimulated Raman spectra but at resolution and absolute uncertainty of wavenumbers about 0.002 cm^{-1} . CARS spectra with resolution about 0.02 cm^{-1} of $^{14}\text{N}_2$ in an electric discharge⁹² enabled observations of vibrational states up to $v=14$, and values of $\Delta G(v)$ and ΔB_v between adjacent vibrational states up to $v=11$ were deduced from these experiments; however, wavenumbers of specific lines were not reported, and later measurements⁹¹ from the same laboratory indicated significant deviations from these results⁹².

Electronic spectra can yield information about the electronic ground state; both Edwards *et al.*⁹³ and Trickl *et al.*⁹⁴ deduced parameters Y_{kl} from selected data from infrared, Raman, and rovibronic spectra in global fits. Both groups rejected some Raman data; Trickl *et al.* alluded to significant inconsistencies between wavenumbers reported from diverse sources for the same transitions. The latter workers excluded measurements of spontaneous Raman scattering by Butcher *et al.*⁸⁷ and modified the CARS data of Gilson *et al.*⁸⁹ with a correction linear in wavenumber. In the same work⁹⁴ an analysis of literature data for vibrational levels $v \geq 4$ indicated the need for coefficients $Y_{k,0}$ in two sets, valid for small and large values of v . One set, consisting of three parameters, reproduces

within 0.05 cm^{-1} the energies of states for $v=0-5$, whereas the other set, consisting of six coefficients, produces errors $<0.42 \text{ cm}^{-1}$ for $v=5-27$.

Available spectral data of $^{15}\text{N}_2$ consist of purely rotational and vibration-rotational Raman transitions measured by Bendtsen⁸⁸ and CARS measurements of Q branches in the bands $1 \leftarrow 0$ and $2 \leftarrow 1$ by Gilson *et al.*⁸⁹; in both cases the resolution is 0.15 cm^{-1} and the calibration is suspect. Hence our present knowledge of eigenenergies of N_2 in its electronic ground state and for any isotopic variant appears capable of improvement.

The objective of the work presented in this chapter was therefore to measure, with much improved accuracy, vibration-rotational transitions of both $^{14}\text{N}_2$ and $^{15}\text{N}_2$ to establish directly the spectral terms in the electronic ground state for $v < 8$. For this purpose coherent anti-Stokes Raman spectra of electrically discharged samples of both nitrogen isotopes were acquired at resolution 0.001 cm^{-1} . We combined our new data with complementary data selected from the literature, all suitably weighted, in order to achieve fits of wavenumbers of transitions of $^{14}\text{N}_2$ and $^{15}\text{N}_2$ to vibrational states up to $v'=8$ and $v'=7$ respectively. Our apparatus included a novel system (see section 3.3 on p. 63) to recirculate a gaseous sample to make economical use of isotopic substances. These measurements and their analysis constitute this chapter.

4.2. Experimental procedure

4.2.1. Apparatus

Although the principal idea of the apparatus used for main spectral measurements of nitrogen is similar to that used for preliminary studies (section 3.2.1), there are some important distinctions (e.g. different dye-laser, longer pulse width, different system for amplification of the Stokes beam, higher resolution, etc.). A short description of the apparatus indicating these distinctions as well as similarities follows.

To populate N_2 in excited vibrational states we subjected flowing gaseous nitrogen to an electric discharge using the cycling system (Figure 3-12), which was described in the previous chapter (section 3.3 on p.63). A power supply (Hipotronics, 25 kV and 50 mA maximum) provided a current 7 - 50 mA, depending on the vibrational state (see section 3.2.4 on p. 56), at a potential difference 900 - 1000 V between tungsten electrodes 25 mm apart. The electrical set-up was identical to that used in the optimization study (see Figure 3-5). The electrodes were cooled with an air stream and the temperature of the vessel's wall was less than 400 K. A minimum rate 0.4 - 0.6 L/min of internal nitrogen flow was required for optimal CARS signal (see section 3.2.6 on p. 61). For measurements on $^{14}N_2$, gas from a commercial cylinder (99.98%) was pumped through the cell at a pressure 30 Torr and exhausted to the atmosphere. Because $^{15}N_2$ (Matheson, 99.9% isotopic purity) is expensive, we recirculated this gas in the way previously discussed in section 3.3 (p. 63). The working pressure of $^{15}N_2$ was 30 Torr for Q branches and 100 Torr for O and S branches. The voltage to the fan of the discharge cell was adjusted to achieve rates of

circulation comparable to those in experiments on $^{14}\text{N}_2$, as judged from the deflection of the discharge zone and the intensity of the CARS signal.

A schematic diagram of the high-resolution CARS apparatus used in the main measurements appears in Figure 4-1. The pulses (532 nm, 50 ns) from a seeded Nd-YAG laser (Continuum, custom laser, 20 Hz) were divided into five parts. Two served as pump beams (each ~ 15 mJ per pulse) to measure the CARS signal in a three-dimensional phase-matching arrangement (folded 'BOXCARS' discussed in section 3.2.1.2 on p. 45). The other three parts were employed to excite three dye cells that amplified the continuous output of a tunable ring dye laser (Coherent, CR-699-29) pumped with an Ar^+ laser (Coherent, Innova 90, 5 W). Dye R6G ($2.55 \cdot 10^{-3}$ M in ethanol) was employed in the dye laser. A dye mixture of R610 and R640 dissolved in methanol was used in the amplifier: $1.6 \cdot 10^{-4}/1.0 \cdot 10^{-4}$ M for first two stages and $1.6 \cdot 10^{-5}/1.0 \cdot 10^{-5}$ M for the third one. For purpose of calibration, a small portion of the (Stokes) output from the dye laser was used to measure absorption of I_2 vapor. The main output from the dye laser after amplification had an energy ~ 1 mJ per pulse. This apparatus to measure coherent Raman spectra has an effective resolution about 0.001 cm^{-1} ⁹⁵. The Stokes beam and two pump beams (532 nm) were focused with a lens (focal length 300 mm) at the downstream edge of the positive column of the glow discharge (see Figure 3-12 and discussion in section 3.2.5 on p. 59). The beam overlap was then adjusted for maximum CARS signal. The CARS beam so generated passed optical filters (Corning CS 5-57 and interference with band pass at 532 nm) and a monochromator (McKee-Pedersen, MP-10118) to a photomultiplier (Hamamatsu R955). The output from this detector was integrated with a signal averager

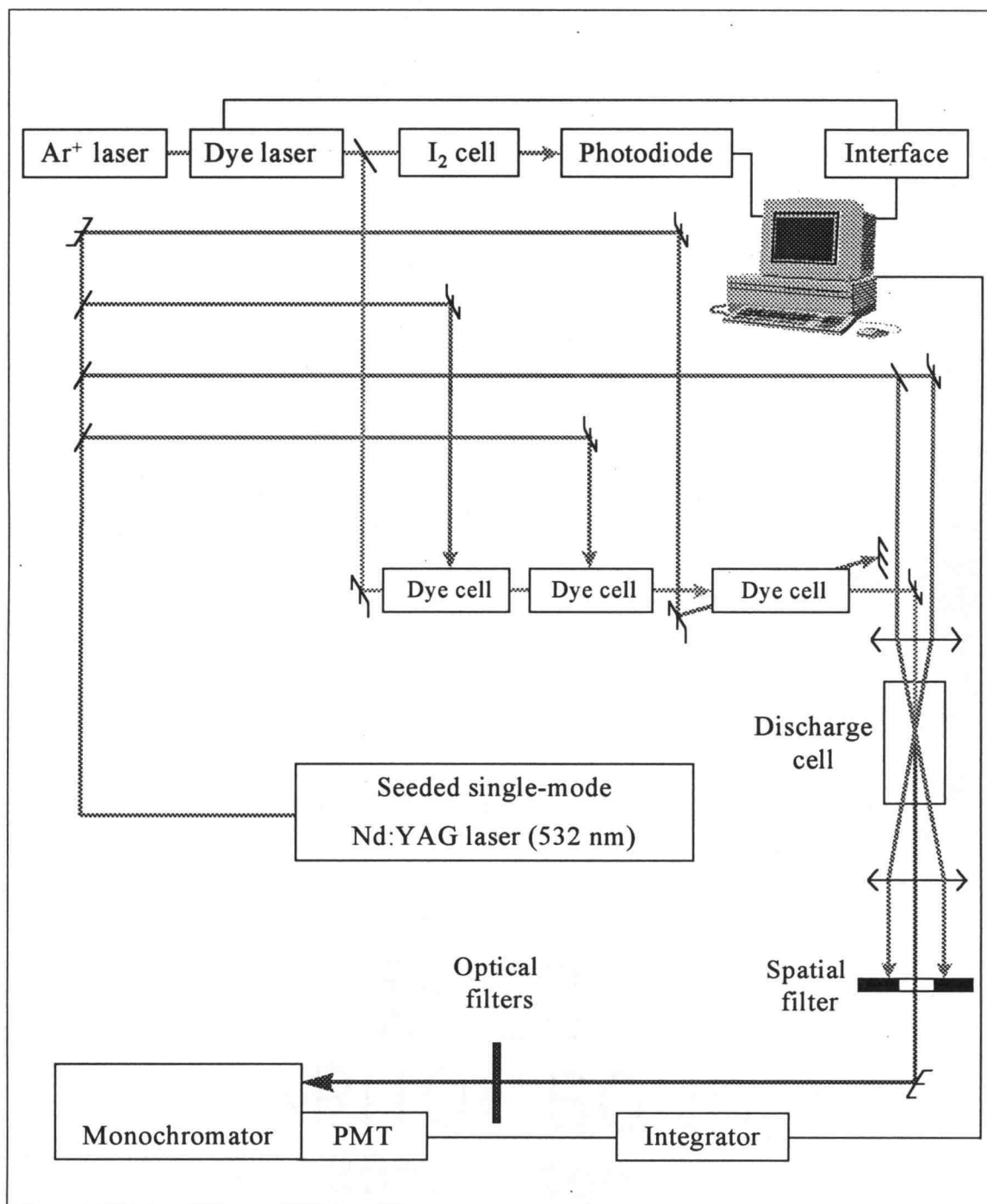


Figure 4-1. Schematic diagram of the high-resolution apparatus used in main spectral measurements of nitrogen isotopes.

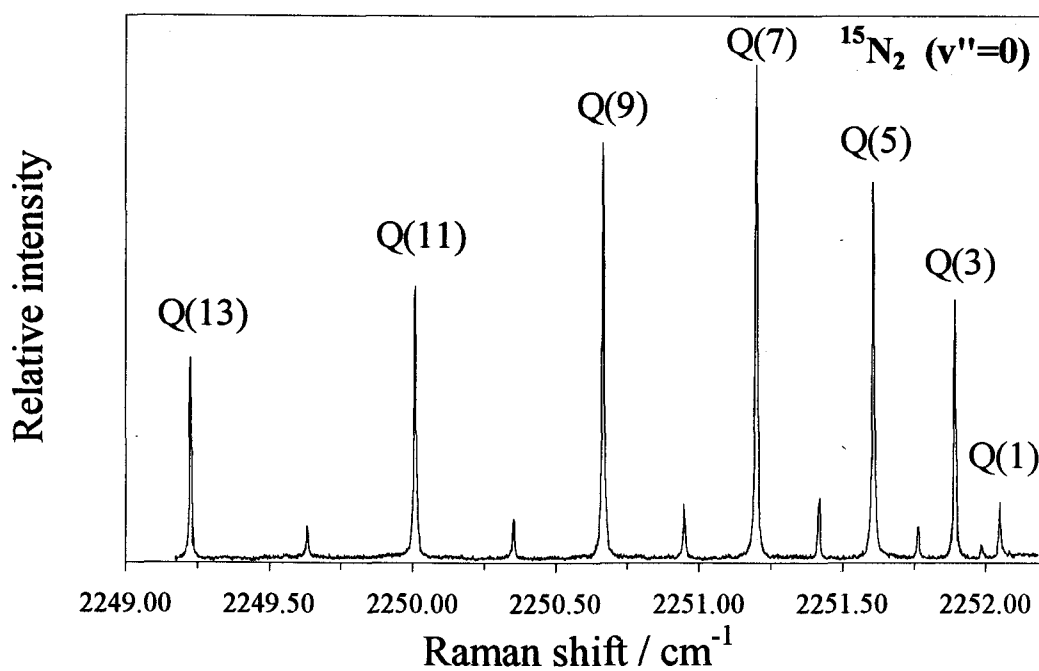
(Stanford Research, SR250), the analog output of which was digitized with a microcomputer, which served also to scan the ring dye laser in steps of 0.001 cm^{-1} .

4.2.2. Measurements

Representative CARS spectra obtained with the above apparatus are shown in Figure 4-2 a and b, which display for $^{15}\text{N}_2$ portions of Q branches in the bands $1\leftarrow 0$ and $7\leftarrow 6$, respectively. The former figure illustrates the ratio of signal to noise for an undischarged sample and the latter figure shows that this ratio degrades, progressively, as the discharge current is increased to populate the higher vibrational levels. The line widths (FWHM) typically were between 0.01 and 0.02 cm^{-1} . For the sample of Figure 4-2 b, the intensities indicate an approximate Boltzmann distribution among rotational levels corresponding to a rotational temperature of about 700 K . In recording these spectra, 10 - 20 shots were averaged at each scan position and a zero level was determined before each scan on by blocking the Stokes beam and averaging a few hundred laser pulses under operating conditions.

Considerable care was taken to ensure that reproducible and accurate wavenumbers of transitions were recorded. To stabilize the frequency of the Nd-YAG and Stokes lasers, we operated the entire system for two hours before measurements began. A typical drift characteristic of the apparatus is shown in Figure 4-3. After stabilization, a reference line $Q_1(10)$ of the fundamental band of $^{14}\text{N}_2$, measured several times over 80 min , is plotted versus time. The standard and the maximum deviations were 0.0004 and 0.0012 cm^{-1} , respectively. In every day operation the reference line $Q_1(10)$

a



b

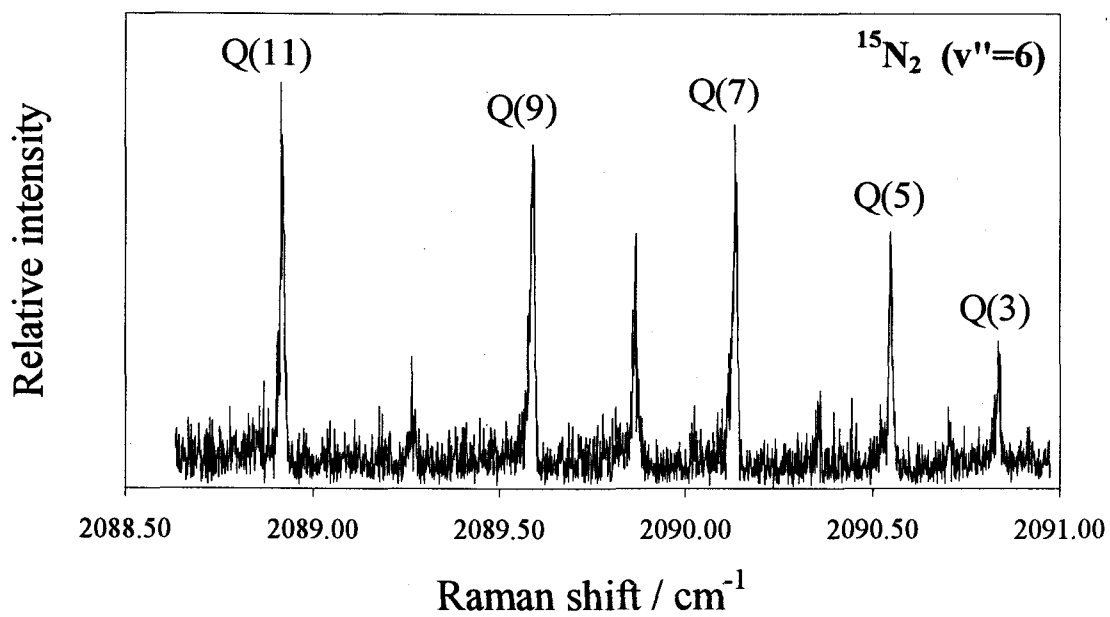


Figure 4-2. Representative CARS spectra of nitrogen. Portion of the Q branch of (a) fundamental band ($v=1\leftarrow 0$) and (b) the hot band ($v=7\leftarrow 6$).

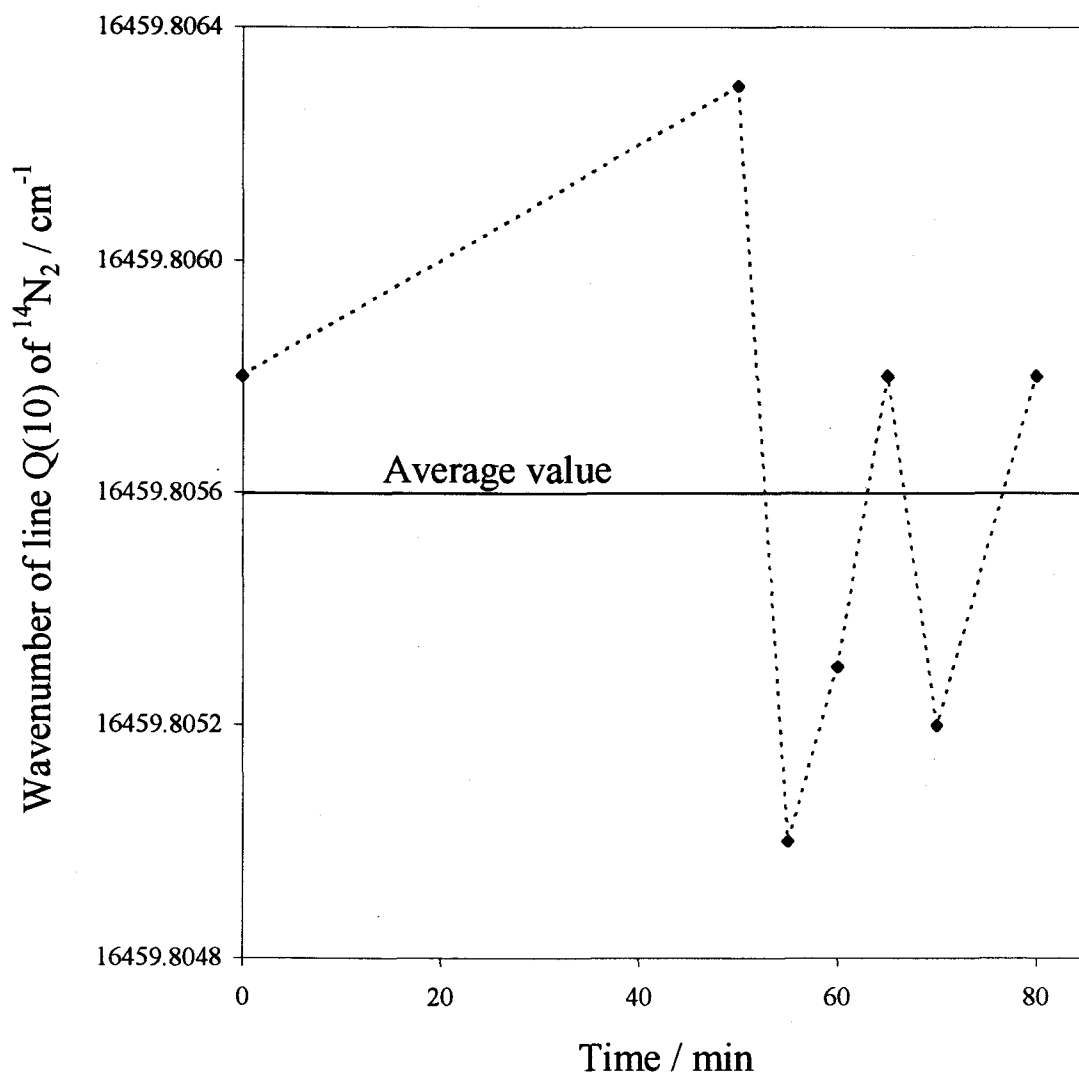


Figure 4-3. Time drift characteristic of the high-resolution apparatus. A wavenumber for reference line, $Q_1(10)$ of the fundamental band of $^{14}\text{N}_2$, is plotted as a function of time of measurement. The worst deviation from the average is 0.0012 cm^{-1} .

was measured few times over 0.5 h to verify that levels of jitter and drift were acceptable, such that the maximum deviation was less than the worst value observed (i.e. 0.0012 cm^{-1}). The same line was recorded before and after each measurement scan of several lines of a particular Q branch of $^{14}\text{N}_2$, which typically took 0.5 h as well. Data were accepted when the wavenumber of the reference line varied less than 0.0012 cm^{-1} .

The wavenumber of line $Q_1(10)$ of $^{14}\text{N}_2$ was also adopted as an absolute standard. The mean value of this standard determined before and after measurements of other lines was set equal to the absolute value 2328.0007 cm^{-1} from stimulated Raman spectra reported by Tabyaoui *et al.*, who cite an absolute uncertainty of 0.0020 cm^{-1} ^{90,91}. Scans of absorption of I_2 were obtained concurrently with measurement of the line $Q_1(10)$ and other lines, and were used to make small corrections of the latter positions relative to this standard line (see section 4.2.3 as well). For measurements on $^{15}\text{N}_2$ an auxiliary standard was analogously used; a line $Q_1(7)$ of $^{15}\text{N}_2$ was measured 13 times with respect to the line $Q_1(10)$ of $^{14}\text{N}_2$; the result is 2251.2028 cm^{-1} and its relative accuracy is estimated to be $\pm 0.0010\text{ cm}^{-1}$.

4.2.3. Precision and accuracy

The frequency of cw Stokes beam was measured with the wavemeter of the dye laser and used to determine the position of all measured lines relative to the standard ($Q_1(10)$ of $^{14}\text{N}_2$). We assessed the precision and relative accuracy of this wavemeter, for which the manufacturer's specifications are reproducibility $\pm 0.00083\text{ cm}^{-1}$ and absolute

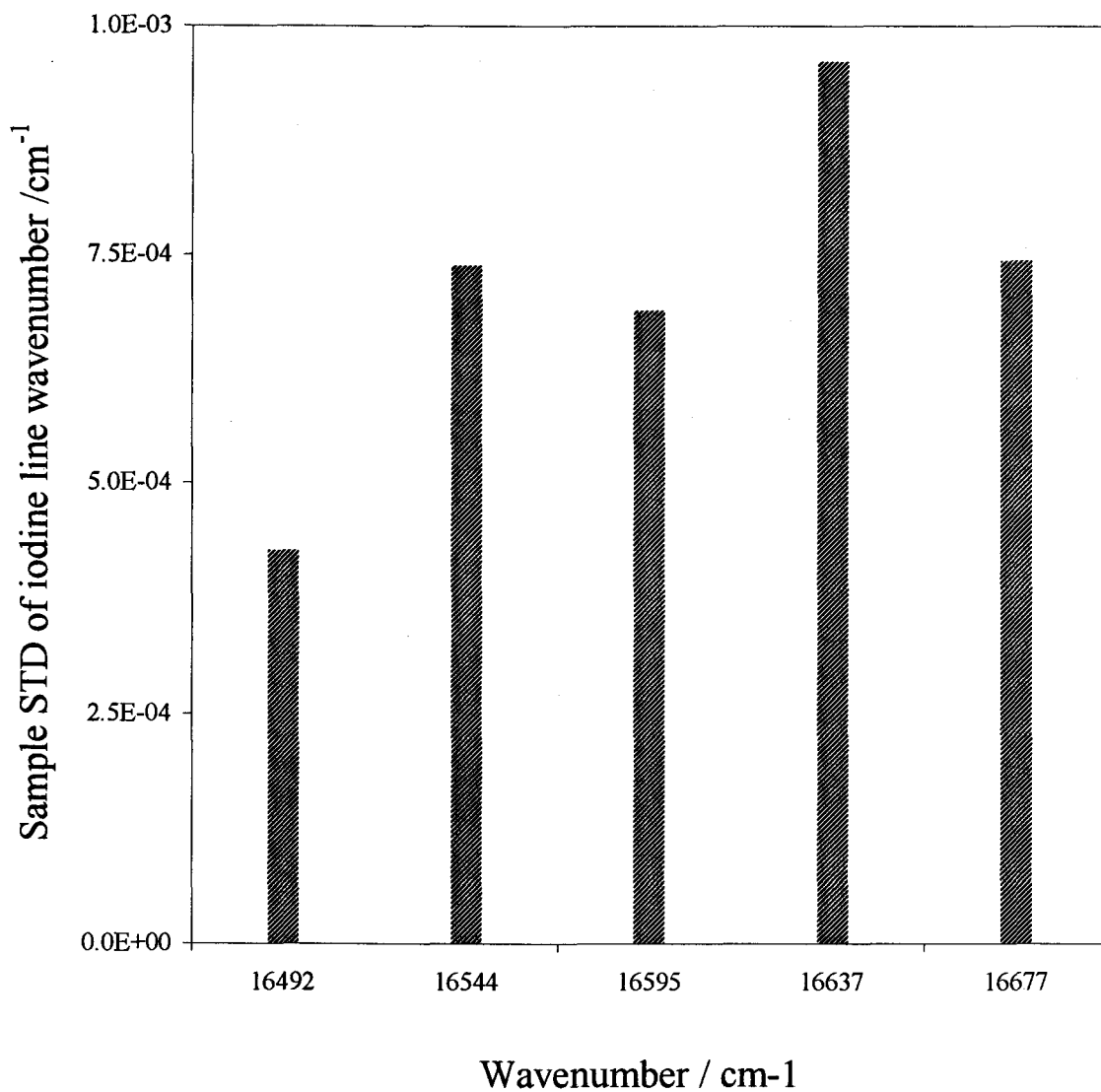


Figure 4-4. Precision of the dye laser wavemeter. Sample STD for five iodine absorption lines is plotted versus their wavenumbers. Each line was measured 10 times. The sample STD varies from 0.0004 to 0.0009 with the mean value of 0.00065 cm⁻¹.

accuracy $\pm 0.0067 \text{ cm}^{-1}$. To test the precision, we measured, ten times each, five lines of I_2 across the region of interest, in each case scanning the dye laser a few hundred cm^{-1} to a random location before resetting it at the beginning of the scan. No adjustment was made to the dye laser or wavemeter during these measurements, and likewise for sample scans. The result of the test is presented in Figure 4-4. As the mean standard error was $\sim 0.00065 \text{ cm}^{-1}$ (0.0004 cm^{-1} at best and 0.0009 cm^{-1} at worst), the precision of the wavemeter is deemed satisfactory under these conditions.

Comparison of the measured I_2 wavenumbers with absolute values from an atlas⁹⁶ showed a small offset that, more importantly, varied by only 0.003 cm^{-1} over the scan range of about 200 cm^{-1} , and in a nearly linear fashion. In practice, this small correction was redetermined for each set of lines in a measurement sequence using scans of absorption of I_2 taken concurrently with scans of N_2 of both the standard line and lines of interest. We estimate that our accuracy relative to the $\text{Q}_1(10)$ line is better than 0.002 cm^{-1} and that absolute accuracy of wavenumbers reported in Table 4-1, Table 4-2 and Table 4-3 is better than 0.004 cm^{-1} , apart from the marked outliers.

4.2.4. Additional sources of uncertainty

In addition to the measurement uncertainties discussed above, several other possible sources of shifts to the Q line positions were considered. The first of these is frequency chirp of the cw Stokes laser due to amplification, which can produce a small shift of the order 10 MHz ⁹⁷. This small effect was not measured; we assumed that it would be about the same for both the standard line $\text{Q}_1(10)$ and other lines, so it was ignored. Also ignored

was any pressure shift of the wavenumbers of the lines. Lavorel *et al.*⁹⁰ determined density coefficients that are nearly constant for Q lines in the fundamental band of $^{14}\text{N}_2$ ($-0.0055 \text{ cm}^{-1}/\text{amagat}$); this shift would be only 0.0002 cm^{-1} at pressures of our samples. Moreover, the shift would cancel because all wavenumbers were measured relative to $\text{Q}_1(10)$, for which the wavenumber was corrected⁹¹ to zero density.

A third effect considered is the AC Stark shift^{98,99}, which was observed for N_2 for highly intense laser beams and which is shown in Figure 4-5 for the standard line for total powers 20 and 40 mJ/pulse of the beam at 532 nm. Displacement of the line center was linearly proportional to the beam energy; at 30 mJ used in all measurements, the shift was about -0.0035 cm^{-1} . For a linear molecule, the AC Stark shift of a vibration-rotational level is⁹⁹

$$\Delta E_{JM} = -E^2 \frac{\alpha}{4} - E^2 \gamma \frac{3M^2 - J(J+1)}{6(2J-1)(2J+3)}, \quad (4.1)$$

in which E is the amplitude of the electric field and α and γ are the spherical and anisotropic invariants of the polarizability tensor. For Q-branch transitions, the α term is the most important; to estimate whether the shift varied significantly from one Q progression to another, we used an approximate relation derived⁹⁸ for a Morse oscillator:

$$\frac{\delta\omega_v}{\omega_v^0} = -\frac{3E^2}{16D_e\beta} \frac{d\alpha}{dq}. \quad (4.2)$$

In this expression the left side is the ratio of the Stark shift to the unperturbed vibrational wavenumber ω_v^0 , D_e and β are conventional parameters of Morse's function for potential energy, and $d\alpha/dq$ is the derivative of polarizability α with respect to the normal coordinate q evaluated at equilibrium separation R_e . The value of the ratio

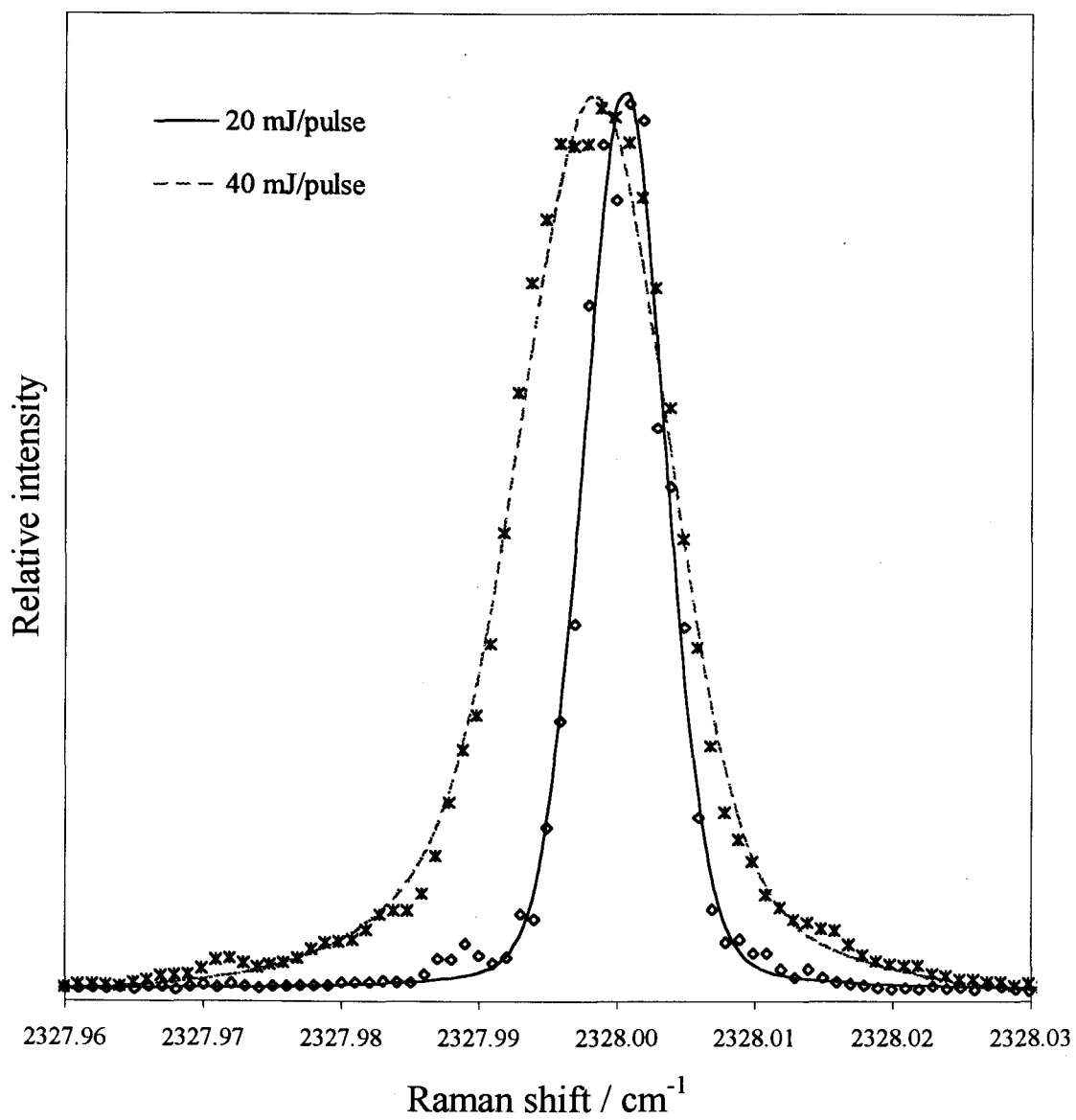


Figure 4-5. Influence of the laser energy on the position of the line $Q_1(10)$ of $^{14}\text{N}_2$.

$\frac{\delta\omega_v}{\omega_v^0}$ from our experiment is 1.5×10^{-6} . As this ratio is expected to be constant, the Stark shift would vary only -0.0031 to -0.0035 cm^{-1} over the range of our measurements. Within the stated experimental uncertainty, all Q lines, including $Q_1(10)$, experience the same Stark shift due to the optical field; hence the absolute accuracy of our measurements is unaffected by this phenomenon.

For lines in O and S branches, the situation differs. The γ term of equation (4.1) has the larger effect and some distortion of lines due to shifts in the M levels is expected; the effect is greatest for small J values and is of opposite sign for O and S branches. We estimate the shifts of the peak maxima to range from about $\pm 0.030 \text{ cm}^{-1}$ down to $\pm 0.003 \text{ cm}^{-1}$ at the average field strength of our experiment. As experimental confirmation of this effect was not made at the time of measurement of O and S branches the wavenumbers of these lines listed in Table 4-3 are uncorrected for the AC Stark effect; for this reason they were excluded from fits to evaluate molecular parameters.

4.3. Analysis of spectra

4.3.1. Interference effects

To obtain accurate wavenumbers of transitions recorded in coherent anti-Stokes Raman spectra, one must take account of small interference shifts that are a consequence of the CARS signal depending on $|\chi|^2$ (see section 2.1.4). For an isolated spectral line the third-order electric susceptibility as a function of wavenumber is expressed²⁷ as

$$\chi = A_{mn} \frac{\delta\omega + i\Gamma_{mn}}{(\delta\omega^2 + \Gamma_{mn}^2)}, \quad (4.3)$$

in which A_{mn} is the amplitude of the transition wavenumber; the remaining symbols were previously defined in section 2.1.4 (see p. 16). The damping constant Γ_{mn} determines the half width of the line at half maximum of intensity. The susceptibility χ has real and imaginary parts,

$$\chi = \chi' + i\chi'', \quad (4.4)$$

in which the real part is given by

$$\chi' = A_{mn} \frac{\delta\omega}{(\delta\omega^2 + \Gamma_{mn}^2)} \quad (4.5)$$

and has a dispersive lineshape; the imaginary part

$$\chi'' = A_{mn} \frac{\Gamma_{mn}}{(\delta\omega^2 + \Gamma_{mn}^2)} \quad (4.6)$$

is Lorentzian and is the form observed in spontaneous and stimulated Raman spectra. The shape of both parts of the third-order susceptibility, real and imaginary, appear in Figure 4-6.

For CARS, the overall shape of a line is given by the square of the susceptibility (see equation (2.34) on p. 14). From equation (4.3) we obtain

$$|\chi|^2 = A_{mn}^2 \frac{|\delta\omega + i\Gamma_{mn}|^2}{(\delta\omega^2 + \Gamma_{mn}^2)^2}, \quad (4.7)$$

$$|\chi|^2 = A_{mn}^2 \frac{1}{(\delta\omega^2 + \Gamma_{mn}^2)}. \quad (4.8)$$

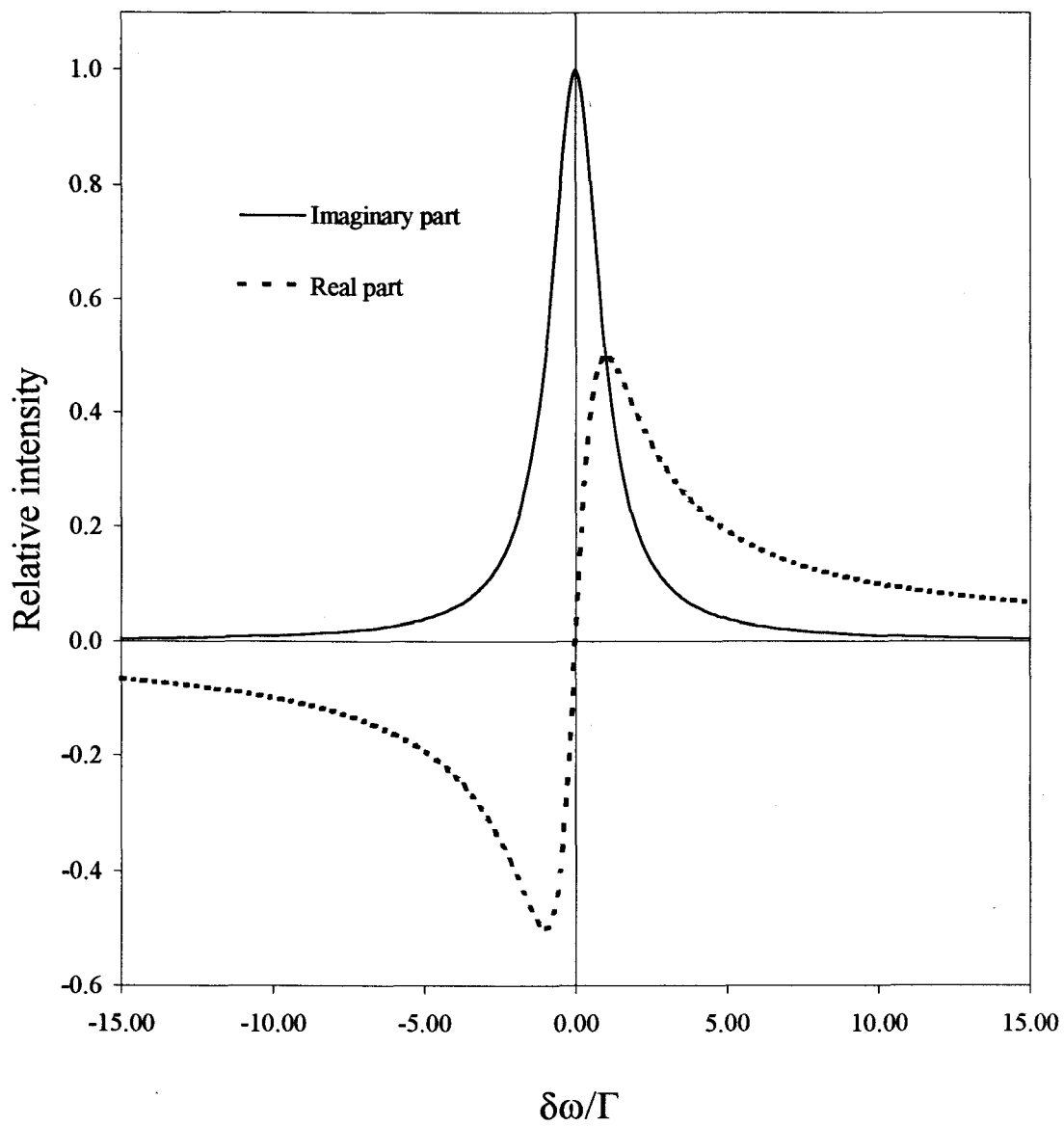


Figure 4-6. The real and imaginary parts of the third-order electric susceptibility.

The last expression can be rewritten as

$$|\chi|^2 = A_{mn} \frac{\Gamma_{mn}}{(\delta\omega^2 + \Gamma_{mn}^2)} \frac{A_{mn}}{\Gamma_{mn}} \quad (4.9)$$

and, comparing this expression with equation (4.6), we see that CARS and Raman lineshapes are identical

$$|\chi|^2 = \chi'' \frac{A_{mn}}{\Gamma_{mn}}. \quad (4.10)$$

Hence the imaginary part of the third-order susceptibility determines the overall shape of a single isolated spectral line. The line is symmetric and the position of maximum intensity defines the wavenumber of the transition.

In the preceding discussion we assumed a negligible value for χ_{nr} , the nonresonant electronic background produced by all molecules in the sample volume, even those not in initial states resonant at ω_{mn} . Because χ_{nr} derives mainly from the real parts of the susceptibility for the (far removed) electronic and purely rotational transitions, it is a simple constant added to the real part of the susceptibility:

$$\chi = (\chi' + \chi_{nr}) + i\chi'' \quad (4.11)$$

Thereby arises an interference term between χ' and χ_{nr} in the expression for $|\chi|^2$ that produces distortion of the line from a symmetric shape: the position of maximum intensity is shifted from the formal wavenumber of the transition. Then the total susceptibility is given by

$$|\chi|^2 = |(\chi' + \chi_{nr}) + i\chi''|^2 \quad (4.12)$$

or

$$|\chi|^2 = \chi_{nr} + 2\chi'\chi_{nr} + (\chi')^2 + (\chi'')^2. \quad (4.13)$$

Moreover, when there are several lines in the same region of the spectrum additional interferences occur within their real and imaginary parts; the line shape is given according to the expression

$$|\chi|^2 = \left| \chi_{nr} + \sum_j \chi'_j + i \sum_j \chi''_j \right|^2. \quad (4.14)$$

To take these effects into account, we used equation (4.14) to simulate the recorded CARS spectra to derive accurate wavenumbers for the transitions. For all spectra the zero level signal, with the Stokes beam blocked, was subtracted before fitting. For each line, the fitting parameters were transition wavenumber ω_{mn} , maximum intensity A_{mn} , and width Γ_{mn} that was about 0.01 cm^{-1} (0.02 cm^{-1} for O and S lines) and due mainly to collisional broadening. A common value of the nonresonant background χ_{nr} (typically a few hundredths of the maximum A_{mn}) was used for all lines in each spectrum. The Doppler broadening was incorporated with convolution of equation (4.14) and a single Gaussian of half width about 0.007 cm^{-1} , with increased widths used for spectra taken at increased discharge currents. The Doppler width effectively accounts also for the Gaussian instrumental half width 0.0005 cm^{-1} . The parameters were then varied in an iterative manner for a best fit according to least squares of residuals between observed and calculated wavenumbers.

An example of such a simulation for the line O(21) of $^{15}\text{N}_2$ appears in Figure 4-7 that illustrates an extreme case of interference caused by χ_{nr} and the wings of the much

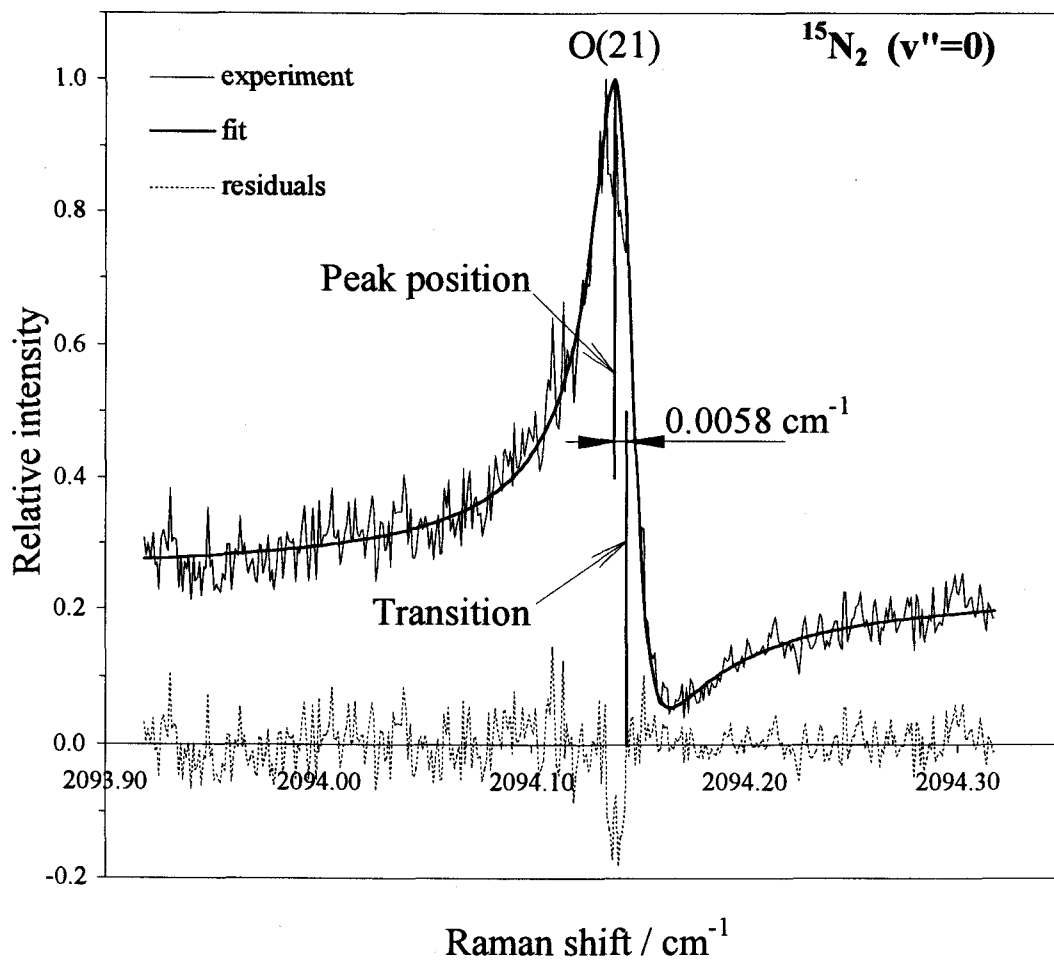


Figure 4-7. Displacement of the CARS peak position from the actual transition due to interference effects.

more intense lines in Q branch. The dispersive contribution of χ_{nr} is evident; the maximum of the line is shifted -0.0058 cm^{-1} from the vertical line that marks ω_{mn} deduced in the fitting. This shift might be due partly to AC Stark distortion of the line, which was not taken into account in the simulation. This distortion is negligible for lines in Q branches and, as χ_{nr} is also relatively less important, the influence of nearby Q transitions plays the major role in determining the interference shifts. The overall Q branch corrections are generally small but tend to increase for transitions at small J for which the spacing between lines is small. For example, for Q lines in the fundamental band of $^{15}\text{N}_2$ (Figure 4-2 a), the shifts vary monotonically from -0.0015 cm^{-1} for $J=12$ to -0.0035 cm^{-1} for $J=1$. The shift of the standard line $Q_1(10)$ of $^{14}\text{N}_2$ was -0.0012 cm^{-1} ; this correction is incorporated in the calculation of all relative Raman shifts.

4.3.2. Parameters in analysis of spectral results

For $^1\Sigma^+$ electronic states of a diatomic molecule containing nuclei of the same atomic number, the expression for spectral terms, given by equation (2.70), simplifies to

$$E_{vJ} = \sum_{k=0} \sum_{l=0} (Y_{kl} + Z_{kl}^v + Z_{kl}^r) (v + \frac{1}{2})^k [J(J+1)]^l, \quad (4.15)$$

in which the parameters were defined in section 2.2.3. The quantities Y_{kl} , deduced from fitting the wavenumbers of spectral lines, are the traditional coefficients: $Y_{10} = \omega_e$, $Y_{01} = B_e$, $Y_{02} = -D_e$, etc.

As it was discussed in section 2.2.3, coefficients Z_{kl} are small terms that represent corrections arising from the approximate nature of the separation of electronic and nuclear motions according to the Born-Oppenheimer model. According to equations (2.71) and

(2.72), they are functions of coefficients u_j , t_j and s_j for adiabatic effects, non-adiabatic rotational and non-adiabatic vibrational effects, respectively. In the case of a homonuclear diatomic molecule, equations (2.67), (2.68) and (2.69) for the latter effects, simplify:

$$V^{AD}(z) = \frac{m_e}{\mu} \sum_{j=0} u_j z^j, \quad (4.16)$$

$$\alpha(z) = \frac{m_e}{\mu} \sum_{j=0} t_j z^j, \quad (4.17)$$

$$\beta(z) = \frac{m_e}{\mu} \sum_{j=0} s_j z^j. \quad (4.18)$$

Because for non-polar diatomic molecules both atomic nuclei have the same protonic number, not only the coefficients Y_{kl} (see equation (2.75)) but also terms Z_{kl} depend on the molecular reduced mass $\mu = M_a M_b / (M_a + M_b)$, rather than Z_{kl} depending on separate reciprocal atomic masses as for heteronuclear diatomic molecules.

One might ask, in determining the different parameters of the above equations, are there any constraints other than vibration-rotational transitions for the various molecular isotopes? For nonadiabatic vibrational effects represented in $\beta(z)$, no such external information is available to combine with wavenumber data in evaluating the potential-energy parameters. For polar molecules, the nonadiabatic rotational $\alpha(z)$ terms can be related to the electric dipole moment and to the rotational g factor, g_J , that is measured by means of the Zeeman effect. For several polar molecules the dipolar moment and g factor have been employed⁵⁷ in fitting wavenumber data to ensure maximal physical significance of resulting spectral and molecular parameters. Although $^{14}\text{N}_2$ and $^{15}\text{N}_2$ lack a permanent electric dipolar moment, a value of g_J is reported for $^{15}\text{N}_2$ ¹⁰⁰, which we used to constrain

the coefficient t_0 during processing of our data of $^{14}\text{N}_2$ and $^{15}\text{N}_2$ to evaluate potential-energy functions.

An alternative expression (2.76) for spectral terms of empirical origin⁶⁶ simplifies for homonuclear molecules to

$$E_{vJ} = \sum_{k=0} \sum_{l=0} U_{kl} \mu^{-(\frac{k}{2}+l)} \left[1 + \frac{m_e}{\mu} \Delta_{kl} \right] \left(v + \frac{1}{2} \right)^k [J(J+1)]^l, \quad (4.19)$$

in which the coefficients U_{kl} are already defined according to equation (2.75). Comparison of equations (4.15) and (4.19) shows that the terms containing the dimensionless parameters Δ_{kl} absorb not only adiabatic and nonadiabatic effects but also coefficients $Y_{kl}^{(2)}$, $Y_{kl}^{(4)}$, etc. in equation (2.74). Both expressions for E_{vJ} were used in our global fits of the data for $^{14}\text{N}_2$ and $^{15}\text{N}_2$.

4.4. Results

The significant results of our measurements are the wavenumbers of about 300 vibration-rotational transitions of $^{14}\text{N}_2$ and $^{15}\text{N}_2$ that are listed in Tables 4-1, 4-2 and 4-3. For $^{14}\text{N}_2$ we list our results for Q branches with $1 \leq v'' \leq 7$. In the fitting procedures we augmented these data with wavenumbers of Q branches with $v''=0$ and 1 from Tabyaoui *et al.*⁹¹ that include the $Q_1(10)$ standard to which all our measurements are referred and of O and S branches of the fundamental band from infrared measurements of quadrupolar absorption⁸⁶. Table 4-2 and Table 4-3 present wavenumbers of our measured lines of $^{15}\text{N}_2$ in Q branches of bands $1 \leftarrow 0$ to $7 \leftarrow 6$ and in the O and S branches of the fundamental band, respectively. Because the Stark shift was uncertain for the latter, they

Table 4-1. Measured wavenumbers (cm^{-1}) of lines in Q branches of $^{14}\text{N}_2$.

	$Q_2(J)$	$Q_3(J)$	$Q_4(J)$	$Q_5(J)$	$Q_6(J)$	$Q_7(J)$	$Q_8(J)$
origins ^a	2301.2521	2272.5574	2243.8200	2215.0479	2186.2254	2157.3625	2128.4530
J							
0	2301.2540	2272.5575	2243.8194	2215.0495			
1	2301.2186	2272.5235	2243.7845	2215.0127			
2	2301.1482	2272.4531	2243.7144	2214.9422	2186.1201	2157.2611*	
3	2301.0421	2272.3502*	2243.6089	2214.8362	2186.0169	2157.1555*	
4	2300.9004	2272.2053	2243.4700	2214.6969	2185.8700	2157.0095	
5	2300.7270	2272.0328	2243.2960	2214.5212	2185.6964	2156.8329	
6	2300.5207	2271.8219	2243.0842	2214.3059	2185.4826	2156.6179	2127.7048
7	2300.2760	2271.5755	2242.8377	2214.0614	2185.2377	2156.3696	2127.4542
8	2299.9952	2271.2962	2242.5560	2213.7798	2184.9538	2156.0861	2127.1708
9	2299.6833	2270.9828	2242.2416	2213.4638	2184.6364	2155.7684	2126.8487
10	2299.3349	2270.6321	2241.8892	2213.1098	2184.2818	2155.4154	2126.5238+
11	2298.9504	2270.2466	2241.5006*	2212.7212	2183.8944	2155.0243	2126.1027
12	2298.5320	2269.8273	2241.0860	2212.2990	2183.4702	2154.5997	2125.6720
13	2298.0794	2269.3724	2240.6300	2211.8418	2183.0153	2154.1402	
14	2297.5894	2268.8805	2240.1374	2211.3515	2182.5184	2153.6404	
15		2268.3588	2239.6127	2210.8239	2181.9900	2153.1116	
16		2267.8000	2239.0482	2210.2595	2181.4244	2152.5469	
17		2267.2028	2238.4603*	2209.6582	2180.8232	2151.9411	
18		2266.5753	2237.8284*	2209.0253		2151.3028	
19		2265.9121	2237.1624*			2150.6333	
20		2265.2115	2236.4590*			2149.9219	
21						2149.1768	
22						2148.3969	
$s^b / 10^{-3}$	1.38	1.25	1.29	1.44	1.60	1.88	2.20

^a Band origins were obtained in a separate fit of each branch.

^b Standard deviation of fit of each separate branch, used for relative weighting ($w=1/s^2$) of lines in global fits. s values for outliers marked with * were increased by a factor of 10, values marked with + were not included in fits.

Table 4-2. Measured wavenumbers (cm^{-1}) of lines in Q branches of $^{15}\text{N}_2$.

	Q ₁ (J)	Q ₂ (J)	Q ₃ (J)	Q ₄ (J)	Q ₅ (J)	Q ₆ (J)	Q ₇ (J)
origins ^a	2252.0802	2225.3303	2198.5441	2171.7222	2144.8605	2117.9640	2091.0316
J							
1	2252.0492	2225.2997	2198.5136	2171.6920		2117.9317	
2	2251.9862	2225.2372	2198.4506			2117.8684	
3	2251.8926	2225.1425	2198.3567	2171.5342	2144.6718	2117.7746	2090.8411
4	2251.7653	2225.0141	2198.2268	2171.4067	2144.5397*	2117.6438	
5	2251.6083	2224.8573	2198.0700	2171.2490	2144.3841	2117.4863	2090.5535
6	2251.4204	2224.6725	2197.8847	2171.0579	2144.1944	2117.2983	
7	2251.2015	2224.4500	2197.6654	2170.8381	2143.9752	2117.0744	2090.1376
8	2250.9502	2224.1994	2197.4113	2170.5833	2143.7211	2116.8218	
9	2250.6666	2223.9192	2197.1268	2170.2969	2143.4340	2116.5362	2089.5944
10	2250.3537	2223.6014	2196.8120	2169.9802	2143.1228	2116.2160	
11	2250.0087	2223.2567	2196.4640	2169.6335	2142.7733	2115.8676	2088.9222
12	2249.6323	2222.8792	2196.0869	2169.2523	2142.3926	2115.4820	
13	2249.2243	2222.4678	2195.6776	2168.8452	2141.9798	2115.0686	2088.1283
14	2248.7860	2222.0330	2195.2337	2168.4104*	2141.5350	2114.6314*	
15	2248.3147	2221.5610	2194.7658	2167.9345*	2141.0584	2114.1511	2087.2003
16	2247.8114	2221.0563	2194.2609	2167.4266*	2140.5502	2113.6397	
17	2247.2804	2220.5220	2193.7255	2166.8923*	2140.0101	2113.0979	2086.1433
18	2246.7154	2219.9552	2193.1558	2166.3181	2139.4461	2112.5263	
19	2246.1217	2219.3568	2192.5592	2165.7158	2138.8417	2111.9211	2084.9647
20	2245.4931	2218.7335	2191.9308	2165.0829	2138.2058	2111.2890*	
21	2244.8352	2218.0708	2191.2675	2164.4219	2137.5396	2110.6191	2083.6583
22	2244.1433	2217.3792	2190.5720	2163.7213	2136.8393	2109.9159	
23	2243.4260	2216.6544	2189.8470	2162.9982	2136.1090	2109.1840	2082.2176
24	2242.6711	2215.9005	2189.0887	2162.2346		2108.4199	
25	2241.8876	2215.1144	2188.2990	2161.4428		2107.6207	2080.6501
26		2214.2941					
27		2213.4447					
$s^b/10^{-3}$	0.96	1.61	1.69	1.73	2.11	1.88	1.76

^{a,b} See footnotes for Table 4-1.

Table 4-3. Measured wavenumbers (cm^{-1}) of lines in O and S branches of $^{15}\text{N}_2$.

J	$O_0(J)$	$S_0(J)$
1		2270.4484
3	2233.4744	2285.0302
5	2218.4600	2299.4783
7	2203.3206	2313.7953
9	2188.0990	2327.9786
11	2172.6957	
13	2157.2079	
15	2141.6095	
17	2125.8955	
19	2110.0745	
21	2094.1443	

were excluded from the fitting calculations; instead we added the purely rotational data of Bendtsen⁸⁸ to our Q-branch data.

4.4.1. Weighting of data

Fitting data to obtain term coefficients Y_{kl} and potential-energy parameters requires assignment of uncertainties s to serve as weights of data (as $1/s^2$) to account for variations in the accuracy of measurements with v and J and in combining data added from other sources. Our procedure involved first fitting each Q branch to a polynomial in $J(J+1)$ to enable us to recognize (a few) outliers, marked with * and + in Table 4-1 and Table 4-2. These were then omitted to obtain, from the remaining lines, the band origins

listed in the tables and a standard deviation that served as an uncertainty assigned to all lines in that branch in a subsequent global fit of all data. Printed at the bottom of each column in the tables, these uncertainties varied only slightly with the branch but increased gradually with v , reflecting the correspondingly degraded ratio of signal to noise. Outliers marked * were included in the fits but were assigned large uncertainties so as to exert negligible effect on fitted parameters. For data used to supplement our measurements, we adopted the uncertainties specified by the original authors. Tests indicated no inconsistency among data from these sources.

4.4.2. Coefficients Y_{kl} and U_{kl}

The wavenumbers of $^{14}\text{N}_2$ and of $^{15}\text{N}_2$ were separately fitted to selected coefficients Y_{kl} , in equation (4.15) with Z_{kl} neglected, of sufficient number to reproduce satisfactorily the lines in each set. Each model was selected on the basis of t-tests and the maximum F-statistic to ensure that only significant parameters were retained in this adjustment (see also Appendix C for a description of the statistical tool of Microsoft Excel 7.0, which was used in our regression analysis, along with related statistical concepts). With nine adjustable parameters the normalized σ and absolute S standard deviations of the fits are 1.12 and 0.0022 cm^{-1} for $^{14}\text{N}_2$, and 1.18 and 0.0023 cm^{-1} for $^{15}\text{N}_2$. The derived values of Y_{kl} appear in Table 4-4.

For $^{14}\text{N}_2$ the coefficients of Table 4-4 reproduce satisfactorily the measured wavenumbers. Figure 4-8 displays with square symbols our residuals (calculated - measured) for the several Q branches; with other symbols also appear the residuals

Table 4-4. Parameters Y_{kl} and U_{kl} for $^{14}\text{N}_2$ and $^{15}\text{N}_2$ ^a.

k	l	Parameter	$^{14}\text{N}_2$	$^{15}\text{N}_2$	$^{14}\text{N}_2 + ^{15}\text{N}_2$
			Y_{kl} / cm^{-1}	Y_{kl} / cm^{-1}	$U_{kl} / (\text{cm}^{-1} \text{u}^{k/2+l})$
1	0	ω_e	2358.54024 ± 0.00039	2278.79126 ± 0.00072	6240.595 ± 0.019
		$\Delta_{1,0}$			0.400 ± 0.039^b
2	0	$-\omega_e x_e$	-14.30577 ± 0.00026	-13.34624 ± 0.00026	-100.1121 ± 0.0096
		$\Delta_{2,0}$			5.1 ± 1.1^b
3	0	$\omega_e y_e / 10^{-3}$	-5.0668 ± 0.055	-6.1977 ± 0.024	-99.8 ± 1.7
4	0	$\omega_e z_e / 10^{-4}$	-1.095 ± 0.036		-44.0 ± 2.8
0	1	B_e	1.9982399 ± 0.0000045	1.865428 ± 0.000021	13.990796 ± 0.000053
1	1	$-\alpha_e / 10^{-2}$	-1.731281 ± 0.000079	-1.564030 ± 0.00033	-32.0945 ± 0.0039
2	1	$\gamma_e / 10^{-5}$	-2.8520 ± 0.018	-1.595 ± 0.082	-117.5 ± 4.3
3	1	$\delta_e / 10^{-7}$		-6.659 ± 0.75	-477 ± 110
0	2	$-D_e / 10^{-6}$	-5.7376 ± 0.010	-5.0706 ± 0.057	-280.92 ± 0.84
1	2	$-\beta_e / 10^{-8}$	-1.02171 ± 0.031	-0.969891 ± 0.40	-112.1 ± 6.7
Range			$0 \leq v \leq 8$	$0 \leq v \leq 7$	
σ^c			1.12	1.18	1.97
S^d			0.0022	0.0023	0.0037

^a Coefficients Y_{kl} are quoted to a sufficient number of significant figures to reproduce experimental wavenumbers to 0.0001 cm^{-1} ; coefficients U_{kl} are obtained from a combined fit of both isotopic variants; reduced masses used: for $^{14}\text{N}_2$ $\mu = 7.0015370037 \text{ u}$, for $^{15}\text{N}_2$ $\mu = 7.5000544865 \text{ u}$; uncertainties correspond to one standard deviation.

^b Coefficients Δ_{kl} have no unit; mass of electron used in their calculation is $5.485799 \cdot 10^{-4} \text{ u}$.

^c Normalized standard deviation.

^d Absolute standard deviation.

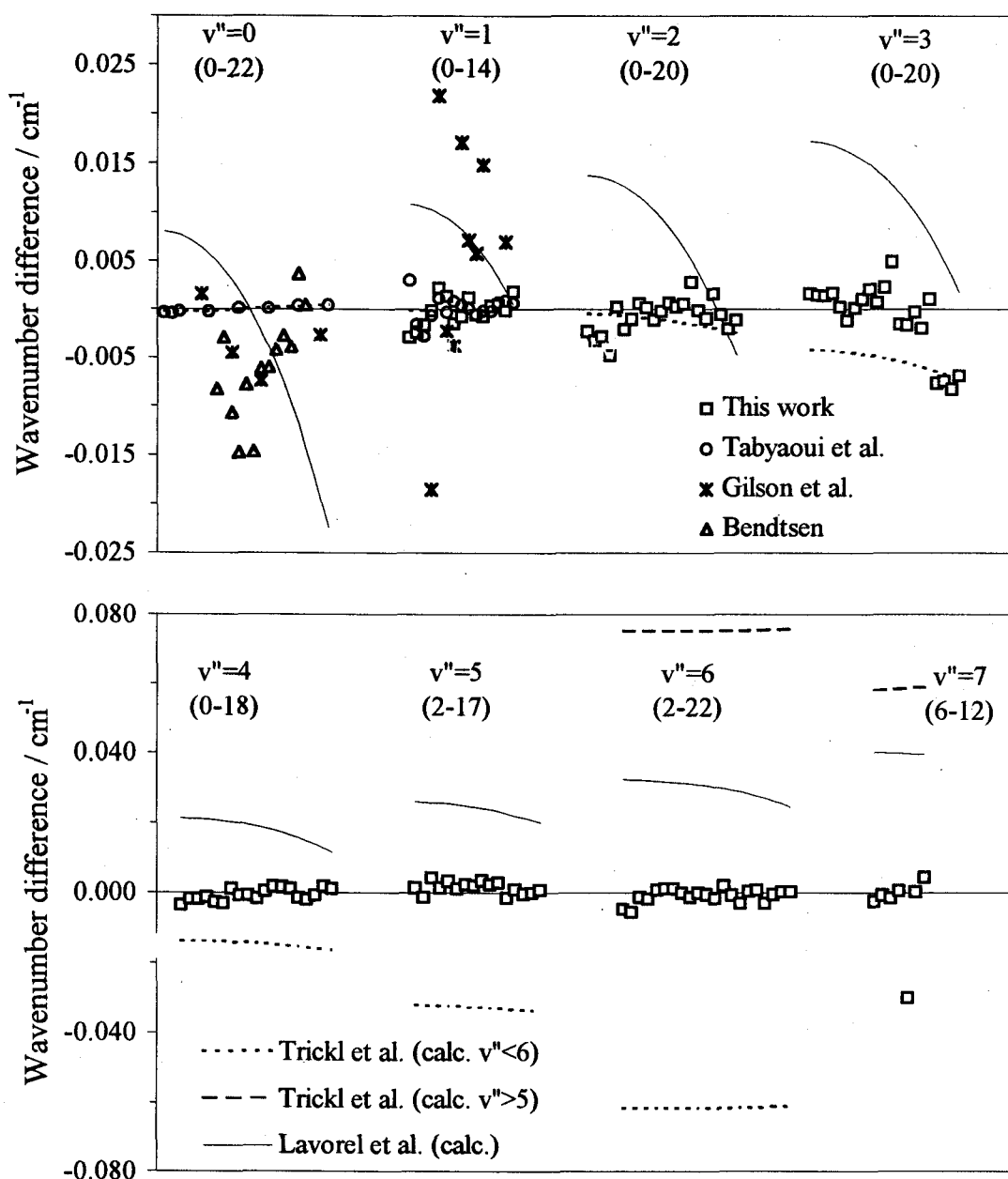


Figure 4-8. Differences between calculated and experimental wavenumbers of Q branches of $^{14}\text{N}_2$ from various sources. Q branches of $^{14}\text{N}_2$ are obtained using coefficients Y_{kl} listed in Table 4-4. Shown with symbols are differences for experimental values from this work, from Tabyaoui *et al.*⁹¹, from Gilson *et al.*⁸⁹, and from Bendtsen⁸⁸. Shown with lines are differences for wavenumbers calculated using coefficients Y_{kl} from Lavorel *et al.*⁹² and two sets of Y_{kl} from Trickl *et al.*⁹⁴, one for $v \leq 5$, the other for $v > 5$. Numbers in parentheses indicate the range of J for each Q branch.

between our calculated values and the experimental measurements for $v'' = 0$ and 1 of Tabyaoui⁹¹, Gilson⁸⁹, and Bendtsen⁸⁸ (and their coworkers). As results of Tabyaoui *et al.* were included in the determination of parameters Y_{kl} , the residuals are small for their $v''=0$ data, as expected, but the improved precision relative to other measurements is evident. The improvement is even greater for our calculated values versus those calculated from coefficients Y_{kl} reported by Trickl *et al.*⁹⁴ (two sets, one for $v \leq 5$ and the other for $v < 27$) and by Lavorel *et al.*⁹². Their results are shown as lines in the figures; these differences greatly exceed the scatter in our residuals.

A similar plot of differences is offered for $^{15}\text{N}_2$ in Figure 4-9, with differences deduced from the only other Raman data, from measurements of Q branches by Bendtsen⁸⁸ and of Gilson *et al.*⁸⁹. A systematic offset about -0.05 cm^{-1} is evident for Bendtsen's Q-branch data⁸⁸; i.e. the latter wavenumbers are slightly too large. The scatter of residuals for Bendtsen's data is comparable to ours, whereas that of data of Gilson *et al.*⁸⁹ is much larger.

The term coefficients Y_{kl} in Table 4-4 are presented to a sufficient number of significant figures to calculate the transitions to 0.0001 cm^{-1} , but the statistical significance of the parameters is limited according to the standard errors listed. Comparisons with previous Y_{kl} results^{86,91,92,94} for $^{14}\text{N}_2$ are hindered by the variation in the number of fitted parameters in the various fits; in general the major Y_{kl} values are consistent but our decreased estimated standard errors imply much increased precision. Our standard errors for Y_{kl} of $^{14}\text{N}_2$ are slightly smaller than those of $^{15}\text{N}_2$, for which no previous extensive data exist for comparison. It should be noted that, because coefficients Y_{kl} result from unconstrained fits, they are equivalent to parameters A_{kl} discussed by Hessel *et al.*¹⁰¹,

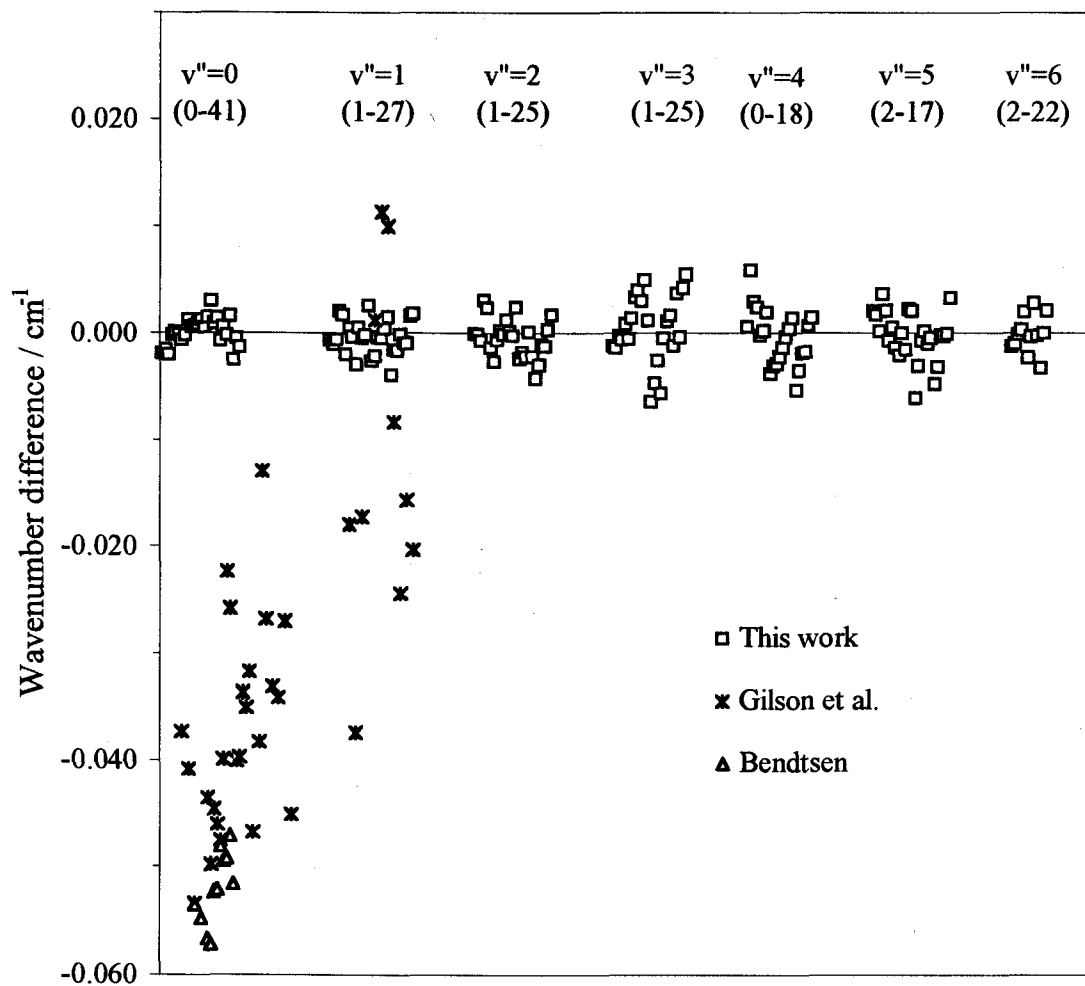


Figure 4-9. Differences between calculated and experimental wavenumbers of Q branches of $^{15}\text{N}_2$ from various sources. Calculated values are obtained using coefficients Y_{kl} listed in Table 4-4; experimental values are taken from this work, from Gilson *et al.*⁸⁹, and from Bendtsen⁸⁸. Numbers in parentheses indicate the range of J for each Q branch.

rather than the constrained parameters implied by Dunham's notation^{38,39,54}. In the latter case, for example, one constraint is $-Y_{0,2} = 4Y_{0,1}^3 / Y_{1,0}^2$. This distinction is minor; for $^{14}\text{N}_2$ and $^{15}\text{N}_2$ the ratio is $5.737 \cdot 10^{-6}$ and $5.000 \cdot 10^{-6} \text{ cm}^{-1}$ respectively, in good accord with $Y_{0,2}$ values deduced from the unconstrained fits.

To the extent that adiabatic and nonadiabatic effects and terms $Y_{kl}^{(2)}$ and higher in equation (2.74) (section 2.2.3) can be described by the Δ_{kl} coefficients, equation (4.19) enables a combined fit of data of $^{14}\text{N}_2$ and $^{15}\text{N}_2$ data in terms of coefficients formally independent of mass. Ten unconstrained parameters U_{kl} and two vibrational correction terms Δ_{10} and Δ_{20} were found to be statistically significant and are listed in Table 4-4. Compared to the two separate fits, the combined analysis decreased the number of parameters from 18 to 12, the values of which can be used for the calculation of transitions of any isotopic variant of N_2 . For example for $^{14}\text{N}^{15}\text{N}$ the parameters yield a value of 2291.34 cm^{-1} for the ω_0 band origin of the fundamental, which is in good accord with the experimental value of 2291.33 cm^{-1} reported by Bendtsen⁸⁸. Overall the combined fit reproduced the wavenumbers of all 356 lines of $^{14}\text{N}_2$ and $^{15}\text{N}_2$ only fairly well; the normalized standard deviation σ increased to 1.97, almost twice that of the separate fits. However, despite the fact that, for the global fit, the absolute standard deviation S also increased by about the same factor, its value is very small (0.0037 cm^{-1}) and does not exceed the estimated absolute uncertainty of our measurements (0.004 cm^{-1}). Addition of further U_{kl} and Δ_{kl} parameters failed to decrease σ and S significantly and led to large standard errors in the fitting parameters. Whether this large value of σ reflected inaccuracy of data or inadequacy of the theoretical model was unclear; hence an

alternative analysis of the mass dependence was made in terms of equation (4.15) and potential-energy coefficients c_j , defined in equation (2.66) (section 2.2.3).

4.4.3. Potential-energy function

To evaluate parameters in a potential-energy function, we made fits with the program *Radiatom*⁶³ on data of $^{14}\text{N}_2$ and $^{15}\text{N}_2$ separately and then combined, employing the same input data sets and uncertainties specified above. The deduced parameters were R_e and coefficients c_j , $0 \leq j \leq 6$ (equation (2.66) section 2.2.3); t_0 in equation (4.17) was constrained to be consistent with the magnitude of the rotational g factor, $|g_J| = 0.2593(5)$, of $^{15}\text{N}_2$ measured in experiments with molecular beams¹⁰⁰, according to the relation $t_0 = g_J \mu/m_p$ in which m_p is the protonic mass; the sign of g_J was assumed to be negative¹⁰⁰. The standard errors of fits (σ and S) were insensitive to the presence or absence of t_0 , but we retained this parameter in the fitting model to ensure maximal significance of other parameters. Resultant values of the parameters appear in Table 4-5; with eight adjustable parameters the normalized and absolute standard deviations of the separate fits are 1.17 and 0.0021 cm^{-1} for $^{14}\text{N}_2$, and 1.18 and 0.0024 cm^{-1} for $^{15}\text{N}_2$. In the combined fit, one additional parameter was found to be significant, as discussed below.

4.5. Discussion

These CARS experiments at resolution 0.001 cm^{-1} provide significantly improved spectral data of $^{14}\text{N}_2$, and, by means of our recirculating system, greatly extended spectral data of $^{15}\text{N}_2$. The Q-branch vacuum wavenumber values of Table 4-1 and Table 4-2

Table 4-5. Parameters for $^{14}\text{N}_2$ and $^{15}\text{N}_2$.

	$^{14}\text{N}_2$	$^{15}\text{N}_2$	$^{14}\text{N}_2$ and $^{15}\text{N}_2$ ^a
Parameter			
c_0 / cm^{-1}	695843.57 ± 0.36	695853.0 ± 3.3	695812.7 ± 1.6
c_1	-1.70398 ± 0.00011	-1.70677 ± 0.00024	-1.70461 ± 0.00015
c_2	1.06160 ± 0.00052	1.0789 ± 0.0012	1.06512 ± 0.00073
c_3	-0.467 ± 0.013	-0.284 ± 0.019	-0.388 ± 0.018
c_4	0.938 ± 0.096	-0.81 ± 0.14	0.31 ± 0.13
c_5	-0.85 ± 0.11	2.12 ± 0.16	-0.06 ± 0.14
c_6	-9.3 ± 2.0	9.7 ± 2.7	-2.0 ± 2.7
(s_0 or $u_2 / 10^5 \text{cm}^{-1}$)			$(1.128 \pm 0.099$ or $7.85 \pm 0.69)$
t_0^b	-1.9307	-1.9307	-1.9307
$R_e / 10^{-10} \text{m}$	1.0976005 ± 0.0000011	1.0976109 ± 0.0000032	1.0975992 ± 0.0000013
Range	$0 \leq v \leq 8$	$0 \leq v \leq 7$	
	$0.95 \leq R / 10^{-10} \text{m} \leq 1.34$	$0.96 \leq R / 10^{-10} \text{m} \leq 1.31$	$0.96 \leq R / 10^{-10} \text{m} \leq 1.31$
σ^c	1.17	1.18	2.10
S^d	0.0021	0.0024	0.0034

^a Parameters are obtained from the global fit of spectral data of $^{14}\text{N}_2$ and $^{15}\text{N}_2$; addition of either s_0 or u_2 , but not both, to parameters c_j and t_0 leads to equivalent fits.

^b Parameter t_0 was fixed during fitting of spectral data (see text).

^c Normalized standard deviation. Uncertainties of parameters correspond to one standard deviation.

correspond to zero pressure and AC Stark field conditions and are believed accurate to $\pm 0.004 \text{ cm}^{-1}$. For the O and S lines of $^{15}\text{N}_2$ (Table 4-3), no Stark shift adjustment was made but this correction is believed to be less than $\pm 0.030 \text{ cm}^{-1}$. Some confirmation of this comes from the comparison of tabulated O and S results with wavenumbers of these transitions calculated from the $^{15}\text{N}_2$ Y_{kl} parameters of Table 4-4; the maximum residual (calc. - obs.) for these is 0.017 cm^{-1} for S(1) and the average difference is 0.004 cm^{-1} .

The adjustable c_j parameters in Table 4-5 define the function for the potential energy $V^{\text{BO}}(z)$ of $^{14}\text{N}_2$ and $^{15}\text{N}_2$ according to equation (2.66) of section 2.2.3. These coefficients from separate fits of data of $^{14}\text{N}_2$ and $^{15}\text{N}_2$ reproduce measured wavenumbers of transitions nearly as well as their counterparts Y_{kl} in Table 4-4, despite the former being one fewer in each set. Several correlation coefficients of parameters c_j have magnitudes about 0.9; for this reason the standard errors associated with each value are only a partial measure of their significance. From the analysis, we obtain values of the equilibrium internuclear separation $R_e/10^{-10} \text{ m} = 1.097601(1)$ for $^{14}\text{N}_2$ and $1.097611(3)$ for $^{15}\text{N}_2$; correspondingly from c_0 , we derive values of the vibrational force coefficient $k_e/\text{N m}^{-1} = 2294.722(2)$ for $^{14}\text{N}_2$ and $2294.710(3)$ for $^{15}\text{N}_2$.

Although the values of coefficients c_3 - c_6 for $^{14}\text{N}_2$ and $^{15}\text{N}_2$ appear disparate, the corresponding potential-energy curves are nearly indistinguishable. Figure 4-10 displays the curve of $^{14}\text{N}_2$ within the range of energy up to the state $v=8$, the highest level to which our measurements pertain. Plotted below the curve is the difference $V^{\text{BO}}(z)$ of $^{14}\text{N}_2$ - $V^{\text{BO}}(z)$ of $^{15}\text{N}_2$, the magnitude of which is less than 3 cm^{-1} over most of the range of validity, $0.96 \leq R/10^{-10} \text{ m} \leq 1.31$. Because such differences divided by the vibrational energy are of the order of the ratio of electronic to nuclear mass for $^{14}\text{N}_2$, they have a magnitude

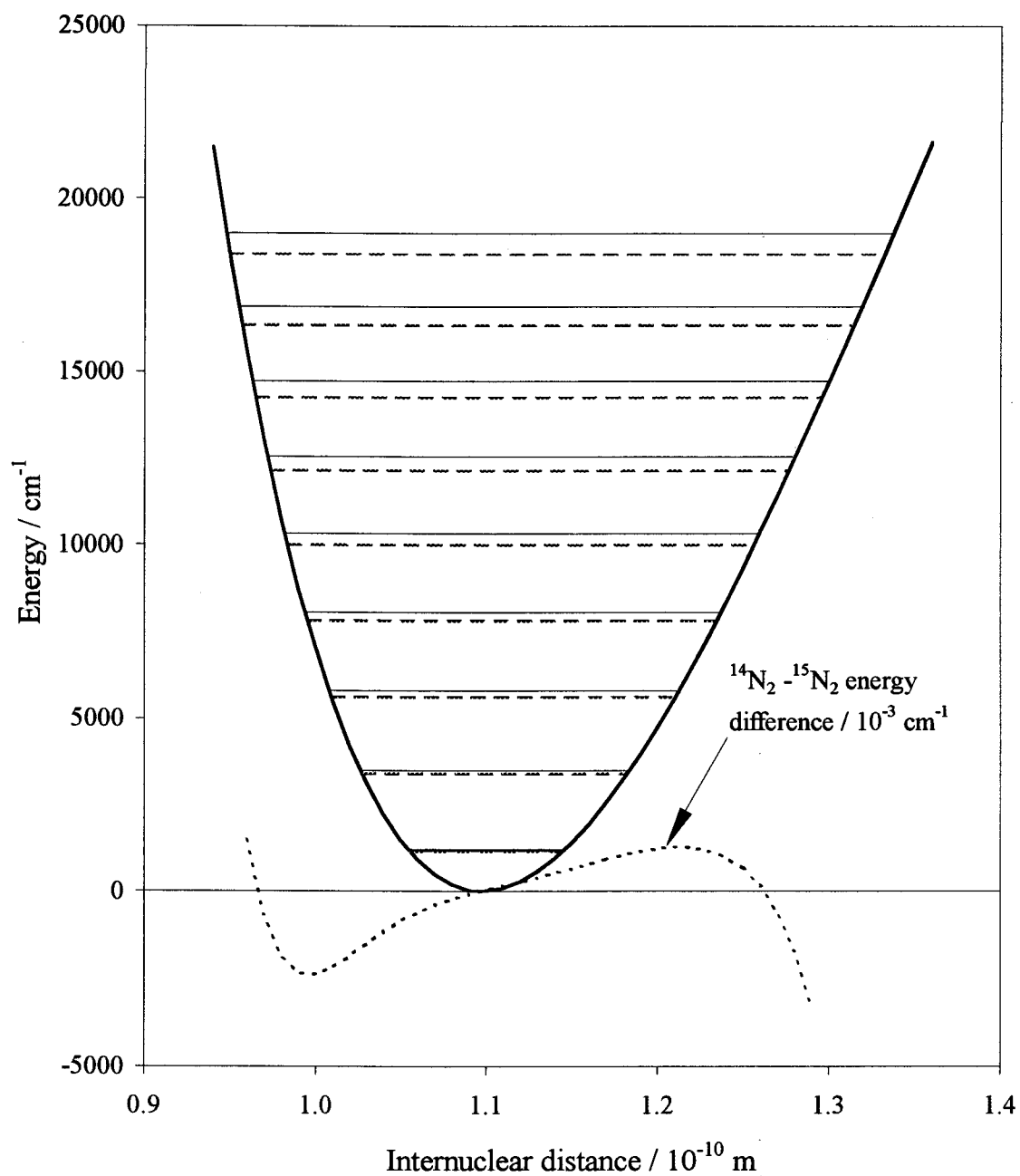


Figure 4-10. Potential-energy curve for dinitrogen. Energies of vibrational levels are shown as horizontal solid (¹⁴N₂) and dashed (¹⁵N₂) lines. The dotted line represents the difference between adiabatic potential energies of ¹⁴N₂ and ¹⁵N₂.

expected for adiabatic effects⁴⁶; thus it might be expected that one could fit well the combined data of $^{14}\text{N}_2$ and $^{15}\text{N}_2$ with $V^{\text{AD}}(z)$ containing coefficients u_j .

However, fits of the combined spectral data to coefficients c_j plus various adjustable u_j , t_j and s_j in equations (4.16), (4.17) and (4.18) showed that, except with unacceptably large magnitudes of the latter parameters, the normalized standard deviation σ of such attempted fits remained slightly greater than 2, in contrast with reduced standard deviations of about 1.2 for the separate isotopic variants. The exception was the addition of either the coefficient s_0 for nonadiabatic vibrational effects (equation (4.18)) or u_2 for adiabatic vibrational effects (equation (4.16)). Either parameter converged to a stable and reasonable value with essentially identical values for the set of coefficients c_j . Although the normalized standard error σ was 2.10 in each case, the absolute standard error S was only 0.0034 cm^{-1} , which is slightly smaller than that for the combined fit with parameters U_{kl} and Δ_{kl} , 0.0037 cm^{-1} (see discussion on p. 98 and Table 4-4 of section 4.4.2). A slight preference for s_0 over u_2 might be had from previous work on polar molecules⁵⁷, in which terms s_j are generally more important than coefficients u_j . However, in view of the relatively large σ of the overall fit, we note that the model represented by equation(4.15) was unable to fit the data to the extent achieved in some other studies, where σ was near unity⁵⁷.

The possibility that there might be a wavenumber error in the $^{15}\text{N}_2$ reference line relative to that of $^{14}\text{N}_2$ was tested by adding a shift parameter δ in the fitting process: δ was found to be negligible and no reduction in σ resulted. Similarly, multiplication with a scaling parameter linear in wavenumber gave essentially a unit value and no improvement. Our conclusion is thus that no such systematic errors exist in our data and that, even at

our measurement accuracy of 0.004 cm^{-1} , random errors preclude quantitative distinction between the small adiabatic and non adiabatic effects in N_2 .

4.6. Summary

At an effective resolution of 0.001 cm^{-1} , we measured Raman spectra of $^{14}\text{N}_2$ and $^{15}\text{N}_2$ that yield improved vibration-rotational terms of states up to $v=8$ of $^{14}\text{N}_2$ and $v=7$ of $^{15}\text{N}_2$ excited in electrical discharges. These terms of each isotopic variant are compactly represented in the form of either nine fitting coefficients Y_{kl} in Table 4-4 or eight fitted parameters of adiabatic potential-energy functions plus one constrained value from the rotational g factor in Table 4-5. Parameters in either set reproduce satisfactorily wavenumbers of transitions in Q branches of the specified bands in our data sets within the estimated absolute uncertainties of measurement.

For nitrogen, mass independent parameters U_{kl} and Δ_{kl} presented in Table 4-4 were reported for the first time. They permit the accurate calculation of energy levels of all isotopic variants of nitrogen, including $^{14}\text{N}^{15}\text{N}$, for which very limited spectral information is available^{88,89}.

Fits of combined spectral data of two isotopic variants of nitrogen, $^{14}\text{N}_2$ and $^{15}\text{N}_2$, yielded a few parameters responsible for extramechanical effects, arising from incomplete separation of electronic and nuclear motion. However, efforts to distinguish adiabatic and nonadiabatic effects were unsuccessful.

5. HYDROGEN SPECTRAL DATA

5.1. Introduction

Hydrogen is another diatomic molecule interesting to consider for the same type of spectral measurements and data analysis as those performed for nitrogen and discussed in Chapter 4. Since it is the lightest diatomic molecule the extramechanical effects should be more pronounced than in any other molecule, including nitrogen. It is also attractive from the point that hydrogen isotopes provide large relative variation in molecular mass (e.g. D_2 and H_2 have the mass ratio of two, whereas for $^{15}N_2$ and $^{14}N_2$ it is only 1.07). Such a variation is required for the global fits of isotopic data using expressions (2.70) and (2.76).

On the other hand, the vibrational lifetime of hydrogen is very small: e.g. $\sim 3 \cdot 10^{-3}$ s for D_2 ¹⁰² and $\sim 4 \cdot 10^{-4}$ s for H_2 ¹³ at a pressure of 1 atm, which is three to four orders of magnitude lower than that for nitrogen¹². The consequence of this fact is that we were not able to observe vibration-rotationally excited states of hydrogen with the DC discharge apparatus described in Chapter 3. Even for oxygen, which has vibrational lifetime of the order of $3 \cdot 10^{-2}$ s at 1 atm¹², we were able to observe Q-branch transitions only in the first hot band with a signal to noise ratio of only about 2. This situation led us to consider possible modifications of the excitation and probing techniques. Before undertaking this task, it seemed reasonable to first assemble spectral data of hydrogen isotopes available in the literature and to analyze them as in the previous chapter to assess their quality.

5.2. Literature overview

There are numerous experimental works on hydrogen published in the literature, however only part of them pursued measurements of **absolute** vibration-rotational wavenumbers, as required for our analysis. In the present chapter we restrict our discussion to such publications. The main optical techniques used by various researchers are quadrupolar absorption¹⁰³⁻¹¹² and linear Raman scattering¹¹³⁻¹²⁰. Only a few groups employed CARS^{121,122} and stimulated Raman scattering (SRS)¹²³. There are also some articles on electronic spectra^{124,125,126}, electric field induced absorption¹²⁷, resonance enhanced multiphoton ionization (REMPI)¹²⁸ and optoacoustic measurements^{129,130} of hydrogen isotopes.

The most studied isotopes are ordinary hydrogen H_2 ^{103-108,111,114-118,121,123,126,127} and deuterium D_2 ^{109,114-118,122,124,127,128}. There are also some articles on tritium T_2 ^{118,120} as well as on mixed isotopes HD ^{110,112,117,118,125,129}, DT ^{113,118,119} and HT ^{118,119,130}. The electric dipole vibrational transitions for the homonuclear isotopes of hydrogen, H_2 , D_2 and T_2 , are rigorously forbidden by symmetry, therefore their molecular spectra were studied mainly by the quadrupolar absorption¹⁰³⁻¹⁰⁹ and the linear^{113-118,120} and nonlinear¹²¹⁻¹²³ Raman scattering techniques. Mixed isotopic variants (HD , DT , HT) also have no electric dipole within the traditional Born-Oppenheimer and adiabatic approximations¹³¹. However, due to nonadiabatic effects (see discussion in section 2.2 on p. 19) such mixed isotopes develop a small electric dipole moment, which is big enough to be detected^{110,112,129,130}.

The claimed absolute accuracy of wavenumber measurements of hydrogen isotopes varies from a few ten thousandths of cm^{-1} for vibration-rotational transitions (e.g. FT quadrupole absorption¹⁰³ and FT Raman¹¹⁵ methods) to 0.4 cm^{-1} for electronic transitions¹²⁵. Transition wavenumbers of hydrogen isotopic variants available in the literature are summarized in Tables 5-1 through 5-6; only the most accurate spectral data with accuracy 0.1 cm^{-1} or better are presented.

For regular hydrogen H_2 , purely rotational, fundamental, the first four hot-band and some overtone transitions are reported in the literature (Table 5-1 and Table 5-2). Many different research groups studied fundamental Q-branch spectra ($v=1\leftarrow 0$; $J=0-6$)^{103,106,114-118,127} and their results generally agree within the uncertainty of measurements, which assures the reliability of the data. Lines with quantum number $J > 6$ in the fundamental Q branch are reported only by Germann and Valentini¹²¹. There are also a few studies on fundamental S-branch^{103,115,118,127} and O-branch^{118, 127} bands of H_2 ; some of these provide very accurate spectral data (see Table 5-2).

The above mentioned work by Germann and Valentini¹²¹ is also the only one in which wavenumbers of lines in Q branches for several H_2 hot bands ($v'=2-5$) are published. To populate higher vibrational levels of hydrogen, Germann and Valentini employed a chemical reaction between hydrogen radical and hydrogen iodide at a total pressure of 10 Torr: $\text{H}\cdot + \text{HI} \rightarrow \text{H}_2^* + \text{I}\cdot$. A limited number of lines in Q_4 branch ($v=4\leftarrow 3$) and a few lines in Q_5 branch ($v=5\leftarrow 4$) were measured by the CARS technique in this work. The authors¹²¹ did not pursue high accuracy and the absolute uncertainty of measured wavenumbers is only 0.05 cm^{-1} .

Table 5-1. Wavenumbers (cm^{-1}) of lines in Q branches of $^1\text{H}_2$ from the literature^a.

J	Q ₁ (J)	Q ₂ (J)	Q ₃ (J)	Q ₄ (J)	Q ₅ (J)
0	4161.161 ± 0.009 ^b	8087.03* ± 0.03 ^c			
1	4155.25469 ± 0.00008 ^c	8075.3114* ± 0.0006 ^c		3462.38 [†] ± 0.05 ^f	
2	4143.4660 ± 0.0003 ^c	8051.991* ± 0.007 ^c			
3	4125.8739 ± 0.0004 ^c	8017.19* ± 0.01 ^c	3661.51 ± 0.05 ^f	3434.19 ± 0.05 ^f	
4	4102.582 ± 0.004 ^c		3639.11 ± 0.05 ^f		
5	4073.74 ± 0.03 ^d		3611.11 ± 0.05 ^f	3384.26 [†] ± 0.05 ^f	3157.59 ± 0.05 ^f
6	4039.45 ± 0.03 ^e		3577.79 ± 0.05 ^f		
7	4000.46 [†] ± 0.05 ^f		3539.82 ± 0.05 ^f	3313.46 [†] ± 0.05 ^f	3086.21 [†] ± 0.05 ^f
8			3496.90 ± 0.05 ^f	3270.42 ± 0.05 ^f	
9	3906.66 ± 0.05 ^f	3676.51 ± 0.05 ^f	449.14 [†] ± 0.05 ^f	3222.86 ± 0.05 ^f	2995.07 ± 0.05 ^f
10	3853.12 ± 0.05 ^f	3623.64 ± 0.05 ^f	3396.91 ± 0.05 ^f		
11	3795.10 [†] ± 0.05 ^f	3566.58 [†] ± 0.05 ^f	3340.35 ± 0.05 ^f		
12	3733.19 ± 0.05 ^f	3505.74 ± 0.05 ^f	3279.87 ± 0.05 ^f		
13		3440.85 ± 0.05 ^f	3215.07 ± 0.05 ^f	2987.85 ± 0.05 ^f	
14		3372.31 ± 0.05 ^f			
15	3525.91 [†] ± 0.05 ^f	3300.74 ± 0.05 ^f			
17	3371.81 ± 0.05 ^f	3147.31 ± 0.05 ^f			
18	3290.79 ± 0.05 ^f				

^a From various sources the most accurate data are selected. Overtone transitions from the ground state are marked with *, and symbol [†] indicates data points not included in the analysis.

^b Jennings *et al.*¹¹⁵

^c Bragg *et al.*¹⁰³

^d Jennings *et al.*¹¹⁴

^e Veirs *et al.*¹¹⁸

^f Germann *et al.*¹²¹

Table 5-2. Wavenumbers (cm^{-1}) of lines in S and O branches of $^1\text{H}_2$ from the literature^a.

J	$S_0(\text{J})$	$S_1(\text{J})$	$O_1(\text{J})$	
0	354.3735 ± 0.0004^b	4497.8391 ± 0.0002^d		
1	587.03211 ± 0.00017^b	4712.9054 ± 0.0002^d		
2	814.42473 ± 0.00008^b	4917.0069 ± 0.0003^d	3806.86 ± 0.03^e	
3	1034.67024 ± 0.00003^b	5108.4040 ± 0.0006^d	3568.24 ± 0.03^e	
4	1246.09811 ± 0.00017^b	5285.63 ± 0.03^e	3329.14 ± 0.03^e	
5	1447.2788 ± 0.0004^b	$5448.04^\dagger \pm 0.03^e$	3091.14 ± 0.03^e	
6	1637.01 ± 0.05^c			
7	1814.50 ± 0.06^c			
9	2130.102 ± 0.004^c			
	$S_2(\text{J})^*$	$O_2(\text{J})^*$	$S_4(\text{J})^*$	$S_5(\text{J})^*$
0	8406.365 ± 0.002^d		15535.7441 ± 0.0056^f	18907.516 ± 0.004^f
1	8604.2189 ± 0.0008^d		15699.801 ± 0.003^f	
2	8785.529 ± 0.006^d	7732.63 ± 0.01^d		
3		7488.28 ± 0.02^d		

^a From various sources the most accurate data are selected. Overtone transitions from the ground state are marked with * and the symbol \dagger indicates data points not included in the analysis. The $S_0(\text{J})$ lines are purely rotational transitions within vibrational state $v=0$.

^b Jennings *et al.*¹⁰⁷

^c Jennings *et al.*¹¹⁴

^d Bragg *et al.*¹⁰³

^e Veirs *et al.*¹¹⁸

^f Ferguson *et al.*¹⁰⁵

A few very accurate low J-number spectral measurements for S- and O-branch overtones of H₂ are also available in the literature from two publications: Bragg *et al.*¹⁰³ and Ferguson *et al.*¹⁰⁵. In both studies quadrupole absorption was measured in a multiple-pass cell at a high pressure of gas (~ 1-4 atm) and room temperature.

Purely rotational S₀ transitions of H₂ as well as of D₂ were comprehensively investigated by Jennings and co-workers. In their studies this group utilized FT quadrupole absorption measurements^{107,108} (H₂ only) in the ~0.5 - 2 atm pressure range and FT Raman scattering at room temperature¹¹⁵ (250 - 600 Torr) and in flames¹¹⁴ (H₂ and D₂). They found no inconsistencies in wavenumbers of the same lines obtained with different methods; however higher purely rotational levels (J"≥6) were accessible only for measurements in a flame¹¹⁴. Purely rotational S₀ transitions of H₂ and D₂ were also investigated by Stoicheff *et al.*¹¹⁷ (J"≤3 of H₂; J"≤4 of D₂) and Veirs *et al.*¹¹⁸ (J"≤5 of H₂; J"≤8 of D). Although their data agree with those of Jennings *et al.*^{107,108,114,115}, the latter is much more accurate; the best subset of these results is shown in Table 5-2 and Table 5-3.

For vibration-rotational transitions of D₂ there is only limited spectral information. Besides fundamental Q₁^{109,114-118,122,127}, and S₁ / O₁^{109,115,118,127} branches only a few Q₂ overtone lines¹¹⁸ with large uncertainty in wavenumbers are available in the literature. The most accurate fundamental Q-, S- and O-branch data were obtained in a quadrupole absorption study of D₂ lines with low J-numbers by McKellar *et al.*¹⁰⁹. Wavenumbers of transitions with higher J-numbers are measured with much larger uncertainty by Brannon *et al.*¹²⁷ (electric field induced absorption) and Veirs *et al.*¹¹⁸ (linear Raman scattering). Reported data from the different sources do not contradict each other. The best results in terms of uncertainty in wavenumbers of these measurements appear in Table 5-3.

Table 5-3. Wavenumbers (cm^{-1}) of lines in Q, S and O branches of $^2\text{H}_2$ from the literature^a.

J	$S_0(\text{J})$	$Q_1(\text{J})$	$S_1(\text{J})$	$O_1(\text{J})$	$Q_2(\text{J})^*$
0	179.068 ± 0.002^b	2993.60 ± 0.02^d	3166.360 ± 0.004^e	2814.546 ± 0.004^e	5868.1 ± 0.1^f
1	297.533 ± 0.003^b	2991.504 ± 0.004^e	3278.522 ± 0.004^e	2693.972 ± 0.004^e	5863.9 ± 0.1^f
2	414.648 ± 0.002^b	2987.296 ± 0.004^e	3387.261 ± 0.005^e	2572.643 ± 0.005^e	5855.6 ± 0.1^f
3	529.900 ± 0.004^b	2980.988 ± 0.004^e	3492.091 ± 0.004^e	2451.05 ± 0.07^f	5843.0 ± 0.1^f
4	642.806 ± 0.004^b	2972.613 ± 0.005^e			5826.3 ± 0.1^f
5	752.900 ± 0.012^c	2962.18 ± 0.04^d	3688.36 ± 0.07^f	2209.23 ± 0.07^f	
6	859.815 ± 0.005^c	2949.69 ± 0.04^d			
7	963.159 ± 0.014^c	2935.2 ± 0.1^f	3863.82 ± 0.07^f		
8	1062.634 ± 0.012^c	2918.8 ± 0.1^f			
9	1157.99 ± 0.03^c	2900.6 ± 0.1^f			
10	$1248.88^\dagger \pm 0.03^c$				
11	$1335.32^\dagger \pm 0.09^c$				
12	$1417.98^\dagger \pm 0.09^c$				

^a From various sources the most accurate data are selected. Overtone transitions from the ground state are marked with * and the symbol \dagger indicates data points not included in the analysis. The $S_0(\text{J})$ lines are purely rotational transitions within vibrational state $v=0$.

^b Jennings *et al.*¹¹⁵

^c Jennings *et al.*¹¹⁴

^d Brannon *et al.*¹²⁷

^e McKellar *et al.*¹⁰⁹

^f Veirs *et al.*¹¹⁸

Unlike D_2 , for the mixed isotope HD spectral information for many transitions has been published (see Table 5-4). However, fewer research groups contributed to this information^{110,112,117,118}, hence a basis for data comparison does not exist, except for fundamental Q-branch lines^{117,118}, where no controversy between the two reported results was found. In their linear Raman scattering experiments, Stoicheff *et al.*¹¹⁷ obtained for a few J values purely rotational S-branch and fundamental Q-branch transition wavenumbers with limited accuracy. The first three lines of the fundamental S branch have been accurately determined in the study of McKellar and co-workers¹¹² by FT room temperature measurements of quadrupole absorption at a relatively low pressure of 0.6 atm. In the same study some fundamental P- and R-branch lines were also observed. We note that no systematic pressure shift measurements were made by these authors¹¹² and, consequently, no corrections to the line positions were applied. However, they believe that the value of such a pressure shift is on average of the order of absolute uncertainty of their measurements, 0.001 cm^{-1} . In earlier work of McKellar *et al.*¹¹⁰, various P- and R-branch overtone lines were determined by measurement of electric dipole absorption at 1 atm and room temperature (see Table 5-4). These authors made estimates of pressure shift coefficients for HD overtones based on the experimental literature value ($-0.0023 \text{ cm}^{-1} / \text{amagat}$)¹³² for fundamental transitions. However, the reported wavenumbers were not corrected to zero pressure. Both articles^{110,112} lack any explicit justification of the claimed accuracy in wavenumbers.

Some spectral information for tritium T_2 and its mixed isotopes (HT and DT) is also available in the literature from a few sources^{113,118-120,130}. The most accurate data are

Table 5-4. Wavenumbers (cm^{-1}) of lines in Q, S, R and P branches of $^1\text{H}^2\text{H}$ from the literature^a.

J	$S_0(\text{J})$	$Q_1(\text{J})$	$S_1(\text{J})$	$R_1(\text{J})$	$P_1(\text{J})$
0	267.09 ± 0.02^b	3632.06 ± 0.05^b	3887.683 ± 0.001^d	3717.532 ± 0.001^d	
1	443.08 ± 0.02^b	$3628.20^\dagger \pm 0.02^b$	4052.196 ± 0.001^d	3798.455 ± 0.001^d	3542.932 ± 0.001^d
2	616.09 ± 0.02^b	$3620.51^\dagger \pm 0.02^b$	4209.963 ± 0.001^d	3874.357 ± 0.001^d	3450.463 ± 0.001^d
3	784.99 ± 0.02^b	$3608.99^\dagger \pm 0.02^b$		3944.720 ± 0.001^d	3355.361 ± 0.001^d
4	948.82 ± 0.02^b			4009.088 ± 0.001^d	
5		3574.9 ± 0.1^c		4067.066 ± 0.001^d	
	$R_3(\text{J})^*$	$P_3(\text{J})^*$	$R_4(\text{J})^*$	$P_4(\text{J})^*$	
0	10445.490 ± 0.007^c		13551.065 ± 0.007^c		
1	10511.443 ± 0.007^c	10278.378 ± 0.007^c	13609.664 ± 0.007^c	13387.646 ± 0.007^c	
2	10564.986 ± 0.007^c	10178.413 ± 0.007^c	13652.215 ± 0.007^c	13283.993 ± 0.007^c	
3	10605.680 ± 0.007^c	10068.365 ± 0.007^c	13678.322 ± 0.007^c	13166.558 ± 0.007^c	
4	10633.213 ± 0.007^c		13687.715 ± 0.007^c		
	$R_5(\text{J})^*$	$P_5(\text{J})^*$	$R_6(\text{J})^*$	$P_6(\text{J})^*$	
0	16486.54 ± 0.02^c		19252.04 ± 0.010^c		
1	16537.84 ± 0.02^c	16326.79 ± 0.02^c	19295.96 ± 0.010^c	19095.99 ± 0.02^c	
2	16569.40 ± 0.02^c	16219.47 ± 0.02^c	19316.54 ± 0.010^c		
3	$16581.01^\dagger \pm 0.02^c$		19313.51 ± 0.010^c		

^a From various sources the most accurate data are selected. Overtone transitions from the ground state are marked with * and the symbol \dagger indicates data points not included in the analysis. The $S_0(\text{J})$ lines are purely rotational transitions within vibrational state $v=0$.

^b Stoicheff *et al.*¹¹⁷

^c Veirs *et al.*¹¹⁸

^d Rich *et al.*¹¹²

^e McKellar *et al.*¹¹⁰

shown in Table 5-5 (T_2 , DT) and Table 5-6 (HT). It should be noted, however, that none of these values was corrected to zero pressure and no estimations of pressure shift coefficients for these isotopes were reported. Such a correction is probably irrelevant for the data of Veirs *et al.*¹¹⁸ due to large absolute uncertainty of their measurements, but is essential for the cases when high accuracy of wavenumbers is claimed (see above mentioned tables).

Edwards *et al.*^{119,120} and Veirs *et al.*¹¹⁸ used linear Raman scattering to study T_2 and DT isotopes (pressure range 500-700 Torr). Linear Raman scattering of DT at ~500 Torr also was measured by Barefield and his co-workers¹¹³. Wavenumbers of lines in the fundamental Q branch and purely rotational S branch for TT and DT molecules reported by Edwards *et al.*^{119,120} generally agree with those of Veirs and his co-workers¹¹⁸ within ~2-3 combined uncertainties of their measurements, however, data presented in the former works^{119,120} are systematically lower than those in the latter¹¹⁸. As follows from Table 5-5, only purely rotational S-branch and fundamental Q-branch transition are known for T_2 and DT molecules, for which lines with higher J values are measured with the relatively large absolute uncertainty of 0.1 cm^{-1} .

The literature spectral data set for the HT isotope is larger than that of T_2 and DT (see Table 5-6). Besides purely rotational S-branch and fundamental Q-branch transitions, fundamental and overtone P- and R-branch wavenumbers were determined with generally high accuracy by electric dipole absorption measurements at 600 Torr of pressure¹³⁰. However, as was mentioned before, these wavenumbers were not corrected to zero pressure. There also exists a large discrepancy of 6 cm^{-1} between fundamental Q-branch data reported by Veirs *et al.*¹¹⁸ and Edwards *et al.*¹¹⁹, i.e. the wavenumbers for the same

Table 5-5. Wavenumbers (cm^{-1}) of lines in Q and S branches of $^3\text{H}_2$ and $^2\text{H}^3\text{H}$ from the literature^a.

J	$^3\text{H}_2$		$^2\text{H}^3\text{H}$	
	$S_0(\text{J})$	$Q_1(\text{J})$	$S_0(\text{J})$	$Q_1(\text{J})$
0	120.049 [†] ± 0.005 ^b	2464.320 ± 0.005 ^b	149.604 ± 0.005 ^d	2743.436 [†] ± 0.005 ^d
1	199.695 [†] ± 0.005 ^b	2463.155 ± 0.005 ^b	248.713 ± 0.005 ^d	2741.813 ± 0.005 ^d
2	278.732 ± 0.005 ^b	2460.822 ± 0.005 ^b	346.866 ± 0.005 ^d	2738.579 ± 0.005 ^d
3	356.954 [†] ± 0.005 ^b	2457.339 ± 0.005 ^b	443.723 ± 0.005 ^d	2733.787 ± 0.005 ^d
4	434.1 ± 0.1 ^c	2452.725 ± 0.005 ^b		2727.448 [†] ± 0.005 ^d
5	510.0 ± 0.1 ^c	2447.021 ± 0.005 ^b		2719.2 ± 0.1 ^c
6	584.3 ± 0.1 ^c	2440.5 ± 0.1 ^c		2709.8 ± 0.1 ^c
7	657.0 [†] ± 0.1 ^c	2432.5 ± 0.1 ^c		2698.5 [†] ± 0.1 ^c
8	727.8 ± 0.1 ^c	2423.5 ± 0.1 ^c		2686.3 ± 0.1 ^c
9	796.7 ± 0.1 ^c	2413.2 ± 0.1 ^c		
10	863.2 ± 0.1 ^c	2402.2 ± 0.1 ^c		
11	927.8 [†] ± 0.1 ^c			

^a From various sources the most accurate data are selected. The symbol [†] indicates data points not included in the analysis. The $S_0(\text{J})$ lines are purely rotational transitions within vibrational state $v=0$.

^b Edwards *et al.*¹²⁰

^c Veirs *et al.*¹¹⁸

^d Edwards *et al.*¹¹⁹

Table 5-6. Wavenumbers (cm^{-1}) of lines in Q, S, R and P branches of $^1\text{H}^3\text{H}$ from the literature^a.

J	$S_0(\text{J})$	$Q_1(\text{J})$	$R_1(\text{J})$	$P_1(\text{J})$
0	237.927 ± 0.005^b	3434.9 ± 0.1^c	3511.020 ± 0.010^d	
1	394.952 ± 0.005^b	3431.6 ± 0.1^c	3583.530 ± 0.010^d	3355.355 ± 0.010^d
2	549.670 ± 0.005^b	3425.1 ± 0.1^c	3651.870 ± 0.010^d	3273.140 ± 0.010^d
3		3415.6 ± 0.1^c	3715.630 ± 0.010^d	
4		3402.8 ± 0.1^c	3774.450 ± 0.010^d	
	$R_4(\text{J})^*$	$P_4(\text{J})^*$	$R_5(\text{J})^*$	$P_5(\text{J})^*$
0	12868.786 ± 0.005^d		15682.984 ± 0.005^d	
1	12922.534 ± 0.005^d	12722.515 ± 0.007^d	15730.589 ± 0.005^d	15539.796 ± 0.010^d
2	12962.825 ± 0.005^d		15761.691 ± 0.005^d	15445.118 ± 0.010^d
3	12989.369 ± 0.005^d		15776.009 ± 0.010^d	
4	13001.917 ± 0.007^d			

^a From various sources the most accurate data are selected. Overtone transitions from the ground state are marked with *. The $S_0(\text{J})$ lines are purely rotational transitions within vibrational state $v=0$.

^b Edwards *et al.*¹¹⁹

^c Veirs *et al.*¹¹⁸

^d Chuang *et al.*¹³⁰

lines from the latter source are systematically lower than those from the former. Analysis of the data indicates that measurements of Edwards *et al.*¹¹⁹ are suspect (see section 5.3).

5.3. Analysis of the experimental literature data

To estimate consistency between spectral data on hydrogen isotopes available in the literature from the different sources and discussed in the previous section 5.2, we subjected them to the analysis similar to that applied to our experimental results on nitrogen isotopes $^{14}\text{N}_2$ and $^{15}\text{N}_2$ (see section 4.3.2 on p. 87). For our fits, we used not only the best data on hydrogen summarized in Tables 5-1 through 5-6, but all available accurate spectral information (absolute uncertainty $\leq 0.1 \text{ cm}^{-1}$). Weights of individual lines $1/s^2$ in these fits were based on the absolute uncertainties s reported by original authors. It should be noted, however, that in certain cases the accuracy of these values was not properly justified or even explained^{110,112}.

5.3.1. Determination of coefficients Y_{kl} for each isotope

The first step of our analysis was a fit of vibration-rotational transition wavenumbers for each hydrogen isotopic variant with the Dunham expression (2.51). This allowed us to single out several outliers (points with normalized residuals greater than 3-4 units), which on average accounted for about 12-13% of all data points. Such outliers are marked with symbol † in the tables of the previous section 5.2 and were eliminated in the final fit of each isotope. Sets of significant coefficients Y_{kl} resulted from these fits are shown in Table 5-7 and Table 5-8.

Table 5-7. Parameters Y_{kl} (cm^{-1}) for $^1\text{H}_2$, $^1\text{H}^2\text{H}$ and $^2\text{H}_2$ ^a.

k	l	Parameter	$^1\text{H}_2$	$^1\text{H}^2\text{H}$	$^2\text{H}_2$
1	0	ω_e	4402.9857 ± 0.0085	3814.050 ± 0.015	3112.633 ± 0.048
2	0	$-\omega_e x_e$	-123.0893 ± 0.0076	-92.388 ± 0.011	-59.511 ± 0.024
3	0	$\omega_e y_e$	1.4661 ± 0.0025	0.9591 ± 0.0029	
4	0	$\omega_e z_e / 10^{-2}$	-8.090 ± 0.025	-4.598 ± 0.023	
0	1	B_e	60.84592 ± 0.00012	45.64913 ± 0.00032	30.44009 ± 0.00026
1	1	$-\alpha_e$	-3.04666 ± 0.00029	-1.98060 ± 0.00054	-1.05476 ± 0.00032
2	1	$\gamma_e / 10^{-2}$	4.983 ± 0.019	2.841 ± 0.024	
3	1	$\delta_e / 10^{-3}$	-3.801 ± 0.035	-1.872 ± 0.028	
0	2	$-D_e / 10^{-2}$	-4.64813 ± 0.00064	-2.6104 ± 0.0016	-1.15803 ± 0.00071
1	2	$-\beta_e / 10^{-3}$	1.6114 ± 0.0057	0.783 ± 0.021	0.2416 ± 0.0087
2	2	$\beta'_e / 10^{-5}$	-4.33 ± 0.19	-2.23 ± 0.45	
0	3	$H_e / 10^{-5}$	4.924 ± 0.020	1.888 ± 0.036	0.5431 ± 0.0035
1	3	$h_e / 10^{-7}$	-8.67 ± 0.18		
2	3	$h'_e / 10^{-8}$	-2.58 ± 0.65		
0	4	$L_e / 10^{-8}$	-6.03 ± 0.28		
0	5	$M_e / 10^{-1}$	5.0 ± 1.2		
Range			$0 \leq v \leq 5$	$0 \leq v \leq 6$	$0 \leq v \leq 2$
σ^b			1.70	1.33	1.06
S^c			0.072	0.032	0.051

^a All accurate literature data with an absolute uncertainty not greater than 0.1 cm^{-1} were used to obtain these parameters. Uncertainties in coefficients Y_{kl} correspond to one standard deviation.

^b Normalized standard deviation (no units).

^c Absolute standard deviation (cm^{-1}).

Table 5-8. Parameters Y_{kl} (cm^{-1}) for $^3\text{H}_2$ and $^2\text{H}^3\text{H}^a$.

k	l	Parameter	$^3\text{H}_2$	$^2\text{H}^3\text{H}$
1	0	ω_e	2464.3085 ± 0.0084	2743.4234 ± 0.0090
0	1	B_e	20.3246 ± 0.0010	25.4045 ± 0.0075
1	1	$-\alpha_e$	-0.58163 ± 0.00088	-0.8050 ± 0.0013
0	2	$-D_e / 10^{-2}$	-0.4870 ± 0.0018	-0.922 ± 0.022
1	2	$-\beta_e / 10^{-3}$	0.171 ± 0.020	0.150 ± 0.036
Range			$0 \leq v \leq 1$	$0 \leq v \leq 1$
σ^b			2.11	1.45
S^c			0.19	0.41

^a All accurate literature data with an absolute uncertainty not greater than 0.1 cm^{-1} were used to obtain these parameters. Uncertainties in coefficients Y_{kl} correspond to one standard deviation. For the $^2\text{H}^3\text{H}$ molecule it was not possible to obtain a reasonable fit (see text).

^b Normalized standard deviation (no units).

^c Absolute standard deviation (cm^{-1}).

The largest set, sixteen parameters, was obtained for the common H₂ molecule. However, it also has large normalized and absolute uncertainties: $\sigma=1.70$ and $S=0.072$ cm⁻¹, respectively. The analysis of residuals of individual lines shows that the main contributor to them is the considerable scatter of the data reported by Germann and Valentini¹²¹. It should be mentioned that this scatter is random and no systematic deviations from the fit were observed. We note that this article¹²¹ is the only source in the literature for wavenumbers of Q-branch lines with high quantum numbers J in the fundamental band and lines in hot bands of H₂ (see Table 5-7), hence it is not sensible to exclude them from the analysis data set.

For the HD molecule, twelve coefficients Y_{kl} proved to be significant (see Table 5-7). In our analysis, data reported by McKellar *et al.*¹¹⁰ were corrected to zero pressure using pressure shift coefficients calculated by these authors¹¹⁰ (see discussion on p. 112). Accordingly, we applied red shifts to their data as follows: -0.0069 cm⁻¹ for $\nu=3\leftarrow 0$ transitions, -0.0092 cm⁻¹ for $\nu=4\leftarrow 0$ transitions, -0.0115 cm⁻¹ for $\nu=5\leftarrow 0$ transitions and -0.0138 cm⁻¹ for $\nu=6\leftarrow 0$ transitions. Although in our fit of the HD spectral data we did not notice any major anomalies, wavenumbers of lines in higher overtone P and R branches ($\nu=4\leftarrow 0$; $\nu=5\leftarrow 0$; $\nu=6\leftarrow 0$) published by McKellar *et al.*¹¹⁰ are systematically higher than those calculated using coefficients Y_{kl} . A possible reason is an underestimation of pressure shifts for these transitions. The normalized and absolute standard errors for HD ($\sigma=1.33$ and $S=0.032$ cm⁻¹) are better than those for H₂ molecule.

We obtained only seven significant parameters Y_{kl} for the D₂ spectral data, but the corresponding fit has the smallest normalized standard error (1.06) among all analyzed isotopic variants (see Table 5-7 and Table 5-8). It should be noted that among outliers we

had to eliminate from our analysis wavenumbers of lines with higher J'' values (10, 11 and 12) in purely rotational S-branch transitions reported by Jennings *et al.*¹¹⁴. These are the only data with such high J -values reported for the D_2 molecule.

Spectral information for tritium containing isotopes T_2 and DT is available in the literature only for a very limited range of quantum number v : $0 \leq v \leq 1$ (see Table 5-5). The consequence of this fact was that only five coefficients Y_{kl} could be determined, among which only one purely vibrational coefficient Y_{10} was statistically meaningful (see Table 5-8). Absolute standard errors are large for both isotopes: 0.19 cm^{-1} for T_2 and 0.41 cm^{-1} for DT. Fit of the T_2 spectral data gave the largest normalized uncertainty (2.11) among all analyzed hydrogen isotopes.

We were not able to obtain a sensible fit for the HT isotope: the normalized standard error was of the order of 200 units. The discrepancy between the data reported by Veirs *et al.*¹¹⁸ and Edwards *et al.*¹¹⁹ (see discussion on p. 114) proved not to be a reason for this; attempts to eliminate from our fits either data set did not solve the problem. Although, for the HT molecule, the v -number range covered by the literature data is larger than in case of T_2 and DT ($v=0, 1, 4, 5$), the range of J -numbers is small ($0 \leq J'' \leq 4$). In addition, the available wavenumbers of HT transitions were not corrected to zero pressure. As a result there is not enough good data to perform a reasonable individual fit for this molecule. However, we used some of the HT data for our global fits (see section 5.3.2 below).

5.3.2. Determination of coefficients U_{kl} and Δ_{kl}

In the second step of our analysis we fitted all transition wavenumbers of hydrogen isotopes analyzed in the above individual fits using expression (2.76), with coefficients Δ_{kl} omitted, to obtain a set of mass independent coefficients U_{kl} of hydrogen isotopes. Such a global fit showed that the HT wavenumbers in the fundamental Q branch reported by Edwards *et al.*¹¹⁹ were systematically and significantly lower than those calculated using coefficients U_{kl} . The absolute value of this offset (6 cm^{-1}) was exactly equal to the discrepancy between data reported by these authors¹¹⁹ and data published by Veirs *et al.*¹¹⁸ (see discussion on p. 114). Data presented in the latter article¹¹⁸ did not show any systematic deviations from the fit, hence we concluded that line positions in the fundamental Q branch of HT measured by Edwards *et al.*¹¹⁹ are inaccurate, and excluded them from the subsequent global fits. This elimination considerably reduced the normalized and absolute standard errors (from ~ 157 down to 35 units and from 0.97 down to 0.43 cm^{-1} , respectively), and increased the number of significant coefficients U_{kl} from 13 to 15. However, in view of such abnormally high errors compared to these of the individual fits (see Table 5-7 and Table 5-8), the global fit is still considered unacceptable.

In the third step of the analysis we performed a fit of the hydrogen spectral data using equation (2.76) without modifications, i.e. parameters Δ_{kl} were not omitted. As it was mentioned before, the latter parameters account for all extramechanical effects as well as for higher order terms in the expression (2.74). In addition to the previously mentioned 15 coefficients U_{kl} , four more parameters proved to be significant: Δ_{10} , Δ_{20} , Δ_{30} and Δ_{01} . Inclusion of these parameters greatly decreased normalized and absolute standard errors to

4.9 and 0.096 cm^{-1} , respectively (see Table 5-9; data set I). Data points corresponding to wavenumbers reported by Edwards *et al.*^{119,120} for T_2 and DT contribute most to normalized error as judged by residuals for individual lines. These wavenumbers are consistently lower than those calculated using coefficients U_{kl} and Δ_{kl} on average by 0.15 cm^{-1} . As mentioned before (see p. 114) data of Edwards and co-workers^{119,120} for T_2 and DT were also systematically below those reported by Veirs *et al.*¹¹⁸. Elimination of the former data^{119,120} from the fit gave a normalized standard error 1.72, an absolute standard error 0.074 cm^{-1} , and the same set of parameters U_{kl} and Δ_{kl} as shown in Table 5-9 (data set II). The relative decrease in the absolute standard error is much smaller than that in the normalized standard error. This fact indicates that wavenumbers of Edwards *et al.*^{119,120} for T_2 and DT molecules are not significantly inaccurate, but their absolute uncertainties are most likely considerably underestimated. For data set II a relatively large random scatter of residuals (difference between calculated and experimental values) was observed for points corresponding to wavenumbers reported by Germann *et al.*¹²¹ (fundamental and hot band Q-branch lines of H_2 ; see Table 5-1), by Ferguson *et al.*¹⁰⁵ (some S- and O-branch overtones for H_2 ; see Table 5-2), by Chuang *et al.*¹³⁰ (fundamental and overtone P and R transitions for HT; see Table 5-6) and Veirs *et al.*¹¹⁸ (different transitions and isotopes shown in Tables 5-1 through 5-6).

5.3.3. Determination of coefficients c , u , t , s

An attempt was made to perform a constrained fit of spectral data in set II with the model (2.70) to obtain coefficients c_j , u_j , t_j and s_j and hence to determine adiabatic and

Table 5-9. Parameters U_{kl} ($\text{cm}^{-1}\text{u}^{k/2+l}$) for hydrogen isotopes^a.

k	l	parameter	Data set I ^b	Data set II ^c
1	0	ω_e	3126.024 ± 0.079	3126.710 ± 0.035
		$\Delta_{1,0}$ /10 ⁻¹	-4.509 ± 0.10676	-4.292 ± 0.039
2	0	$-\omega_e x_e$	-61.269 ± 0.074	-61.870 ± 0.032
		$\Delta_{2,0}$ /10 ⁻¹	-4.391 ± 1.90461	-9.15 ± 0.69
3	0	$\omega_e y_e$ /10 ⁻¹	2.74 ± 0.24	4.57 ± 0.10
		$\Delta_{3,0}$	15.782 ± 4.99733	-2.6 ± 1.1
4	0	$\omega_e z_e$ /10 ⁻²	1.26 ± 0.32	-1.12 ± 0.14
5	0	$\omega_e z_e'$ /10 ⁻³	-1.61 ± 0.16	-0.459 ± 0.066
0	1	B_e	30.66800 ± 0.00046	30.66772 ± 0.00017
		$\Delta_{0,1}$	-2.09 ± 0.13	-2.036 ± 0.047
1	1	$-\alpha_e$	-1.09001 ± 0.00023	-1.089804 ± 0.000083
2	1	γ_e /10 ⁻²	1.270 ± 0.010	1.2608 ± 0.0037
3	1	δ_e /10 ⁻⁴	-6.82 ± 0.12	-6.7226 ± 0.0423
0	2	$-D_e$ /10 ⁻²	-1.17994 ± 0.00016	-1.179928 ± 0.000057
1	2	$-\beta_e$ /10 ⁻⁴	2.936 ± 0.014	2.9334 ± 0.0049
2	2	$-\beta'_e$ /10 ⁻⁶	-6.43 ± 0.15	-6.406 ± 0.054
0	3	H_e /10 ⁻⁶	6.202 ± 0.011	6.2023 ± 0.0040
1	3	h_e /10 ⁻⁸	-8.46 ± 0.16	-8.424 ± 0.059
0	4	L_e /10 ⁻⁹	-3.135 ± 0.028	-3.136 ± 0.010
σ^d			4.86	1.72
S^e			0.095	0.074

^a Reduced masses used: for H $\mu = 1.0078250319$ u; for D $\mu = 2.0141017779$ u; for T $\mu = 3.0160492677$ u. Coefficients Δ_{kl} have no units; the mass of electron used in their calculation is $5.485799 \cdot 10^{-4}$ u. Uncertainties in coefficients correspond to one standard deviation.

^b All literature data excluding HT wavenumbers from Edwards *et al.*¹¹⁹ (see text).

^c All literature data excluding all wavenumbers from Edwards *et al.*^{119,120} (see text).

^d Normalized standard error (no units).

^e Absolute standard deviation (cm^{-1}).

nonadiabatic effects but this proved to be unsuccessful. Due to random error in experimental data, no convergence in the regression was achieved for different sets of coefficients. For this fit we used program *Radiatom*⁶³, which was also employed in the analogous analysis of our nitrogen data.

5.3.4. Results of theoretical studies of extramechanical effects

Although we could not separately evaluate adiabatic and nonadiabatic effects from the data available in the literature for hydrogen isotopes, we were able to estimate changes in energy levels due to the combined effect of all extramechanical corrections to the Dunham model, which is based on the Born-Oppenheimer approximation, using coefficients Δ_{ki} derived in the course of our analysis. Since for hydrogen, there is a lot of work published on theoretical calculations of these corrections, it was interesting to compare the results of our analysis of experimental data and those of theoretical studies. The overwhelming majority of the theoretical work has been restricted to calculations of corrections to the potential-energy curve derived from the Born-Oppenheimer approximation. In Figure 5-1 we show the most recent result in this field¹³³. These corrections are very small on the scale of the overall potential-energy curve (note that the former are multiplied by 1000 in the figure). Besides these adiabatic corrections, the figure displays the relativistic corrections as well. The latter makes up for the fact that the Schrodinger equation used to obtain the Born-Oppenheimer potential does not take into account the relativistic mass effect of the electron arising from its high speed (comparable to that of light). As seen in the figure,

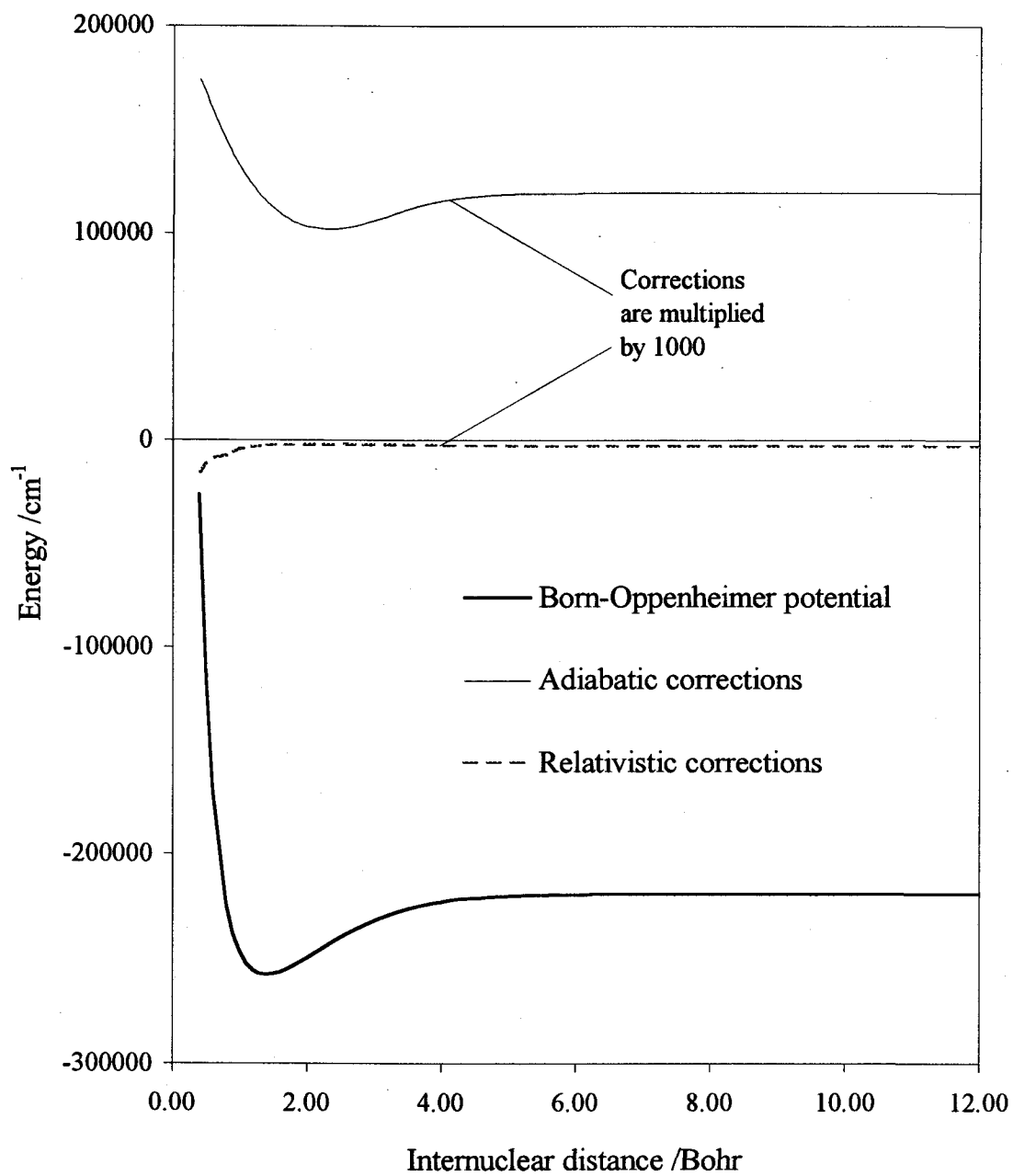


Figure 5-1. Born-Oppenheimer potential-energy curve for ${}^1\text{H}_2$ molecule and adiabatic and relativistic corrections to it¹³³.

the relativistic term is small compared to the adiabatic corrections. It also has a negligible effect on vibration-rotational energy¹³⁴ and is mentioned only for completeness sake.

In contrast, adiabatic and nonadiabatic corrections make a considerable difference in the energy levels of hydrogen. It is important to note that the nonadiabatic term is kinetic in origin and does not contribute to the potential energy; it does, however, affect directly the molecular energy levels. Figure 5-2 illustrates changes in energies of purely vibrational levels ($J=0$) due to adiabatic¹³⁵ and nonadiabatic¹³⁶ corrections derived from *ab initio* calculations, as well as their combined effect (total extramechanical corrections). In the same figure we also show the energy changes due to total extramechanical effects derived from experimental measurements. These were calculated using coefficients Δ_{kl} determined in the analysis of the literature data for hydrogen isotopes (Table 5-9, set II) described above in section 5.3.2. Although the sign, the order, and the overall trend in energy corrections due to combined adiabatic and nonadiabatic effects is similar for experiment and theory, there is an obvious offset between them. The absolute values of theoretical corrections are approximately from 5 cm^{-1} ($v=0$ level) to 11 cm^{-1} ($v=8$ level) larger than those based on experiment. The corresponding discrepancy in corrections to the (rotationless) vibrational wavenumbers increases from 0.5 cm^{-1} for the fundamental Q branch to 2 cm^{-1} for $v=8 \leftarrow 7$ transition. Which part of this discrepancy is due to inconsistency in experimental data from the different studies and which is due to inaccuracy in *ab initio* results remains to be seen.

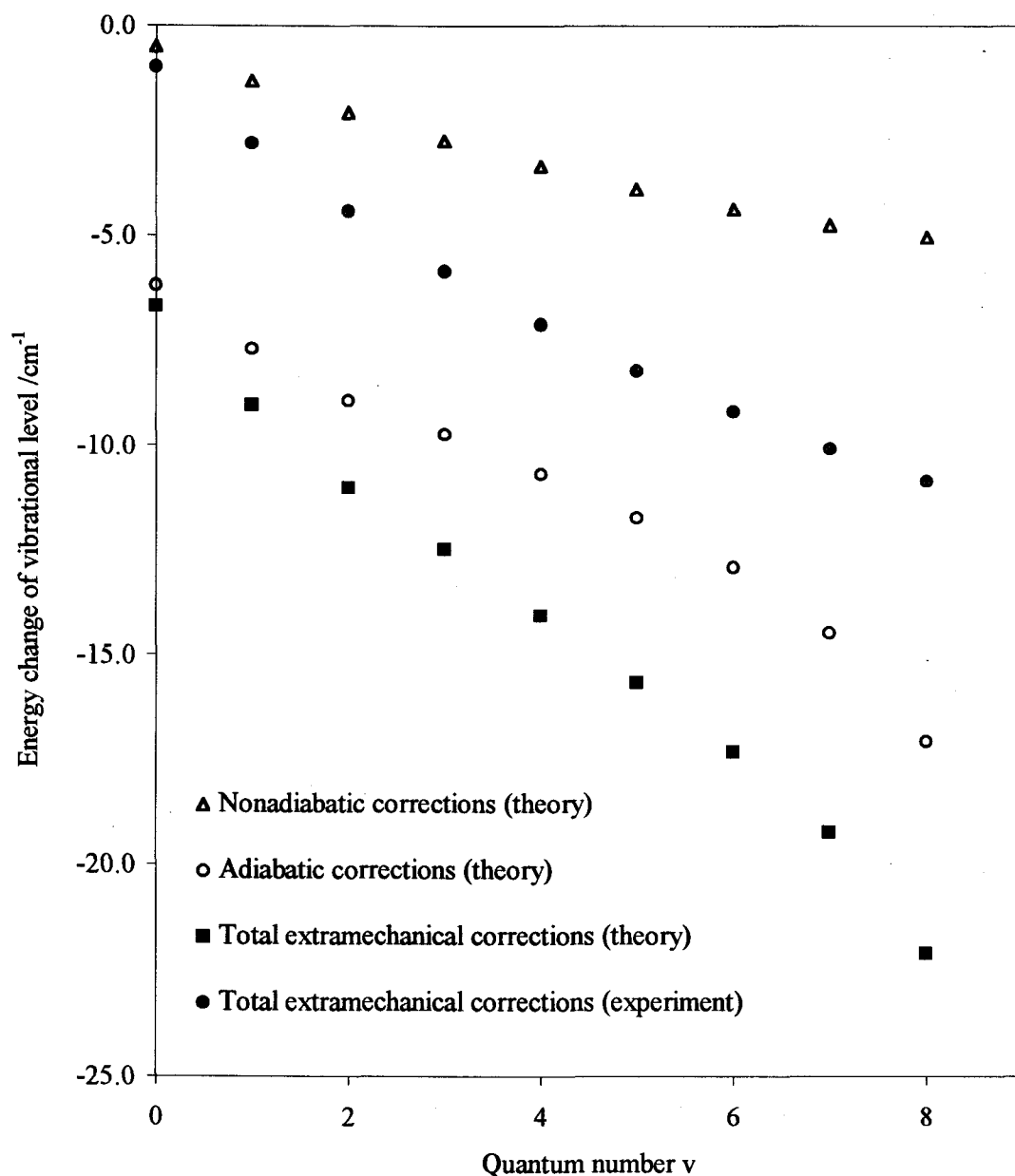


Figure 5-2. Influence of adiabatic and nonadiabatic corrections on energy of vibrational levels of $^1\text{H}_2$ molecule. Literature data for adiabatic¹³⁵ and nonadiabatic¹³⁶ corrections were used to calculate theoretical energy change of vibrational levels. Experimental energy changes are calculated using coefficients Δ_{ki} derived in the course of analysis of the experimental data on hydrogen isotopes accomplished in this work.

5.4. Summary

From the literature overview of spectral data of hydrogen isotopes, it is seen that numerous articles have been published in this area. The majority of this work was devoted to experimental determination of wavenumbers of lines in the vibration-rotational fundamental and first hot bands as well as in the purely rotational band. In general the most accurate measurements of these wavenumbers were for lines with low values of the J-quantum number. In our analysis described in section 5.3, these data did not show any anomalies, whereas points corresponding to higher J values were either main contributors to the standard errors (e.g. the fundamental Q branch of H_2^{121}) or were among outliers (e.g. lines with $J''=10-12$ in purely rotational S branch of D_2^{114}). Therefore it seems desirable to re-measure these lines to check their accuracy.

Some spectral information about higher energy levels ($v \geq 2$) is also available from a limited number of literature sources for several isotopic variants in the form of wavenumbers for higher hot band Q-branch transitions (H_2^{121}) and overtones ($\text{H}_2^{103,105}$, HD^{110} and HT^{130}). However, the hot band Q-branch transitions of H_2^{121} were not of high accuracy and, along with overtones of H_2^{105} and HT^{130} , contributed most to the standard errors in the Dunham fit in the course of our analysis of individual isotopes. In addition overtone wavenumbers of HD^{110} and all wavenumbers available in the literature for HT were not corrected to zero pressure, although high accuracy of measurements was claimed.

Analysis of individual hydrogen isotopic variants with the Dunham model showed high absolute standard errors S of fits ranging from 0.032 to 0.41 cm^{-1} , which is 1-2 orders

of magnitude higher than those in case of nitrogen data measured in this work (see Table 4-4, Table 5-7 and Table 5-8). The global fit also gave high absolute standard deviation of 0.074 cm^{-1} , revealed some inaccurate data for HT molecule¹¹⁹ and indicated that accuracy for T₂ and DT measurements claimed by authors^{119,120} might be overestimated. In this fit, four parameters Δ_{kl} proved to be statistically significant, addition of which to parameters U_{kl} in the model (2.76) considerably reduced the standard errors. This agrees with the expectation that hydrogen possesses pronounced extramechanical effects. Comparison of energy changes in vibrational levels of H₂ due to extramechanical effects calculated using coefficients Δ_{kl} derived from experimental literature data with such changes derived from *ab initio* computations shows 5 - 11 cm^{-1} disagreement.

In light of these observations and the fact that attempts to fit the best hydrogen isotopic data available in the literature with model (2.70) failed, we conclude that there is a need for systematic and accurate spectral measurements of hydrogen isotopes to experimentally assess extramechanical effects in this molecular system. The special need exists for accurate data for vibration-rotational transitions with higher values of v - and J -quantum numbers.

6. CONCLUSIONS

An optical method for high resolution CARS measurements of molecular species vibration-rotationally excited in a glow discharge plasma was developed in our laboratory. The influence of different discharge parameters on the excitation efficiency of nitrogen molecule was analyzed. In the course of this analysis the optimum electrode configuration and pressure range were established. It was also shown that for each vibrational level there exist different optimum values of discharge current, which increase with increasing vibrational quantum number v . Our study revealed the necessity of a gas flow of about 0.4 - 0.6 L/min through the discharge cell in order to greatly increase (factor of ~ 150) the CARS signal from vibration-rotationally excited nitrogen molecules. It was determined that with such a gas flow the maximum concentration of excited molecules exist at the downstream border of the positive column of a glow discharge. To make an economical use of precious gases (e.g. nitrogen isotope $^{15}\text{N}_2$) a novel cycling system for optical measurements in a glow discharge at low pressures required in our experiments was developed. Figures of merit of our experimental apparatus were carefully evaluated. Account of precision and nonlinearity of scans of dye laser as well as of overall frequency time drift of dye and Nd:YAG lasers was taken. It was shown that on average the precision of the whole system is better than 0.001 cm^{-1} .

At an effective resolution of 0.001 cm^{-1} our method was used for spectral measurements of isotopic variants of nitrogen: $^{14}\text{N}_2$ and $^{15}\text{N}_2$. Specifically we obtained wavenumbers of lines in Q branches of bands with $\Delta v=1$ up to $v'=8$ for $^{14}\text{N}_2$ and $v'=7$ for $^{15}\text{N}_2$, and O and S branches of the fundamental band of $^{15}\text{N}_2$. In our wavenumber

determination procedure we accounted for corrections due to the Stark effect, pressure shift, interference effects, and frequency chirps due to amplification of the dye-laser Stokes beam. The absolute uncertainty of our Q-branch measurements is 0.004 cm^{-1} . In terms of accuracy these data significantly improved existing spectral information for $^{14}\text{N}_2$ and greatly extended that for $^{15}\text{N}_2$.

Our accurate spectral data allowed us for the first time to determine coefficients Y_{kl} for each of two nitrogen isotopes $^{14}\text{N}_2$ and $^{15}\text{N}_2$ valid in the wide range of vibrational quantum numbers v : 0-8 and 0-7, respectively. Also performed for the first time, the global fit of spectral data for both nitrogen isotopes yielded mass-independent coefficients U_{kl} and Δ_{kl} , which can be used to calculate energy levels of all isotopic variants of nitrogen, including $^{14}\text{N}^{15}\text{N}$, for which very limited spectral information is available. Although normalized standard errors in combined regression analysis of all isotopic spectral data were larger than those in separate fits, the value of the former was only two units. The absolute standard error of combined fits was small and did not exceed the stated accuracy of our measurements. We conclude that coefficients Δ_{kl} presented in Table 4-4 quantitatively characterize extramechanical effects in nitrogen molecule. However, even at our measurement accuracy of 0.004 cm^{-1} , attempts to distinguish between adiabatic and nonadiabatic effects in nitrogen proved to be unsuccessful.

Along the line of future extension of this type of study, the literature spectral data for hydrogen isotopes were analyzed. We showed that accurate and reliable data are available only for purely rotational transitions and vibration-rotational transitions in the fundamental and the first hot bands. Even for these transitions, accurate information for higher rotational levels is very much limited. Analysis of literature data for individual

isotopic variants of hydrogen and of all these data combined, similar to that performed for our nitrogen wavenumbers, gave values of the absolute standard errors from 1 to 2 orders of magnitude higher than those in case of nitrogen. The coefficients Δ_{kl} resulting from such an analysis of hydrogen spectral data were used to estimate the shifts of vibrational energy levels of H_2 molecule due to extramechanical effects. Comparison of these energy level shifts with those predicted for hydrogen by theory displayed disagreement of the order of 5-11 cm^{-1} . Whether this discrepancy is due to internal inconsistency of the experimental data set or is due to inaccuracy of theoretical calculations, or both, remains to be checked. From the above observations we conclude that there is a need of accurate and systematic spectral measurements of hydrogen isotopes in a wide range of vibrational and rotational quantum numbers.

BIBLIOGRAPHY

- ¹ J. P. Taran, "CARS spectroscopy and applications", Conf. NATO/ASI on Applied Laser Spectroscopy, San Miniato, 3-15 September, 1989.
- ² J. P. Taran, *Pure & Appl. Chem.* **59**, 1295 (1987).
- ³ W. M. Shaub, J. W. Nibler, and A. B. Harvey, *J. Chem. Phys.* **67**, 1883 (1977).
- ⁴ J. W. Nibler, J. R. McDonald, and A. B. Harvey, *Opt. Commun.* **18**, 371 (1976).
- ⁵ J. P. Taran and M. Pealat, "Practical CARS temperature measurements", 6th Symposium on Temperature, its Measurement and Control in Science and Industry, Washington, 14-15 March, 1982.
- ⁶ K. Muller-Dethlefs *et al.*, *Ber. Bunsenges, Phys. Chem.* **85**, 803 (1981).
- ⁷ F. Moya *et al.*, "Flame Investigation by Coherent Anti-Stokes Raman Scattering", AIAA 14th Aerospace Science Meeting, Washington, 26-28 January, 1976.
- ⁸ J. L. Kohl, L. Strachan, and L. D. Gardner, *Astrophys. J.* **465**, L141 (1996).
- ⁹ J. L. Linsky and B.E. Wood, *Astrophys. J.* **463**, 254 (1996).
- ¹⁰ S. Pak, D. T. Jaffe, and L. D. Keller, *Astrophys. J.* **457**, L43 (1996).
- ¹¹ F.M. Fernandez and J.F. Ogilvie, *Chin. J. Phys.* **30**, 177 (1992).
- ¹² R. Frey, J. Lukasik, and J. Ducuing, *Chem. Phys. Lett.* **14**, 514 (1972).
- ¹³ M.M. Audibert, C. Joffrin, and J. Ducuing, *Chem. Phys. Lett.* **25**, 158 (1974).
- ¹⁴ G. J. Germann and J. J. Valentini, *J. Phys. Chem.* **92**, 3792 (1988).
- ¹⁵ J. R. Ferraro and K. Nakamoto, "Introduction to Raman Spectroscopy", Academic Press, London, U. K., 1994.
- ¹⁶ G. L. Easley, "Coherent Raman Spectroscopy", Pergamon Press, New York, 1981.
- ¹⁷ D. A. Long, "Raman Spectroscopy", McGraw-Hill, London, U. K., 1977.

- ¹⁸ "Raman Spectroscopy of Gases and Liquids. Topics in Current Physics", edited by A. Weber, Vol. 11, Springer-Verlag, Berlin, 1979.
- ¹⁹ "The Raman Effect", ed. by A. Anderson, Marcel Dekker, New York, 1973.
- ²⁰ C. V. Raman and K. S. Krishnan, *Nature* **121**, 501 (1928).
- ²¹ A. Smekal, *Naturwiss.* **11**, 873 (1923).
- ²² G. Landsberg and L. Mandelstam, *Naturwiss.* **16**, 557 and 772 (1928).
- ²³ E. G. Woodbury and W. K. Ng, *Proc. IRE* **50**, 2367 (1962).
- ²⁴ T. Yajima and M. Takatsuji, *J. Phys. Japan* **19**, 2343 (1964).
- ²⁵ P. D. Maker and R. W. Terhune, *Phys. Rev. A* **137**, 801 (1965).
- ²⁶ N. Bloembergen, "Nonlinear Optics", Benjamin Press, New York, 1965.
- ²⁷ J. W. Nibler and G. V. Knighten, *in* "Raman Spectroscopy of Gases and Liquids. Topics in Current Physics", edited by A. Weber, Vol. 11, p. 253, Springer-Verlag, Berlin, 1979.
- ²⁸ J. W. Nibler *et al.*, *in* "Vibrational Spectra and Structure", edited by J. Durig, Vol. 6, p. 173, Elsevier, Amsterdam, 1977.
- ²⁹ Y.R. Shen, "The Principles of Nonlinear optics", John Wiley, New York, 1984.
- ³⁰ "Chemical Applications of Nonlinear Raman Spectroscopy", edited by A. B. Harvey, Academic Press, New York, 1981.
- ³¹ S. Maeda *et al.*, *Appl. Spectrosc. Rev.* **21**, 211 (1985).
- ³² A. Yariv, "Quantum Electronics", John Wiley, New York, 1975.
- ³³ S. Druet and J. P. Taran, *Prog. Quant. Electr.* **7**, 1 (1982).
- ³⁴ W. M. Tolles, J. W. Nibler, J. R. MacDonald, and A. B. Harvey, *Appl. Spectrosc.* **31**, 253 (1977).

- ³⁵ R. W. Maker and P. D. Terhune, *in* "Lasers", edited by A. K. Levine, Vol. 2, Marcel Dekker, New York, 1968.
- ³⁶ J. W. Nibler and J. J. Yang, *Ann. Rev. Phys. Chem.* **38**, 349 (1987).
- ³⁷ M. Born and J. R. Oppenheimer, *Ann. Phys. Leipzig* **84**, 457 (1927).
- ³⁸ J. L. Dunham, *Phys. Rev.* **41**, 713 (1932).
- ³⁹ J. L. Dunham, *Phys. Rev.* **41**, 721 (1932).
- ⁴⁰ G. Wentzel, *Zeit. f. Phys.* **38**, 518 (1926).
- ⁴¹ L. Brillouin, *Comptes Rendus* **183**, 24 (1926).
- ⁴² H. A. Kramers, *Zet. F. Phys.* **39**, 828 (1926).
- ⁴³ R. M. Herman and S. Short, *J. Chem. Phys.* **50**, 572 (1970).
- ⁴⁴ R. H. Tipping and J. F. Ogilvie, *J. Mol. Structure* **35**, 1 (1976).
- ⁴⁵ A. G. Maki, W. B. Olson, and G. Thompson, *J. Mol. Spectrosc.* **144**, 257 (1990).
- ⁴⁶ J. F. Ogilvie, *Ber. Bunsen-Ges. Phys. Chem.* **100**, 1906 (1996).
- ⁴⁷ J. H. Van Vleck, *J. Chem. Phys.* **4**, 327 (1936).
- ⁴⁸ B. Rosenblum, A. H. Nethercot, and C. H. Townes, *Phys. Rev.* **109**, 400 (1958).
- ⁴⁹ R. M. Herman and A. Asgharian, *J. Mol. Spectrosc.* **19**, 305 (1966).
- ⁵⁰ P. R. Bunker, *J. Mol. Spectrosc.* **28**, 422 (1968).
- ⁵¹ P. R. Bunker, *J. Mol. Spectrosc.* **35**, 306 (1970).
- ⁵² P. R. Bunker, *J. Mol. Spectrosc.* **68**, 367 (1977).
- ⁵³ P. R. Bunker and R. E. Moss, *Mol. Phys.* **33**, 417 (1977).
- ⁵⁴ J. K. G. Watson, *J. Mol. Spectrosc.* **80**, 411 (1980).

- ⁵⁵ J. F. Ogilvie, *Spectrochim. Acta* **A46**, 43 (1990).
- ⁵⁶ J. F. Ogilvie and S. C. Liao, *Chem. Phys. Lett.* **226**, 281 (1994).
- ⁵⁷ J. F. Ogilvie, *Mol. Phys.* **88**, 1055 (1996).
- ⁵⁸ W. Kolos and L. Wolniewicz, *J. Chem. Phys.* **41**, 3663 (1964).
- ⁵⁹ J. F. Ogilvie, "The vibrational and rotational spectrometry of diatomic molecules", to be published.
- ⁶⁰ F. M. Fernandez, *Phys. Rev.* **A50**, 2953 (1994).
- ⁶¹ J. F. Ogilvie, *Proc. R. Soc. London* **A378**, 287 (1981).
- ⁶² J. F. Ogilvie, *J. Chem. Phys.* **88**, 2804 (1988).
- ⁶³ J. F. Ogilvie, *J. Phys.* **B27**, 47 (1994).
- ⁶⁴ J. F. Ogilvie, *Chem. Phys. Lett.* **267**, 590 (1997).
- ⁶⁵ J. F. Ogilvie, *J. Molec. Spectrosc.* **148**, 243 (1991).
- ⁶⁶ A. H. M. Ross, R.S. Eng, and H. Kildal, *Opt. Commun.* **12**, 433 (1974).
- ⁶⁷ M. Faraday, *Res. Elec.* **1**, 663 (1839).
- ⁶⁸ H. Davy, *Phil. Trans.* **111**, 427 (1821).
- ⁶⁹ W. Crookes, *Phil. Trans.* **1**, 152 (1879).
- ⁷⁰ E. Nasser, "Fundamentals of Gaseous Ionization and Plasma Electronics", John Wiley-Interscience, New York, 1971.
- ⁷¹ A. M. Howatson, "An introduction to gas discharges", Pergamon Press, New York, 1976.
- ⁷² J. D. Cobine, "Gaseous Conductors. Theory and Engineering Applications", McGraw-Hill, New York, 1941.
- ⁷³ J. S. Townsend, "Electricity in Gases", Clarendon Press, Oxford, U. K., 1915.

- ⁷⁴ R. Popoular, "Electric Phenomena in Gases", American Elsevier, New York, 1965.
- ⁷⁵ L. B. Loeb, "Fundamental Processes of Electrical Discharge in Gases", John Wiley, New York, 1939.
- ⁷⁶ A. Engle, "Ionized gases", Clarendon Press, Oxford, U. K., 1965 (p. 181).
- ⁷⁷ J. M. Meek and J. D. Craggs, "Electrical Breakdown in Gases", Clarendon Press, Oxford, U. K., 1953.
- ⁷⁸ "Handbook of Thin Film Technology", edited by L. I. Maissel and R. Glang, McGraw Hill, New York, 1970.
- ⁷⁹ R. K. Marcus, "Glow Discharge Spectroscopy", Plenum Press, New York, 1993.
- ⁸⁰ M. L. Orlov, J. F. Ogilvie, and J. W. Nibler, *J. Mol. Spectrosc.* **185**, 128 (1997).
- ⁸¹ P. R. Minarik, Ph. D. thesis, Oregon State University, 1997.
- ⁸² J. W. Nibler and G. A. Pubanz, *in* "Advances in Non-linear Spectroscopy", edited by R. J. Clark and R. E. Hester, p. 1, John Wiley, London, U. K., 1987.
- ⁸³ B. Massabieaux *et al.*, *J. Physique* **48**, 1939 (1987).
- ⁸⁴ Lumonics HyperDye Pulsed Dye Lasers, Users Manual, 105 Schneider Rd., Kanata, Ontario, Canada K2K 1Y3; tel. 613-592-1460.
- ⁸⁵ D. Reuter, D. E. Jennings, and J. W. Brault, *J. Mol. Spectrosc.* **115**, 294 (1986).
- ⁸⁶ P. Rinsland *et al.*, *J. Mol. Spectrosc.* **148**, 274 (1991).
- ⁸⁷ R. J. Butcher, D. V. Willetts, and W. J. Jones, *Proc. Roy. Soc. London A***324**, 231 (1971).
- ⁸⁸ J. Bendtsen, *J. Raman Spectrosc.* **2**, 133 (1974).
- ⁸⁹ T. R. Gilson *et al.*, *J. Raman Spectrosc.* **9**, 361 (1980).
- ⁹⁰ B. Lavorel, R. Chaux, R. Saint-Loup and H. Berger, *Opt. Commun.* **62**, 25 (1987).

- ⁹¹ A. Tabyaoui, B. Lavorel, G. Millot, R. Saint-Loup, R. Chaux and H. Berger, *J. Raman Spectrosc.* **21**, 809 (1990).
- ⁹² B. Lavorel, G. Millot, M. Lefebvre and M. Pealat, *J. Raman Spectrosc.* **19**, 375 (1988).
- ⁹³ S. Edwards *et al.*, *J. Mol. Spectrosc.* **162**, 257 (1993) and references therein.
- ⁹⁴ T. Trickl, D. Proch, and K. L. Kompa, *J. Mol. Spectrosc.* **171**, 374 (1995).
- ⁹⁵ M. Leuchs, M. Crew, J. Harrison, M. F. Hineman, and J. W. Nibler, *J. Chem. Phys.* **105**, 4885 (1996).
- ⁹⁶ S. Gerstenkern and P. Luc, "Atlas du Spectra d'Absorption de la Molecule d'Iode", Centre National de la Recherche Scientifique, Paris, France, 1978.
- ⁹⁷ T. Trickl, D. Proch and K. L. Kompa, *J. Mol. Spectrosc.* **162**, 184 (1993).
- ⁹⁸ L. A. Rahn, R. L. Farrow, M. L. Koszykowski and P. L. Mattern, *Phys. Rev. Lett.* **45**, 620 (1980).
- ⁹⁹ R. L. Farrow and L. A. Rahn, *Phys. Rev. Lett.* **48**, 395 (1982).
- ¹⁰⁰ S. I. Chan, M. R. Baker, and N. F. Ramsey, *Phys. Rev. A* **136**, 1224 (1964).
- ¹⁰¹ M. M. Hessel, and C. R. Vidal, *J. Chem. Phys.* **70**, 4439 (1979).
- ¹⁰² J. Lukasik, and J. Ducuing, *Chem. Phys. Lett.* **27**, 203 (1974).
- ¹⁰³ S. L. Bragg, J. W. Brault, and W. H. Smith, *Astrophys. J.* **263**, 999 (1982).
- ¹⁰⁴ V. De Cosmo, H. P. Gush, and M. Halpern, *Can. J. Phys.* **62**, 1713(1984).
- ¹⁰⁵ D. W. Ferguson *et al.*, *J. Mol. Spectrosc.* **160**, 315 (1993).
- ¹⁰⁶ U. Fink, T. A. Wiggins, and D. H. Rank, *J. Mol. Spectrosc.* **18**, 384 (1965).
- ¹⁰⁷ D. E. Jennings and J. W. Brault, *J. Mol. Spectrosc.* **102**, 265 (1983).
- ¹⁰⁸ D. E. Jennings and J. W. Brault, *Astrophys. J.* **256**, L29 (1982).
- ¹⁰⁹ A. R. W. McKellar and T. Oka, *Can. J. Phys.* **56**, 1315 (1978).

- ¹¹⁰ A. R. W. McKellar, W. Goetz, and D. A. Ramsay, *Astrophys. J.* **207**, 663 (1976).
- ¹¹¹ J. Reid and A. R. W. McKellar, *Phys. Rev.* **A18**, 224 (1978).
- ¹¹² N. H. Rich, J. W. Johns, and A. R. W. McKellar, *J. Mol. Spectrosc.* **95**, 432 (1982).
- ¹¹³ J. E. Barefield, L. H. Jones, and R. Liepens, *J. Mol. Spectrosc.* **80**, 233 (1980).
- ¹¹⁴ D. E. Jennings, A. Weber, and J. W. Brault, *J. Mol. Spectrosc.* **126**, 19 (1987).
- ¹¹⁵ D. E. Jennings, A. Weber, and J. W. Brault, *Appl. Opt.* **25**, 284 (1986).
- ¹¹⁶ E. C. Looi, J. C. Stryland, and H. L. Welsh, *Can. J. Phys.* **56**, 1102 (1978).
- ¹¹⁷ B. P. Stoicheff, *Can. J. Phys.* **35**, 730 (1957).
- ¹¹⁸ D. K. Veirs and G. M. Rosenblatt, *J. Mol. Spectrosc.* **121**, 401 (1987).
- ¹¹⁹ H. G. M. Edwards *et al.*, *J. Raman Spectrosc.* **8**, 251 (1979).
- ¹²⁰ H. G. M. Edwards, D. A. Long, and H. R. Mansour, *J. Chem. Soc. Faraday Trans. II* **74**, 1203 (1978).
- ¹²¹ G. J. Germann and J. J. Valentini, *J. Phys. Chem.* **92**, 3792 (1987).
- ¹²² M. A. Hennesian *et al.*, *Opt. Lett.* **1**, 149 (1977).
- ¹²³ D. E. Jennings, L. A. Rahn, and A. Owyong, *Astrophys. J.* **291**, L15 (1985).
- ¹²⁴ H. Bredohl and G. Herzberg, *Can. J. Phys.* **51**, 867 (1973).
- ¹²⁵ I. Dabrowski and G. Herzberg, *Can. J. Phys.* **54**, 525 (1976).
- ¹²⁶ I. Dabrowski, *Can. J. Phys.* **62**, 1639 (1984).
- ¹²⁷ P. J. Brannon, C. H. Church, and C. W. Peters, *J. Mol. Spectrosc.* **27**, 44 (1968).
- ¹²⁸ A. J. R. Heck, W. M. Huo, R. N. Zare, and D. W. Chandler, *J. Mol. Spectrosc.* **173**, 452 (1995).
- ¹²⁹ F. W. Dalby and J. Vigue, *Phys. Rev. Lett.* **43**, 1310 (1979).

- ¹³⁰ M. -C. Chuang and R. N. Zare, *J. Mol. Spectrosc.* **121**, 380 (1987).
- ¹³¹ W. Kolos and L. Wolniewicz, *J. Chem. Phys.* **45**, 944 (1966).
- ¹³² P. Dion and A. D. May, *Can. J. Phys.* **51**, 36 (1973).
- ¹³³ L. Wolniewicz, *J. Chem. Phys.* **99**, 1851 (1993).
- ¹³⁴ T. Orlikowski and L. Wolniewicz, *Chem. Phys. Lett.* **24**, 461 (1974).
- ¹³⁵ J. D. Poll and G. Karl, *Can. J. Phys.* **44**, 1467 (1966).
- ¹³⁶ L. Wolniewicz, *J. Chem. Phys.* **103**, 1792 (1995).

APPENDICES

APPENDIX A. EXPRESSIONS FOR SOME OF PARAMETERS Y_{kl} AND Z_{kl}

$$Y_{0,0} = B_e \left(-\frac{7c_1^2}{32} - \frac{c_1}{8} + \frac{3c_2}{8} + \frac{1}{16} \right) + \dots$$

$$Y_{0,1} = B_e + \frac{B_e^3}{\omega_e^2} \left(\frac{21c_1^3}{4} + \frac{27c_1^2}{4} - \frac{23c_1c_2}{2} + \frac{35c_1}{8} - 8c_2 + \frac{15c_3}{2} + 2 \right) + \dots$$

$$Y_{0,2} = -\frac{4B_e^3}{\omega_e^2} + \frac{B_e^5}{\omega_e^4} \left(\begin{array}{l} -126c_1^4 - \frac{495c_1^3}{2} - \frac{23c_1c_2}{2} + 333c_1^2c_2 - \frac{933c_1^2}{4} + 434c_1c_2 - 205c_1c_3 \\ -147c_1 - 92c_2^2 + 194c_2 - 200c_3 + 90c_4 - \frac{535}{8} \end{array} \right)$$

$$Y_{0,3} = \frac{16B_e^5}{\omega_e^4} (c_1 + 2) + \dots$$

$$Y_{1,0} = \omega_e + \frac{B_e^2}{\omega_e} \left(\begin{array}{l} -\frac{1155c_1^4}{256} - \frac{111c_1^3}{32} + \frac{459c_1^2c_2}{32} - \frac{33c_1^2}{64} + \frac{61c_1c_2}{8} - \frac{951c_1c_3}{8} + \frac{3c_1}{8} \\ -\frac{67c_2^2}{16} - \frac{c_2}{16} - \frac{15c_3}{4} + \frac{254c_4}{4} - \frac{3}{32} \end{array} \right)$$

$$Y_{2,0} = B_e \left(-\frac{15c_1^2}{8} + \frac{3c_1}{2} + \frac{3c_2}{2} - \frac{3}{4} \right) + \dots$$

$$Y_{3,0} = \frac{B_e^2}{\omega_e} \left(\begin{array}{l} -\frac{705c_1^4}{64} + \frac{15c_1^3}{8} + \frac{225c_1^2c_2}{8} + \frac{57c_1^2}{16} - \frac{17c_1c_2}{2} - \frac{35c_1c_3}{2} - 2c_1 \\ -\frac{17c_2^2}{4} - \frac{3c_2}{4} - 5c_3 + 5c_4 + \frac{1}{2} \end{array} \right)$$

$$Y_{1,1} = \frac{6B_e^2c_1}{\omega_e} + \dots$$

$$Y_{1,2} = \frac{6B_e^4}{\omega_e^3} (-9c_1^2 - 12c_1 + 8c_2 - 4) + \dots$$

$$Y_{2,1} = \frac{B_e^3}{\omega_e^2} \left(45c_1^3 + 27c_1^2 - 78c_1c_2 + \frac{3c_1}{2} + 30c_3 \right) + \dots$$

$$Y_{2,2} = \frac{B_e^5}{\omega_e^4} \left(\begin{array}{l} -1080c_1^4 + 1566c_1^3 + 1992c_1c_2 + 2484c_1^2c_2 - 981c_1^2 - 1140c_1c_3 \\ -396c_1 - 624c_2^2 + 264c_2 - 480c_3 + 360c_4 - \frac{87}{2} \end{array} \right)$$

$$Z_{0,0}^{v,a} \frac{M_a}{m_e} = u_0^a$$

$$Z_{0,1}^{v,a} \frac{M_a}{m_e} = \gamma^2 u_1^a$$

$$Z_{0,2}^{v,a} \frac{M_a}{m_e} = B_e \gamma^4 s_0^a + \gamma^4 \left[u_1^a \left(-\frac{3c_1}{2} - 2 \right) + u_2^a \right]$$

$$Z_{0,3}^{v,a} \frac{M_a}{m_e} = B_e \gamma^2 \left[s_0^a \left(-\frac{3c_1}{2} - \frac{9}{2} \right) + \frac{s_1^a}{2} \right] + \gamma^6 \left[u_1^a \left(\frac{9c_1^2}{2} - 2c_2 + 9c_1 + \frac{25}{4} \right) + u_2^a (-3c_1 - 4) + u_3^a \right]$$

$$Z_{1,0}^{v,a} \frac{M_a}{m_e} = B_e \gamma^{-1} s_0^a + \gamma \left[u_1^a \left(-\frac{3c_1}{2} + 1 \right) + u_2^a \right]$$

$$Z_{2,0}^{v,a} \frac{M_a}{m_e} = B_e \left[s_0^a \left(-\frac{15c_1^2}{8} + \frac{3c_2}{2} + \frac{3c_1}{2} - \frac{3}{4} \right) + s_1^a \left(-\frac{3c_1}{4} + \frac{1}{2} \right) + \frac{s_2^a}{2} \right] + \gamma^2 \left[u_1^a \left(-\frac{45c_1^3}{8} + \frac{39c_1c_2}{4} - \frac{15c_3}{4} + \frac{3c_1^2}{8} - \frac{3c_2}{2} + \frac{9c_1}{8} - \frac{3}{8} \right) + u_2^a \left(\frac{15c_1^2}{4} - \frac{3c_2}{2} - \frac{3c_1}{2} \right) + u_3^a \left(-\frac{15c_1}{4} + \frac{3}{2} \right) + \frac{3u_4^a}{2} \right]$$

$$Z_{0,1}^{r,a} \frac{M_a}{m_e} = B_e t_0^a$$

$$Z_{0,2}^{r,a} \frac{M_a}{m_e} = B_e \gamma^2 \left[s_0^a - \frac{s_1^a}{2} - 2t_0^a + t_1^a \right]$$

$$Z_{0,3}^{r,a} \frac{M_a}{m_e} = B_e \gamma^4 \left[s_0^a \left(\frac{3c_1}{2} + \frac{9}{2} \right) - \frac{s_1^a}{2} + t_0^a (3c_1 + 6) + t_1^a \left(-\frac{3c_1}{2} - 4 \right) + t_2^a \right]$$

$$Z_{1,1}^{r,a} \frac{M_a}{m_e} = B_e \gamma \left[s_0^a \left(\frac{3c_1}{2} + \frac{3}{2} \right) - \frac{s_1^a}{2} + 3t_0^a c_1 + t_1^a \left(-\frac{3c_1}{2} - 1 \right) + t_2^a \right]$$

APPENDIX B. VISUAL BASIC PROGRAM FOR SPECTRAL DATA ACQUISITION

This program is written in Visual Basic III for computer interfacing of the medium resolution apparatus used in our optimization study of nitrogen excitation in a glow discharge (see Chapter 2). It is compatible with Windows 3.1 and Windows 95 platforms.

Interface program "Lumonics 17" by M. L. Orlov

Option Explicit

frmPanelForm

Sub btnScan_Click ()

'This procedure performs scan of Lumonics
'and data collection from ADC channels of Lab Master

Dim Result\$, i%, Dummy%

'General initialization of frmWin* and their objects

'arrow mouse pointer

frmWin2.MousePointer = 1

frmWin3.MousePointer = 1

frmWin4.MousePointer = 1

'enable/disable objects

frmWin2.lblCoordinates2.Caption = ""

frmWin3.lblCoordinates3.Caption = ""

frmWin4.lblCoordinates4.Caption = ""

frmWin2.mnuControlPanel.Enabled = False

frmWin2.mnuTitle.Enabled = False

frmWin2.mnuSaveAs.Enabled = False

frmWin2.mnuBoxes.Enabled = False

frmWin2.mnuHelp.Enabled = False

frmWin2.btnSize2.Enabled = False

frmWin3.btnSize3.Enabled = False

```

frmWin4.btnSize4.Enabled = False
frmWin2.btnPrint2.Enabled = False
frmWin3.btnPrint3.Enabled = False
frmWin4.btnPrint4.Enabled = False
frmWin2.mnuStop.Enabled = True
frmWin2.mnuPause.Enabled = True
frmWin2.txtTitle.Visible = False
frmWin2.txtPrmtrVrt.Visible = False
frmWin2.txtPrmtrHrz.Visible = False
*****

*****

'Read ADC channel to use for "Bad shot" detector
*****

' Check if "Bad shot" channel number is valid
Dummy = CInt(txtWindow(1).Text)
If Dummy < 0 Or Dummy > 7 Then
    MsgBox WrongBadShotChannel, 16
    Exit Sub
End If
Window(1) = Dummy
*****

*****

'Read ADC channels to display in Windows 2-4.
'Program is set up so, that first the Window with lower number should be selected for
display e.g. Window3 could be used only if Window2 is also engaged . The following
block checks if this condition is fulfilled
*****

'for info on WinCode see GEN_PROC.BAS-> declarations
WinCode = 0
For i = 2 To 4
    'check if any ADC channel is assigned for ith Window
    If txtWindow(i).Text <> "None" And txtWindow(i).Text <> "none" And
txtWindow(i).Text <> "" Then
'read # of ADC channel selected for ith Window
    Dummy = CInt(txtWindow(i).Text)
    'Check if ADC channel number is valid
    If Dummy < 0 Or Dummy > 7 Then
        MsgBox WrongADCchannel, 16
        Exit Sub
    End If
    'store ADC channel number to display in ith Window
    Window(i) = Dummy
    'calculate code number for Window selection

```

```

        WinCode = WinCode + i
    End If
Next i
'check if Windows were selected for display
'in continuous increasing order
If WinCode <> 2 And WinCode <> 5 And WinCode <> 9 Then
    MsgBox WrongWindowSelection, 16
    Exit Sub
End If
*****
'Get number of shots to average from "Data Collection Parameters"
Shots = CInt(txtShots.Text)
'Make sure that scan is stopped
StopSCU
'Make sure that units are set to wave numbers. Make sure that mode is set to "Burst".
See the current GEN_PROC.BAS
CheckUnitsMode
'Write scan parameters from the panel to SCU
WriteBasicPrmtrs
'Place SCU to the start position by initiating scan and waiting until delay time is expired.
'Indication: the first letter of SCU respond is "@"
Do: Loop Until Left$(TalkSCU("G"), 1) = "@"
'Define global parameters for ScaleWin* procedures
PsnEnd = CSng(txtPumpBeam.Text) - CSng(frmPanel.txtFinalPsn.Text)
Increment = CSng(frmPanel.txtIncrement.Text)
PsnStart = CSng(txtPumpBeam.Text) - CSng(ReadPresPsn())
Wdth = PsnEnd - PsnStart
'Note: Hght is defined in frmPanel Form_Load
'Calculate total number of data points "TotalPts" see GEN_PROC.BAS
TotalPts = (PsnStart - PsnEnd) / Increment + 1
'Dimension arrays for Frequency storage
ReDim Frequency(2, TotalPts)
'Initialize data point counter
CurPoint = 1
'Set up FlagScanOn
FlagScanOn = 1
'Store current position (dye laser and Raman shift)
StoreFrq
'Hide all the windows
Hidewindows
'Set up size of selected Windows
'and place them on the screen
SizeWindows
'Clear and scale selected Windows
ScaleWindows

```

```

'Show selected Windows
ShowWindows
'Dimension arrays for Signal storage after MaxWinNum is determined in ShowWindows
ReDim Signal(MaxWinNum, TotalPts)
'Collect signal from ADC channels selected by user from the "ControlPanel" during run-
'time, average them for number of "Shots" and store them in array "Signal". "Signal"
'described in GEN_PROC.BAS (declarations)
AvgSignal
'default file name + date + time to display on frmWin2
FileDateStamp
'Display digital result for current point in frmSpectra.Caption (for Starting point)
Display
*****

*****

'Perform scan (including repetitions)
*****

Do
  'Make Lumonics do one step
  StepSCU
  DoEvents
  'Check if scan is finished and exit loop if so
  If StatusSCU() = "S" Then Exit Do
  'Check if scan is paused
  ElseIf StatusSCU() = "P" Then
    'Put on hold until scan is resumed by user
    Do
      DoEvents
    Loop Until StatusSCU() = "@"
  End If
  CurPoint = CurPoint + 1
  'Store current position (dye laser and Raman shift)
  StoreFrq
  'get signals from Lab Master ADC channels and store them
  AvgSignal
  'Display digital result for current point in frmSpectra.Caption
  Display
Loop

'Store real # of points in spectrum
NumPtsTaken = CurPoint
*****

```

```

*****
'Post-initialization
*****
'Slew back to the start position
SlewSCU (txtStartPsn)
'Check what the current position is after scan is finished
txtPresPsn = ReadPresPsn()
'Post-scan initialization of objects
PostScanIni      'See Gen_Proc.Bas
'Save current settings to INI file: shots to average; ADC Channels; pump beam
'wavelength; slew position
WriteIni         'See Gen_Proc.BAS
*****
End Sub

Sub btnShowWindows_Click ()
'
'-----
'Shows those windows for which ADC channels were
'selected
'-----
Select Case WinCode
Case 2
    frmWin2.Show
Case 5
    frmWin2.Show
    frmWin3.Show
Case 9
    frmWin2.Show
    frmWin3.Show
    frmWin4.Show
Case Else
    MsgBox "No spectrum." + NL + "Nothing to show yet!", 16
Exit Sub
End Select
End Sub

Sub btnSlew_Click ()
'Disable rest of form controls
mnuFile.Enabled = False
btnScan.Enabled = False
btnShowWindows.Enabled = False
btnWriteAdvdPrmtrs.Enabled = False
'make sure scan is stoped
StopSCU
'now slew

```

```

SlewSCU (txtSlewPsn.Text)
Do: Loop Until StatusSCU() = "S"
'Enable controls after slew is done
mnuFile.Enabled = True
btnScan.Enabled = True
btnShowWindows.Enabled = True
btnWriteAdvdPrmtrs.Enabled = True
End Sub

```

```

Sub btnWriteAdvdPrmtrs_Click ()
Dim n%
n = MsgBox("Warning!" + NL + NL + "Usually there is no need to change these
parameters." + NL + "Change of them might upset the system. (E.g. change" + NL + "of
'Pres. Position' might destroy calibration)." + NL + NL + "Are you sure you still want
change them?", 1)
'Exit sub if other then "OK" button was selected
If n <> 1 Then
    ReadAdvdPrmtrs
    Exit Sub
End If
'write Advanced Parameters and check their actual values
WriteAdvdPrmtrs
ReadAdvdPrmtrs
End Sub

```

```

Sub Form_Load ()
On Error Resume Next
Dim i%
frmPanel.Show
'Line <CR> and line feed
NL$ = Chr$(13) + Chr$(10)
*****
'Texts for informative messages
*****
WrongCommSCU$ = "Dear Customer:" + NL + NL + "This program can use only
Comm1 or Comm2" + NL + "to communicate with SCU. You have to change" + NL +
"CommSCU' constant in SCU_Proc.Bas under declarations and restart the program" +
NL + NL + "Sorry, about that!"
Unchangable$ = "Dear Valuable Customer:" + NL + NL + "We have to inform you, that
this" + NL + "is one of unchangable parameters!" + NL + NL + "(Note: Comm Port
could be changed at" + NL + "design time. See SCU_PROC.BAS)" + NL + NL + "See
you soon!"
WrongADCchannel = "Dear Valuable Customer:" + NL + NL + "You have selected
invalid ADC channel!" + NL + "For LabMaster use ADC channels 0 - 7." + NL + NL +
"Take care."

```

WrongBadShotChannel = "Dear Valuable Customer:" + NL + NL + "You have selected invalid ADC channel" + NL + "for 'Bad shot' detector use channels 0 - 7." + NL + NL + "Take care."

WrongTotalPts = "Error during calculation of" + NL + "total number of points!" + NL + "Please restart scan!" + NL + NL + "Sorry about that!"

WrongWindowSelection = "Dear Valuable Customer:" + NL + NL + "Select windows in increasing order starting with lower numbers. Thus, Window2 should be always selected for display some ADC channel and Window3 should not be skipped, if Window4 is selected." + NL + NL + "Have a nice scan!"

NoScanTaken = "Dear Valuable Customer:" + NL + NL + "No scan taken yet. Do not try to save nothing please!"

Greeter = "Dear Valuable Customer:" + NL + NL + "Before you can use this program for taking spectra you should initialize the SCU by clicking on corresponding menu." + NL + NL + "Have a nice scan!"

Help = "Dear Valuable Customer:" + NL + NL + "The following is how to use Windows of this program." + NL + NL + "1. Buttons 'Size"

Help1 = " toggels between maximized and normal Window state." + NL + "2. Button 'Print' prints the corresponding Window as it is at the moment of the click." + NL + "3. Left Mouse click on a Window marks this position with Raman shift (cm-1) and Intensity (Volts)." + NL + "4. Right Mouse click removes all marks from the corresponding Window" + NL + "5. Double click on Title box and Text boxes of Window2 hide them keeping all information typed on them. To bring them back just click on 'Title' or corresponding 'Text boxes' menu. Right Mouse click on these objects clears their content." + NL + "6. Menu 'SaveAs' saves all information shown from all Windows shown except marked positions." + NL + "7. When program is exited the following current information is stored: pump beam wavelength; Slew position; channels in Windows 1-4; shots to average; content of boxes on Window2"

WrongProgram = "Dear Valuable Customer:" + NL + NL + "This file was greated with another version of the program, so it could not be opened." + NL + NL + "Sorry for any inconvenience!"

'Set up defaults and show some of them

'Get from INI file:

'- # of shots to average from ADC channels; used in the

' function AvgSignal (see GEN_PROC.BAS).

'- Default Slew Position

'- Default pump beam wavelength

'- Define default ADC channels to collect data from and assign

' them to one of four display Windows

ReadINI 'See GEN_PROC.BAS

'Defaults for ScaleWin* procedures in GEN_PROC.BAS

ScaleMin = 0: ScaleMax = 10: Ticks = 6

```

Hght = ScaleMax - ScaleMin
'common dialog box "cmdBox" settings
frmPanel.cmdBox.Filter = "ASCII (*.prn)|*.prn|All files (*.*)|*.*"
frmPanel.cmdBox.FilterIndex = 1
'Default file name for common dialog boxes
frmPanel.cmdBox.FileName = "Spectrum.prn"
*****

*****

'Initialize flags
*****

'FlagScanOn: 0 - (no scan); 1 - (scan in progress)
FlagScanOn = 0
'no sacn taken yet
FlagScanTaken = 0
'No About form shown - show is "stopped"
StopAboutFlag = 1
*****

'Show greeter
MsgBox Greeter, 64
End Sub

Sub Form_Unload (Cancel As Integer)
WriteIni
End Sub

Sub lblCommPortT_Click ()
MsgBox Unchangable, 64 'text see frmPanel Form_Load
End Sub

Sub lblScanModeT_Click ()
MsgBox Unchangable, 64 'text see frmPanel Form_Load
End Sub

Sub lblWNumb_Click ()
MsgBox Unchangable, 64 'text see frmPanel Form_Load
End Sub

Sub mnuAbout_Click ()
Dim d&, i&
About.Show
StopAboutFlag = 0
Randomize
Do While StopAboutFlag = 0
    d = Int(Rnd * 10000000#)

```

```

    If d > &HFFFFFF Then d = &HFFFFFF
    About.BackColor = d
    For i = 1 To 100000: Next i 'dummy delay
    DoEvents
Loop
End Sub

```

```

Sub mnuExit_Click ()
Hidewindows
Unload frmPanel
End
End Sub

```

```

Sub mnuIntlSCU_Click ()

```

```

'Initialize communications with SCU

```

```

InitializeSCU
'disable after initialization is done once
mnuIntlSCU.Enabled = False
'enable controls on Control Panel
btnShowWindows.Enabled = True
btnScan.Enabled = True
btnWriteAdvdPrmtrs.Enabled = True
btnSlew.Enabled = True
End Sub

```

```

Sub mnuOpen_Click ()
FileOpen
End Sub

```

```

Sub mnuSaveAs_Click ()
'See GEN_PROC.BAS
SaveAs
End Sub

```

```

*****
*****

```

frmWIN2.frm

```

Sub btnPrint2_Click ()
'disable objects on froms frmWin2-4
PrePrint
lblCoordinates2.Visible = False

```

```

txtTitle.BackColor = &H80000005    'white
txtPrmtrVrt.BackColor = &H80000005    'white
txtPrmtrHrz.BackColor = &H80000005    'white
PrintForm
lblCoordinates2.Visible = True
txtTitle.BackColor = &HFFFF00        'blue
txtPrmtrVrt.BackColor = &HC0C0C0     'gray
txtPrmtrHrz.BackColor = &HC0C0C0     'gray
'Enable objects on forms frmWin2-4
AfterPrint
End Sub

Sub btnSize2_Click ()
If frmWin2.WindowState <> 2 Then
    frmWin2.WindowState = 2
    frmPanel.ZOrder 0
    ScaleWin2
    Redraw
    frmWin2.ZOrder 0
ElseIf frmWin2.WindowState <> 0 Then
    frmWin2.WindowState = 0
    frmPanel.ZOrder 0
    ScaleWin2
    Redraw
    ShowWindows
End If
End Sub

Sub Form_DragDrop (Source As Control, X As Single, Y As Single)
'


---


'Move objects on frmWin2 form upon drag/drop is over


---


If Source = lblCoordinates2 Then
    lblCoordinates2.Move X - ScaleWidth / 30, Y - ScaleHeight / 100
ElseIf Source.Tag = "1" Then
    txtTitle.Move X - ScaleWidth / 30, Y - ScaleHeight / 100
ElseIf Source.Tag = "3" Then
    txtPrmtrVrt.Move X - ScaleWidth / 30, Y - ScaleHeight / 100
ElseIf Source.Tag = "2" Then
    txtPrmtrHrz.Move X - ScaleWidth / 30, Y - ScaleHeight / 100
ElseIf Source = lblFileDate Then
    lblFileDate.Move X - ScaleWidth / 30, Y - ScaleHeight / 100
End If
End Sub

```

```

Sub Form_MouseDown (Button As Integer, Shift As Integer, X As Single, Y As Single)
If FlagScanOn = 1 Then Exit Sub
'Label current point on the screen with a red dot
If Button = Left_Button Then
    Circle (X, Y), -ScaleWidth / 600, RGB(255, 0, 0)
    PSet (X + ScaleWidth / 150, Y)
    Print Format$(X, "0.000") + "; " + Format$(Y, "0.00")
End If
'Clear all labels by graph redrawing
If Button = Right_Button Then
    frmPanel.ZOrder 0
    Redraw
    ShowWindows
    frmWin2.ZOrder 0
End If
End Sub

Sub Form_MouseMove (Button As Integer, Shift As Integer, X As Single, Y As Single)
If FlagScanOn = 1 Then Exit Sub
lblCoordinates2.Caption = "Raman shift (cm-1): " + Format$(X, "0.000") + " Intensity
(V): " + Format$(Y, "0.00")
End Sub

Sub lblCoordinates2_MouseDown (Button As Integer, Shift As Integer, X As Single, Y
As Single)
If Button = Left_Button Then
    lblCoordinates2.Drag 1 'start of Drag
End If
End Sub

Sub lblCoordinates2_MouseDown (Button As Integer, Shift As Integer, X As Single, Y
As Single)
If Button = Left_Button Then
    lblCoordinates2.Drag 1 'start of Drag
End If
End Sub

Sub lblCoordinates2_MouseUp (Button As Integer, Shift As Integer, X As Single, Y As
Single)
If Button = Left_Button Then lblCoordinates2.Drag 2 'end of Drag
End Sub

Sub lblFileDate_MouseDown (Button As Integer, Shift As Integer, X As Single, Y As
Single)
If Button = Left_Button Then lblFileDate.Drag 1 'start of Drag

```

```
If Button = Right_Button Then lblFileDate.Caption = "" 'clear Title
End Sub
```

```
Sub lblFileDate_MouseUp (Button As Integer, Shift As Integer, X As Single, Y As
Single)
If Button = Left_Button Then lblFileDate.Drag 2 'end of Drag
End Sub
```

```
Sub mnuHelp_Click ()
MsgBox Help + Help1
End Sub
```

```
Sub mnuHrz_Click ()
txtPrmtrHrz.Visible = True
End Sub
```

```
Sub mnuPause_Click ()
frmWin2.mnuStop.Enabled = False
frmWin2.mnuPause.Enabled = False
frmWin2.mnuResume.Enabled = True
PauseSCU
End Sub
```

```
Sub mnuResume_Click ()
```

```
'Resume paused scan
```

```
Dim Result$
mnuResume.Enabled = False
frmWin2.mnuStop.Enabled = True
frmWin2.mnuPause.Enabled = True
frmWin2.lblCoordinates2.Caption = ""
frmWin3.lblCoordinates3.Caption = ""
frmWin4.lblCoordinates4.Caption = ""
PSet (Frequency(2, CurPoint - 1), Signal(2, CurPoint - 1))
Result = TalkSCU("G")
End Sub
```

```
Sub mnuSaveAs_Click ()
'See GEN_PROC.BAS
SaveAs
End Sub
```

```
Sub mnuStop_Click ()
StopSCU
End Sub
```

```
Sub mnuTitle_Click ()
txtTitle.Visible = True
End Sub
```

```
Sub mnuVrt_Click ()
txtPrmtrVrt.Visible = True
End Sub
```

```
Sub txtPrmtrHrz_MouseDown (Button As Integer, Shift As Integer, X As Single, Y As Single)
If Button = Left_Button Then txtPrmtrHrz.Drag 1
If Button = Right_Button Then txtPrmtrHrz.Text = "" 'clear Title
End Sub
```

```
Sub txtPrmtrHrz_MouseUp (Button As Integer, Shift As Integer, X As Single, Y As Single)
If Button = Left_Button Then txtPrmtrHrz.Drag 2
End Sub
```

```
Sub txtPrmtrVrt_MouseDown (Button As Integer, Shift As Integer, X As Single, Y As Single)
If Button = Left_Button Then txtPrmtrVrt.Drag 1
If Button = Right_Button Then txtPrmtrVrt.Text = "" 'clear Title
End Sub
```

```
Sub txtPrmtrVrt_MouseUp (Button As Integer, Shift As Integer, X As Single, Y As Single)
If Button = Left_Button Then txtPrmtrVrt.Drag 2
End Sub
```

```
Sub txtTitle_MouseDown (Button As Integer, Shift As Integer, X As Single, Y As Single)
If Button = Left_Button Then txtTitle.Drag 1
If Button = Right_Button Then txtTitle.Text = "" 'clear Title
End Sub
```

```
Sub txtTitle_MouseUp (Button As Integer, Shift As Integer, X As Single, Y As Single)
If Button = Left_Button Then txtTitle.Drag 2
End Sub
```

```
*****
*****
```

frmWIN3.frm

```

Sub btnPrint3_Click ()
'disable objects on frmWin2-4
PrePrint
lblCoordinates3.Visible = False
PrintForm
lblCoordinates3.Visible = True
'Enable objects on frmWin2-4
AfterPrint
End Sub

```

```

Sub btnSize3_Click ()
If frmWin3.WindowState <> 2 Then
    frmWin3.WindowState = 2
    frmPanel.ZOrder 0
    ScaleWin3
    Redraw
    frmWin3.ZOrder 0
ElseIf frmWin3.WindowState <> 0 Then
    frmWin3.WindowState = 0
    frmPanel.ZOrder 0
    ScaleWin3
    Redraw
    ShowWindows
End If
End Sub

```

```

Sub Form_DragDrop (Source As Control, X As Single, Y As Single)
If Source = lblCoordinates3 Then
    lblCoordinates3.Move X - ScaleWidth / 30, Y - ScaleHeight / 100
End If
End Sub

```

```

Sub Form_MouseDown (Button As Integer, Shift As Integer, X As Single, Y As Single)
If FlagScanOn = 1 Then Exit Sub
'label current point on the screen with a red dot
If Button = Left_Button Then
    Circle (X, Y), -ScaleWidth / 600, RGB(255, 0, 0)
    PSet (X + ScaleWidth / 150, Y)
    Print Format$(X, "0.000") + "; " + Format$(Y, "0.00")
End If
'Clear all labels by graph redrawing
If Button = Right_Button Then

```

```

    frmPanel.ZOrder 0
    Redraw
    ShowWindows
    frmWin3.ZOrder 0
End If

```

```

Sub Form_MouseMove (Button As Integer, Shift As Integer, X As Single, Y As Single)
If FlagScanOn = 1 Then Exit Sub
lblCoordinates3.Caption = "Raman shift (cm-1): " + Format$(X, "0.000") + " Intensity
(V): " + Format$(Y, "0.00")
End Sub

```

```

Sub lblCoordinates3_MouseDown (Button As Integer, Shift As Integer, X As Single, Y
As Single)
If Button = Left_Button Then
    lblCoordinates3.Drag 1 'start of Drag
End If
End Sub

```

```

Sub lblCoordinates3_MouseUp (Button As Integer, Shift As Integer, X As Single, Y As
Single)
If Button = Left_Button Then lblCoordinates3.Drag 2 'end of Drag
End Sub

```

```

*****
*****

```

frmWIN4.frm

```

Sub btnPrint4_Click ()
'disable objects on frmWin2-4
PrePrint
lblCoordinates4.Visible = False
PrintForm
lblCoordinates4.Visible = True
'enable objects on frmWin2-4
AfterPrint
End Sub

```

```

Sub btnSize4_Click ()
If frmWin4.WindowState <> 2 Then
    frmWin4.WindowState = 2
    frmPanel.ZOrder 0
    ScaleWin4
    Redraw
    frmWin4.ZOrder 0

```

```

ElseIf frmWin4.WindowState <> 0 Then
    frmWin4.WindowState = 0
    frmPanel.ZOrder 0
    ScaleWin4
    Redraw
    ShowWindows
End If
End Sub

```

```

Sub Form_DragDrop (Source As Control, X As Single, Y As Single)
If Source = lblCoordinates4 Then
    lblCoordinates4.Move X - ScaleWidth / 30, Y - ScaleHeight / 100
End If
End Sub

```

```

Sub Form_MouseDown (Button As Integer, Shift As Integer, X As Single, Y As Single)
If FlagScanOn = 1 Then Exit Sub
'label current point on the screen with a red dot
If Button = Left_Button Then
    Circle (X, Y), -ScaleWidth / 600, RGB(255, 0, 0)
    PSet (X + ScaleWidth / 150, Y)
    Print Format$(X, "0.000") + "; " + Format$(Y, "0.00")
End If
'Clear all labels by graph redrawing
If Button = Right_Button Then
    frmPanel.ZOrder 0
    Redraw
    ShowWindows
    frmWin4.ZOrder 0
End If

```

```

Sub Form_MouseMove (Button As Integer, Shift As Integer, X As Single, Y As Single)
If FlagScanOn = 1 Then Exit Sub
lblCoordinates4.Caption = "Raman shift (cm-1): " + Format$(X, "0.000") + " Intensity
(V): " + Format$(Y, "0.00")
End Sub

```

```

Sub lblCoordinates4_MouseDown (Button As Integer, Shift As Integer, X As Single, Y
As Single)
If Button = Left_Button Then
    lblCoordinates4.Drag 1 'start of Drag
End If
End Sub

```

```
Sub lblCoordinates4_MouseUp (Button As Integer, Shift As Integer, X As Single, Y As Single)
```

```
If Button = Left_Button Then lblCoordinates4.Drag 2 'end of Drag
```

```
End Sub
```

```
*****
*****
```

GEN_PROC.BAS

```
*****
```

```
'This module contains definitions of general procedures and variables responsible for
'processing of the signal obtained from ADC. Those specific for LabMaster's ADC and
'communication with SCU could be found in IO-Board.Bas and SCU_Proc.Bas
'respectively
```

```
*****
```

```
'Declarations for mhelp.vbx
```

```
Declare Function Inp% Lib "mhelp.vbx" (ByVal PortNum%)
```

```
Declare Sub OUT Lib "mhelp.vbx" (ByVal PortNum%, ByVal DataByte%)
```

```
Global NLS 'line feed and <CR>
```

```
'Strings to hold texts for different messages
```

```
'Texts are initialized in frmPanel Form_Load
```

```
Global Unchangable$
```

```
Global WrongADCchannel$
```

```
Global WrongBadShotChannel$
```

```
Global WrongTotalPts$
```

```
Global WrongWindowSelection$
```

```
Global NoScanTaken$
```

```
Global Greeter$
```

```
Global Help$
```

```
Global Help1$
```

```
Global WrongProgram$
```

```
'# of shots to be averaged for each data point
```

```
'Is the same value for all active channels
```

```
Global Shots%
```

```
'Matrix to store final averaged signals: Signal(i,j)
```

```
'i: 1 - Signal from ADC channel assigned to Window1 ("bad shots")
```

```
' 2 - Signal from ADC channel assigned to Window2
```

```
' 3 - Signal from ADC channel assigned to Window3
```

```
' 4 - Signal from ADC channel assigned to Window4
```

```
'j: # of data point
```

```
Global Signal!()
```

```
'Matrix to store frequencies: Frequency(i,j)
```

```
'i: 1 - dye laser frequency in wave numbers
```

```
' 2 - Raman shift in wave numbers
```

```
'j: # of data point
```

```

Global Frequency!()
'Number of the current data point
Global CurPoint%
'Total number (calculated) of data points
Global TotalPts%
'Real # of points in spectrum after it is stopped.
'Could be different from TotalPts if scan was interrupted
Global NumPtsTaken%
'Array to store numbers of ADC channels to show in Windows
Global Window%(4)
'Code number, which represent sum of Window numbers selected for display of ADC
'channels. E.g. if Window2 and Window3 are selected WinCode=5. Valid values: 2, 5, 9
Global WinCode%
'Max Window number selected to display ADC channels
Global MaxWinNum%
'Scan Parameters used in ScaleWin*, CalcTotalPts procedures etc. in Gen_PROC.BAS
'Calculated upon btnScan_Click() on frmPanel
'Note: PsnStart and PsnEnd are Raman shifts in cm-1
Global Wdth!, Hght!, ScaleIncrement!, Ticks%, ScaleMin!, ScaleMax!
Global PsnStart!, PsnEnd!, Increment! '(i.e step size of scan)
*****
FL A G S   F L A G S   F L A G S
*****
'FlagScanOn: 0 - (no scan); 1 - (scan in progress)
Global FlagScanOn%
'FlagScanOn: 0 - (no scan); 1 - (at least 1 scan taken)
Global FlagScanTaken%
'About form show is terminated: 0 - About is ON; 1 - OFF
Global StopAboutFlag%
*****

Sub AfterPrint ()
'


---


'Enable/make visible objects after print is finished
'


---


frmWin2.mnuControlPanel.Enabled = True
frmWin2.mnuTitle.Enabled = True
frmWin2.mnuSaveAs.Enabled = True
frmWin2.mnuBoxes.Enabled = True
frmWin2.mnuHelp.Enabled = True
frmWin2.btnSize2.Visible = True
frmWin3.btnSize3.Visible = True
frmWin4.btnSize4.Visible = True
frmWin2.btnPrint2.Visible = True
frmWin3.btnPrint3.Visible = True

```

```
frmWin4.btnPrint4.Visible = True
End Sub
```

```
Sub AvgSignal ()
```

```
'
'-----
'This procedure averages number of shots specified by Global variable "Shots" (set by
'user from the "Control Panel"-> "txtShots.Text" during run-time) on ADC channels
'determined by user from the "Control Panel" -> "Data Collection Parameters" during run-
'time and stores average signals in array "Signal". Default Shots = 10 (defined in
'frmPanel Sub Form_Load)
'
```

```
ReDim Sum(MaxWinNum)
```

```
Dim i%, j%, Channel%, Dummy!
```

```
'Zero sum accumulator for signals
```

```
For i = 2 To MaxWinNum: Sum(i) = 0: Next i
```

```
*****
```

```
'Calculate sum of signals for selected channels
```

```
*****
```

```
For i = 1 To Shots
```

```
'-----
'Bad shot check
'-----
```

```
'Number of "Bad shot" channel read from Window0
```

```
Channel = Window(1)
```

```
'Enable "external trigger" of STC (ADC)
```

```
PrepADC 1
```

```
'Read "Bad shot" detector on channel from Window1
```

```
Dummy = ReadADC(Channel)
```

```
'If shot is bad do not count and store it
```

```
If Dummy < .5 Then
```

```
    i = i - 1
```

```
    'display warning in captions of Window*
```

```
    frmWin2.Caption = "B A D  S H O T S  !!!"
```

```
    frmWin3.Caption = "B A D  S H O T S  !!!"
```

```
    frmWin4.Caption = "B A D  S H O T S  !!!"
```

```
    GoTo 1
```

```
End If
```

```
'-----
'Set mode of I/O board ADC to "software trigger"
```

```
PrepADC 0          'see IO_BOARD.BAS
```

```
For j = 2 To MaxWinNum
```

```
    'Note: Array "Window" is defined in btnScan_Click
```

```
    'accumulate signals from selected channels use software start of conversion
```

```
    'SoftADC
```

```

        Sum(j) = Sum(j) + SoftADC(Window(j))
    Next j
1 Next i
*****
'Calculate and store average values in "Signal" for selected windows .
For i = 2 To MaxWinNum
    Signal(i, CurPoint) = Sum(i) / Shots
Next i
End Sub

Sub CheckUnitsMode ()
'
-----
'Makes sure that selected units are wave numbers
'and selected Mode is "Burst"
'
-----
Dim Result$, n%
*****
'Check Units
*****
'Read current selected units
Result = Mid$(TalkSCU("0"), 2, 1)
'Give warning if it is not cm-1
If Result <> "W" And Result <> "w" Then
    MsgBox "Dear valuable Customer:" + NL + NL + "This program is designed to use
'cm-1' only!" + NL + "Thus units have been changed back to wave numbers." + NL + NL
+ "Talk to you later!", 64
    "Scroll" units until wave numbers are selected
'Indication: second character in SCU respond is "W" or "w"
Do
    'Change current selected units
    Result = Mid$(TalkSCU("U"), 2, 1)
Loop Until Result = "W" Or Result = "w"
End If
*****

*****
'Check Mode
*****
'Read code letter for Units/Mode from SCU respond
n = Asc(Result)
'Detrmine if it is Upper or Lower case
'Lower case means "Linear" scan mode
'Upper case means "Burst" scan mode
If n >= 97 And n <= 122 Then

```

```
MsgBox "Dear valuable Customer:" + NL + NL + "This program does not support
'Linear' mode," + NL + "so 'Scan Mode' is changed back to 'Burst'" + NL + NL + "Take
care.", 64
```

```
'change back to "Burst": "B" toggels between two modes
```

```
Do
```

```
n = Asc(Mid$(TalkSCU("B"), 2, 1))
```

```
Loop Until n >= 65 And n <= 90
```

```
End If
```

```
*****
```

```
End Sub
```

```
Sub Display ()
```

```
'Display current point in Caption of frmSpectra
```

```
'Laser frequency;Raman shift; Signals on ADC
```

```
'channels and draw Volts=f(Raman shift)
```

```
Dim Result$
```

```
'Window2
```

```
Result = "Window2:      " + "Channel: " + Str$(Window(2)) + "      Laser: " +
Format$(Frequency(1, CurPoint), ".00")
```

```
Result = Result + "      Raman: " + Format$(Frequency(2, CurPoint), ".00")
```

```
Result = Result + "      Volts:"
```

```
Result = Result + Format$(Signal(2, CurPoint), "0.00")
```

```
frmWin2.Caption = Result
```

```
frmWin2.Line -(Frequency(2, CurPoint), Signal(2, CurPoint))
```

```
If WinCode = 2 Then Exit Sub 'the rest is not displayed
```

```
'Window3
```

```
Result = "Window3:      " + "Channel: " + Str$(Window(3)) + "      Laser: " +
Format$(Frequency(1, CurPoint), ".00")
```

```
Result = Result + "      Raman: " + Format$(Frequency(2, CurPoint), ".00")
```

```
Result = Result + "      Volts:"
```

```
Result = Result + Format$(Signal(3, CurPoint), "0.00")
```

```
frmWin3.Caption = Result
```

```
frmWin3.Line -(Frequency(2, CurPoint), Signal(3, CurPoint))
```

```
If WinCode = 5 Then Exit Sub 'the rest is not displayed
```

```
'Window4
```

```
Result = "Window4:      " + "Channel: " + Str$(Window(4)) + "      Laser: " +
Format$(Frequency(1, CurPoint), ".00")
```

```
Result = Result + "      Raman: " + Format$(Frequency(2, CurPoint), ".00")
```

```
Result = Result + "      Volts:"
```

```
Result = Result + Format$(Signal(4, CurPoint), "0.00")
```

```
frmWin4.Caption = Result
```

```
frmWin4.Line -(Frequency(2, CurPoint), Signal(4, CurPoint))
```

```
End Sub
```

```
Sub FileDateStamp ()
```

```
'Show current file name and date/time on form frm.Win2
```

```
frmWin2.lblFileDate.Caption = frmPanel.cmdBox.FileName + Format$(Now, " mm/dd/yy  
hh:mm")  
End Sub
```

```
Sub FileOpen ()
```

```
'Load old file from disk into program
```

```
Dim i&, j%, t$, Dummy$, Result$, x%, y%, a$, b$  
frmPanel.cmdBox.Flags = OFN_PATHMUSTEXIST Or OFN_FILEMUSTEXIST
```

```
'Action "Open"
```

```
frmPanel.cmdBox.Action = 1
```

```
If frmPanel.cmdBox.FileName = "" Then
```

```
    MsgBox "No file selected!", 16
```

```
    Exit Sub
```

```
End If
```

```
Open frmPanel.cmdBox.FileName For Input As #1
```

```
'Read version of the program used to save this file
```

```
Line Input #1, t$
```

```
If t <> "Lumonics17a" Then
```

```
    MsgBox WrongProgram, 16
```

```
    Close
```

```
    Exit Sub
```

```
End If
```

```
frmPanel.MousePointer = 11
```

```
'Read date and time file was taken
```

```
Line Input #1, t
```

```
frmWin2.lblFileDate.Caption = frmPanel.cmdBox.FileName + " " + t
```

```
'Read blank line
```

```
Line Input #1, t
```

```
' "Scan Title"
```

```
Line Input #1, Dummy$ '(discard "Scan Title")
```

```
Result = ""
```

```
Line Input #1, Dummy$
```

```
a = Dummy$
```

```
If a <> "Text from Vertical Parameter Box" Then
```

```
    Do
```

```
        Line Input #1, Dummy$
```

```
        b = Dummy$
```

```
        If b = "Text from Vertical Parameter Box" Then
```

```

        Result = Result + a
    Exit Do
Else
    Result = Result + a + NL
    a = b
End If
Loop
End If
frmWin2.txtTitle.Text = Result
' "Text from Vertical Parameter Box"
Result = ""
Line Input #1, Dummy$
a = Dummy$
If a <> "Text from Horizontal Parameter Box" Then
    Do
        Line Input #1, Dummy$
        b = Dummy$
        If b = "Text from Horizontal Parameter Box" Then
            Result = Result + a
            Exit Do
        Else
            Result = Result + a + NL
            a = b
        End If
    Loop
End If
frmWin2.txtPrmtrVrt.Text = Result
' "Text from Horizontal Parameter Box"
Result = ""
Line Input #1, Dummy$
a = Dummy$
If a <> "End of text" Then
    Do
        Line Input #1, Dummy$
        b = Dummy$
        If b = "End of text" Then
            Result = Result + a
            Exit Do
        Else
            Result = Result + a + NL
            a = b
        End If
    Loop
End If
frmWin2.txtPrmtrHrz.Text = Result

```

```

'Read blank line
Line Input #1, t
'Read actual number of points taken
Line Input #1, t: NumPtsTaken = Val(t)
'Read Maximum Window Number was used
Line Input #1, t: MaxWinNum = Val(t)
'Set up corresponding "WinCode"
WinCode = 0
For i = 2 To MaxWinNum
    WinCode = WinCode + i
Next i
'Read blank line
Line Input #1, t
'Read/discard header
Line Input #1, t
*****
*****
ReDim Frequency!(2, NumPtsTaken), Signal(MaxWinNum, NumPtsTaken)
For i = 1 To NumPtsTaken
    Line Input #1, t
    Frequency(1, i) = Val(Mid$(t, 2, 8))
    Frequency(2, i) = Val(Mid$(t, 16, 8))
For j = 2 To MaxWinNum
    Signal(j, i) = Val(Mid$(t, 29 + (j - 2) * 14, 6))
Next j
Next i
*****
PsnStart = Frequency(2, 1)
PsnEnd = Frequency(2, NumPtsTaken)
Wdth = PsnEnd - PsnStart
Close
'Size windows selected for display and place them on screen
SizeWindows
'draw loaded file in corresponding windows
Redraw
ShowWindows
'Initialize screen objects
PostScanIni
frmPanel.MousePointer = 1
End Sub

Sub Hidewindows ()
frmWin2.Hide
frmWin3.Hide
frmWin4.Hide

```

End Sub

Sub InitializeSCU ()

'Initialize communication with SCU of Lumonics

Dim Dummy\$

'Initialize CommPort for communications with SCU

'CommSCU is defined in SCU_Proc.Bas as Global Const

CommSCUini (CommSCU)

'Make sure scan is stopped

StopSCU

'Make sure that "LoopBack" flag of SCU is "0". See Lumonics manual p. 5-7 for more information

Dummy = TalkSCU("908:0")

'Make sure that units are set to wave numbers. Make sure that mode is set to "Burst".

'See the current GEN_PROC.BAS

CheckUnitsMode

'Read current "Basic Scan Parameters" and current "Advanced Scan Parameters" from SCU

ReadAllScanPrmtrs 'See GEN_PROC.BAS

End Sub

Sub PostScanIni ()

'Post initialization of frmWin* and their objects

'Mouse Pointer to cross

frmWin2.MousePointer = 2

frmWin3.MousePointer = 2

frmWin4.MousePointer = 2

'enable/disable objects on formWin*

frmWin2.mnuStop.Enabled = False

frmWin2.mnuPause.Enabled = False

frmWin2.mnuResume.Enabled = False

frmWin2.mnuControlPanel.Enabled = True

frmWin2.mnuTitle.Enabled = True

frmWin2.mnuSaveAs.Enabled = True

frmWin2.mnuBoxes.Enabled = True

frmWin2.mnuHelp.Enabled = True

frmWin2.btnSize2.Enabled = True

frmWin3.btnSize3.Enabled = True

frmWin4.btnSize4.Enabled = True

frmWin2.btnPrint2.Enabled = True

frmWin3.btnPrint3.Enabled = True

```

frmWin4.btnPrint4.Enabled = True
'no scan in progress
FlagScanOn = 0
'at least one scan taken
FlagScanTaken = 1
End Sub

```

```

Sub PrePrint ()

```

```

'Disable/make invisible unnecessary objects

```

```

frmWin2.mnuControlPanel.Enabled = False
frmWin2.mnuTitle.Enabled = False
frmWin2.mnuSaveAs.Enabled = False
frmWin2.mnuBoxes.Enabled = False
frmWin2.mnuHelp.Enabled = False
frmWin2.btnSize2.Visible = False
frmWin3.btnSize3.Visible = False
frmWin4.btnSize4.Visible = False
frmWin2.btnPrint2.Visible = False
frmWin3.btnPrint3.Visible = False
frmWin4.btnPrint4.Visible = False
End Sub

```

```

Sub ReadAdvdPrmtrs ()

```

```

'This procedure reads current "Advanced Scan Parameters" from SCU and displays them
'on the Control Panel

```

```

Dim Result$, n%
'read present position and display it
frmPanel.txtPresPsn.Text = ReadPresPsn()
'read from SCU and display other SCU "Advanced Scan Parameters"
frmPanel.txtScanDelay.Text = Format$(Right$(TalkSCU("6"), 8), "#0.00")
frmPanel.txtFrequency.Text = Format$(Right$(TalkSCU("7"), 8), "#0.00")
frmPanel.txtBurstQuantity.Text = Format$(Right$(TalkSCU("8"), 8), "#")
'Show number of Comm Port used for communications with SCU
frmPanel.lblCommPortT.Caption = Str$(CommSCU)
End Sub

```

```

Sub ReadAllScanPrmtrs ()

```

```

'Read from SCU and display all scan parameters
'on Control Panel

```

```

ReadBasicPrmtrs
ReadAdvdPrmtrs
End Sub

```

```

Sub ReadBasicPrmtrs ()

```

```

This procedure reads current "Basic Scan Parameters" from
'SCU and displays them on the "Control Panel"

```

```

frmPanel.txtStartPsn.Text = Format$(Right$(TalkSCU("1"), 8), ".00")
frmPanel.txtFinalPsn.Text = Format$(Right$(TalkSCU("2"), 8), ".00")
frmPanel.txtIncrement.Text = Format$(Right$(TalkSCU("3"), 8), "#0.00")
frmPanel.txtScanRepeat.Text = Format$(Right$(TalkSCU("5"), 8), "#")
End Sub

```

```

Sub ReadINI ()

```

```

Read INI file from C:\windows

```

```

Dim Dummy$, Result$, a$, b$
Open "c:\windows\Lumonics.ini" For Input As #2
' "Shots to average"
Input #2, Dummy$
Input #2, Dummy$
frmPanel.txtShots.Text = Dummy$
' "Bad shot channel"
Input #2, Dummy$
Input #2, Dummy$
frmPanel.txtWindow(1).Text = Dummy$
' "Window2 ADC channel"
Input #2, Dummy$
Input #2, Dummy$
frmPanel.txtWindow(2).Text = Dummy$
' "Window3 ADC channel"
Input #2, Dummy$
Input #2, Dummy$
frmPanel.txtWindow(3).Text = Dummy$
' "Window4 ADC channel"
Input #2, Dummy$
Input #2, Dummy$
frmPanel.txtWindow(4).Text = Dummy$
' "Pump Beam Wavelength in cm-1"
Input #2, Dummy$
Input #2, Dummy$
frmPanel.txtPumpBeam.Text = Dummy$

```

```

' "Default Slew position in cm-1"
Input #2, Dummy$
Input #2, Dummy$
frmPanel.txtSlewPsn.Text = Dummy$
' "Scan Title"
Input #2, Dummy$ '(discard "Scan Title")
Result = ""
Input #2, Dummy$
a = Dummy$
If a <> "Text from Vertical Parameter Box" Then
  Do
    Input #2, Dummy$
    b = Dummy$
    If b = "Text from Vertical Parameter Box" Then
      Result = Result + a
      Exit Do
    Else
      Result = Result + a + NL
      a = b
    End If
  Loop
End If
frmWin2.txtTitle.Text = Result
' "Text from Vertical Parameter Box"
Result = ""
Input #2, Dummy$
a = Dummy$
If a <> "Text from Horizontal Parameter Box" Then
  Do
    Input #2, Dummy$
    b = Dummy$
    If b = "Text from Horizontal Parameter Box" Then
      Result = Result + a
      Exit Do
    Else
      Result = Result + a + NL
      a = b
    End If
  Loop
End If
frmWin2.txtPrmtrVrt.Text = Result
' "Text from Horizontal Parameter Box"
Result = ""
Input #2, Dummy$
a = Dummy$

```

```

If a <> "End" Then
  Do
    Input #2, Dummy$
    b = Dummy$
    If b = "End" Then
      Result = Result + a
      Exit Do
    Else
      Result = Result + a + NL
      a = b
    End If
  Loop

End If
frmWin2.txtPrmtrHrz.Text = Result
Close #2
End Sub

Sub Redraw ()
'


---


Redraws last spectrum taken in main Window2
'Note: It does not show forms if they are invisible
'


---


'Clear selected Windows and scale them
ScaleWindows
'draw graphs in selected Windows
For CurPoint = 1 To NumPtsTaken
  Display
Next CurPoint
End Sub

Sub SaveAs ()
'


---


Sav scan if any taken
'


---


Dim i%, j%, Result$
'check if there is anything to save
If FlagScanTaken = 0 Then
  MsgBox NoScanTaken, 16
  Exit Sub
End If
'common dialog box "cmdBox" settings
frmPanel.cmdBox.Flags = OFN_PATHMUSTEXIST Or OFN_OVERWRITEPROMPT
'Save as action
frmPanel.cmdBox.Action = 2

```

```

'check if any name was selected
If frmPanel.cmdBox.FileName = "" Then
    MsgBox "No file selected!", 16
    Exit Sub
End If
'default file name + date + time to display on frmWin2
FileDateStamp
frmPanel.MousePointer = 11
frmWin2.MousePointer = 11
frmWin3.MousePointer = 11
frmWin4.MousePointer = 11
Open frmPanel.cmdBox.FileName For Output As #1
Print #1, "Lumonics17a"
Print #1, Format$(Now, "mm/dd/yy hh:mm")
'blank line
Print #1,
'Save Title if it is visible
Print #1, "Scan Title"
If frmWin2.txtTitle.Visible = True Then
    Print #1, frmWin2.txtTitle.Text
End If
'Save Vertical Parameter Box if it is visible
Print #1, "Text from Vertical Parameter Box"
If frmWin2.txtPrmtrVrt.Visible = True Then
    Print #1, frmWin2.txtPrmtrVrt.Text
End If
'Save Horizontal Parameter Box if it is visible
Print #1, "Text from Horizontal Parameter Box"
If frmWin2.txtPrmtrHrz.Visible = True Then
    Print #1, frmWin2.txtPrmtrHrz.Text
End If
Print #1, "End of text"
'blank line
Print #1,
'save actual number of points in spectrum
Print #1, NumPtsTaken

'save maximum window number used (tells how many channels were used)
'e.g. 2 - means only window2 was used; 3 - means window2 and window3
Print #1, MaxWinNum
'blank line
Print #1,
Print #1, "Laser, cm-1", "Raman, cm-1", "Window2", "Window3", "Window4"
For i = 1 To NumPtsTaken
    'save frequencies: Laser and Raman

```

```

Print #1, Frequency(1, i), Frequency(2, i),
'save Signals for selected channels
For j = 2 To MaxWinNum
    Print #1, Format$(Signal(j, i), "0.00"),
Next j
'save nothing after the last Signal
'needed to force next entry to be on a new line
Print #1,
Next i
Close #1
frmPanel.MousePointer = 1
frmWin2.MousePointer = 2
frmWin3.MousePointer = 2
frmWin4.MousePointer = 2
End Sub

Sub ScaleWin2 ()
'


---


Scales Window2 and draws axes on it
'


---


Dim j%
frmWin2.Cls

frmWin2.Scale (PsnStart - Wdth * .01, ScaleMax + Hght * .03)-(PsnEnd + Wdth * .1,
ScaleMin - Hght * .06)
'*****draw axes on Window2 'horizontal line*****
frmWin2.Line (PsnStart, ScaleMin)-(PsnEnd, ScaleMin), RGB(250, 0, 0)
'vertical line
frmWin2.Line (PsnStart, ScaleMin)-(PsnStart, ScaleMax), RGB(250, 0, 0)
'***** draws appropriate numbers on X axis *****
ScaleIncrement = Wdth / (Ticks - 1)
For j = 0 To 5
    frmWin2.Line (PsnStart + ScaleIncrement * j, ScaleMin)-(PsnStart + ScaleIncrement *
j, ScaleMin - Hght * .01), RGB(250, 0, 0)
    frmWin2.CurrentY = ScaleMin - Hght * .01
    frmWin2.Print Format$(PsnStart + ScaleIncrement * j, ".000");
Next j
End Sub

Sub ScaleWin3 ()
'


---


Scales Window3
'


---


frmWin3.Cls

```

```

frmWin3.Scale (PsnStart - Wdth * .01, ScaleMax + Hght * .03)-(PsnEnd + Wdth * .1,
ScaleMin - Hght * .06)
frmWin3.PSet (PsnStart, ScaleMin)
End Sub

```

```

Sub ScaleWin4 ()

```

```

Scales Window4

```

```

frmWin4.Cls
frmWin4.Scale (PsnStart - Wdth * .01, ScaleMax + Hght * .03)-(PsnEnd + Wdth * .1,
ScaleMin - Hght * .06)
frmWin4.PSet (PsnStart, ScaleMin)
End Sub

```

```

Sub ScaleWindows ()

```

```

'Clear and set up scale of selected windows. Selected windows are indicated by WinCode
'WinCode is calculated under btnScan_Click

```

```

Select Case WinCode

```

```

Case 2

```

```

    frmWin2.Cls
    ScaleWin2

```

```

Case 5

```

```

    frmWin2.Cls
    frmWin3.Cls
    ScaleWin2
    ScaleWin3

```

```

Case 9

```

```

    frmWin2.Cls
    frmWin3.Cls
    frmWin4.Cls
    ScaleWin2
    ScaleWin3
    ScaleWin4

```

```

End Select

```

```

'Put current point in the lower left corner of Scale

```

```

frmWin2.PSet (PsnStart, ScaleMin)
frmWin3.PSet (PsnStart, ScaleMin)
frmWin4.PSet (PsnStart, ScaleMin)
End Sub

```

```
Sub ShowWindows ()
```

```
,
```

```
'Show selected Windows in their current state
```

```
,
```

```
Select Case WinCode
```

```
Case 2
```

```
    frmWin2.Show
```

```
    MaxWinNum = 2
```

```
Case 5
```

```
    frmWin2.Show
```

```
    frmWin3.Show
```

```
    MaxWinNum = 3
```

```
Case 9
```

```
    frmWin2.Show
```

```
    frmWin3.Show
```

```
    frmWin4.Show
```

```
    MaxWinNum = 4
```

```
End Select
```

```
End Sub
```

```
Sub SizeWindows ()
```

```
,
```

```
'Set up size of windows and place them on the screen
```

```
,
```

```
Select Case WinCode
```

```
Case 2
```

```
    frmWin2.Top = 0
```

```
    frmWin2.Left = 0
```

```
    frmWin2.Height = 7320
```

```
Case 5
```

```
    frmWin2.Left = 0
```

```
    frmWin2.Top = 2130
```

```
    frmWin2.Height = 5025
```

```
    frmWin3.Left = 0
```

```
    frmWin3.Top = 0
```

```
    frmWin3.Height = 2130
```

```
Case 9
```

```
    frmWin2.Left = 0
```

```
    frmWin2.Top = 3135
```

```
    frmWin2.Height = 4065
```

```
    frmWin3.Left = 0
```

```
    frmWin3.Top = 1560
```

```
    frmWin3.Height = 1580
```

```
    frmWin4.Left = 0
```

```
    frmWin4.Top = 0
```

```

    frmWin4.Height = 1575
End Select
End Sub

```

```

Sub StoreFrq ()

```

```

'Stores current position of dye laser, calculates and
'stores corresponding Raman shift (all in cm-1)

```

```

Dim Result!

```

```

'If error occurs in reading Present position try to read it once again: go to the beginning
On Error Resume Next

```

```

'get and store dye laser position discard any erroneous position due to not complete
'reading of the position (MSD are cut off)

```

```

'Do

```

```

    Result = CSng(ReadPresPsn())

```

```

'Loop Until Result >= PsnStart * .95

```

```

Frequency(1, CurPoint) = Result

```

```

'calculate and store Raman shift

```

```

Frequency(2, CurPoint) = CSng(frmPanel.txtPumpBeam.Text) - Result

```

```

End Sub

```

```

Sub WriteAdvdPrmtrs ()

```

```

'This procedure takes SCU "Advanced scan parameters" from the
'"Control Panel" on the screen and writes them to SCU

```

```

Dim Result$

```

```

Result = TalkSCU("0:" + LTrim$(Str$(Val(frmPanel.txtPresPsn.Text))))

```

```

Result = TalkSCU("6:" + LTrim$(Str$(Val(frmPanel.txtScanDelay.Text))))

```

```

Result = TalkSCU("7:" + LTrim$(Str$(Val(frmPanel.txtFrequency.Text))))

```

```

Result = TalkSCU("8:" + LTrim$(Str$(Val(frmPanel.txtBurstQuantity.Text))))

```

```

'Scan mode is fixed to "Burst" for this program; can't change

```

```

'CommSCU (port for SCU) could be changed only at design time

```

```

'Change value of CommSCU (see SCU_PROC.BAS->declarations)

```

```

End Sub

```

```

Sub WriteBasicPrmtrs ()

```

```

'This procedure takes "Basic scan parameters" from the
'"Control Panel" on the screen and writes them to SCU

```

```

Dim Result$

```

```

Result = TalkSCU("1:" + LTrim$(Str$(Val(frmPanel.txtStartPsn.Text))))

```

```

Result = TalkSCU("2:" + LTrim$(Str$(Val(frmPanel.txtFinalPsn.Text))))

```

```

Result = TalkSCU("3:" + LTrim$(Str$(Val(frmPanel.txtIncrement.Text))))
Result = TalkSCU("5:" + LTrim$(Str$(Val(frmPanel.txtScanRepeat.Text))))
End Sub

```

```

Sub WriteIni ()

```

```

'Write INI file Lumonics.ini to C:\Windows

```

```

Open "c:\windows\Lumonics.ini" For Output As #2

```

```

Print #2, "Shots to average"

```

```

Print #2, frmPanel.txtShots.Text

```

```

Print #2, "Bad shot channel"

```

```

Print #2, frmPanel.txtWindow(1).Text

```

```

Print #2, "Window2 ADC channel"

```

```

Print #2, frmPanel.txtWindow(2).Text

```

```

Print #2, "Window3 ADC channel"

```

```

Print #2, frmPanel.txtWindow(3).Text

```

```

Print #2, "Window4 ADC channel"

```

```

Print #2, frmPanel.txtWindow(4).Text

```

```

Print #2, "Pump Beam Wavelength in cm-1"

```

```

Print #2, frmPanel.txtPumpBeam.Text

```

```

Print #2, "Default Slew position in cm-1"

```

```

Print #2, frmPanel.txtSlewPsn.Text

```

```

Print #2, "Scan Title"

```

```

Print #2, frmWin2.txtTitle.Text

```

```

Print #2, "Text from Vertical Parameter Box"

```

```

Print #2, frmWin2.txtPrmtrVrt.Text

```

```

Print #2, "Text from Horizontal Parameter Box"

```

```

Print #2, frmWin2.txtPrmtrHrz.Text

```

```

Print #2, "End"

```

```

Close #2

```

```

End Sub

```

```

*****

```

```

*****

```

IO_BOARD.BAS

```

*****

```

```

'In general IO_BOARD.BAS contains procedures responsible

```

```

'for control of I/O board used for ADC of the signal to be

```

```

'collected and processed by PC. Should be modified in the

```

```

'case I/O board is changed.

```

```

*****

```

```

'THE LABMASTER'S ADC SHOULD BE CONFIGURED AS FOLLOWS:

```

```

'
'   - BINARY OUTPUT FORMAT
'   - UNIPOLAR 0 - 10 V INPUT RANGE
'
'OTHERWISE "READADC()" FUNCTION SHOULD BE MODIFIED
'

```

Addresses of Lab Master

```

'Base address
Global Const ADDRESS = 816
'Addresses of the 8255 parallel I/O chip
Global Const portA = ADDRESS + 12
Global Const portB = ADDRESS + 13
Global Const portC = ADDRESS + 14
Global Const control8255 = ADDRESS + 15 'control port
'Control/Status byte (control if write, status if read)
Global Const ContStatus = ADDRESS + 4

```

Sub PrepADC (Mode%)

```

'This procedure sets mode of ADC
'

```

```

Dim x As Integer      'dummy
'reset done flipflop by reading HI byte
    x = Inp(ADDRESS + 6)
'write control byte to board
'mode=0 means software start convert
'mode-1 means external start convert
    OUT ContStatus, 128 + 4 * Mode%
End Sub

```

Function ReadADC! (Channel%)

```

This function returns converted input from ADC registers for channel defined by formal
'parameter "Channel"and translates it into Voltage
'THIS PROCEDURE NEEDS TO BE MODIFIED IN CASE OF CHANGE
'OF IO BOARD CONFIGURATION: POLARITY, INPUT RANGE ETC.
'

```

```

Dim Low%, High%, Result&
'Select ADC channel # of I/O board board
OUT ADDRESS + 5, Channel%
'Wait until EOC (bit 7 goes HI)
Do: Loop While Inp%(ContStatus) < 128
'Read Low byte and High half-bytes
Low = (Inp(ADDRESS + 5) And 255) 'mask bits 0-7

```

```

High = (Inp(ADDRESS + 6) And 15) 'mask off bits 4-7
'Combine two parts to 12-bit word
Result = 256 * High + Low
'Convert counts -> volts
'(LabMaster is configured in binary output format and
'and 0 - 10 V unipolar input range)
ReadADC = Result / 409.6
End Function

```

```

Function SoftADC! (Channel%)

```

```

This procedure performs ADC triggered by software
'THIS PROCEDURE NEEDS TO BE MODIFIED IN CASE OF CHANGE
'OF IO BOARD CONFIGURATION: POLARITY, INPUT RANGE ETC.

```

```

Dim Low%, High%, Result&
'Select ADC channel # of I/O board board
OUT ADDRESS + 5, Channel%
'Software start of conversion
OUT ADDRESS + 6, 0
'Wait until EOC (bit 7 goes HI)
Do: Loop While Inp%(ContStatus) < 128
'Read Low byte and High half-bytes
Low = (Inp(ADDRESS + 5) And 255) 'mask bits 0-7
High = (Inp(ADDRESS + 6) And 15) 'mask off bits 4-7
'Combine two parts to 12-bit word
Result = 256 * High + Low
'Convert counts -> volts
'(LabMaster is configured in binary output format and 0 - 10 V unipolar input range)
'Read converted data
SoftADC = Result / 409.5
End Function

```

```

*****
*****

```

SCU_PROC.BAS

```

*****
The SCU_PROC.BAS contains functions responsible for communications with SCU of
'Lumonics
*****

```

```

'Register layout for Comm ports see in Hogan,"Programmer's PC source book", 430.
'Copy of relevant pages is attached to the Program listing Program listing is in file cabinet
'under Dye Laser: Lumonics

```

'Holds message to show in case invalid Comm port was selected. Text itself is initialized in 'Form_Load (frmPanel). Valid Comm port number for SCU: 1 or 2
 Global WrongCommSCU\$
 'Code of Comm Port used for communicatios with SCU. This parameter is used in "Peak" and "Poke" routines (See current module: SCU_PROC.BAS)
 Global SCU_Port_Code%
 'Number of Comm Port used for communications with SCU. Valid values are 1 or 2
 Global Const CommSCU = 1

Function CheckSum% (Strng\$)

'

 Calculates actual checksum of message from SCU. Compares it with one send by SCU to PC. Returns -1 in case they are different - bad reading. Returns 1 in case they are same - good reading. Note: last three characters in message from SCU contain encoded Checksum value; first part of the whole message is "informative" message itself
 '_____

Dim L%, aSum%, i%

Dim CheckSumCode\$

'Calculate actual checksum of SCU informative message received

aSum = 0

For i = 1 To Len(Strng) - 3

 aSum = aSum + Asc(Mid\$(Strng, i, 1))

Next i

'calculate letter code for CheckSum of informative message received

CheckSumCode = Chr\$((aSum And 15) + 96) + Chr\$((Int(aSum / 16) And 15) + 96) + Chr\$(13)

'compare letter code of computed CheckSum with one received from SCU

If CheckSumCode = Right\$(Strng, 3) And aSum > 0 Then

 CheckSum = 1 'O.K reading

Else

 CheckSum = -1 'bad reading

End If

End Function

Sub CommSCUini (Port%)

'

 'This procedure checks if the choice of new Comm port for communications with SCU is valid and initializes it
 '_____

If Port <> 1 And Port <> 2 Then

 MsgBox WrongCommSCU\$, 16

 End

Else

 PortEncode (Port) 'see current SCU_PROC.BAS

End If

```
'Open selected port
frmPanel.Comm1.CommPort = Port
frmPanel.Comm1.Settings = "9600,n,8,2" 'Establish settings
frmPanel.Comm1.PortOpen = True
'Initialize handshaking lines: DTR & RTS (LO: PC ready). It turned out that there is no
'need for "normal" handshaking since modern PC are faster than SCU. Therefore it is
'sufficient to drop DTR & RTS once.
OUT SCU_Port_Code * &H100 + &H2FC, 3
End Sub
```

```
Sub PauseSCU ()
```

```
'Pause the scan in progress
```

```
Do: Loop Until Left$(TalkSCU("P"), 1) = "P"
End Sub
```

```
Function Peak () As String
```

```
'This procedure returns a character read from Comm port. Number of port is defined by
'variable "CommSCU". Code for CommSCU is stored in variable "SCU_Port_Code"
```

```
'Wait for bit 0 in Line Status register go HI : DATA RECEIVED
Do: Loop Until (Inp(SCU_Port_Code * &H100 + &H2FD) And 1) = 1
'Read a byte from the RX buffer
Peak = Chr$(Inp(SCU_Port_Code * &H100 + &H2F8) And 127)
End Function
```

```
Sub Poke (c$)
```

```
'This procedure sends a character C$ to Comm port. Number of port is defined by
'variable "CommSCU". Code for CommSCU is stored in variable "SCU_Port_Code"
```

```
'Wait for bit 5 in Line Status register is HI. (Trans-hold-register is empty)
Do: Loop Until (Inp(SCU_Port_Code * &H100 + &H2FD) And &H20) = &H20
'Send a byte C$ to TX buffer
OUT SCU_Port_Code * &H100 + &H2F8, Asc(c$)
End Sub
```

```
Sub PortEncode (Num%)
```

```
'This procedure establishes code for Comm port to be used for communications with SCU.
'"SCU_Port_Code" parameter is used in "Peak" and "Poke" procedures of the
SCU_PROC.BAS
```

```

Select Case Num
  Case 1
    SCU_Port_Code = 1
  Case 2
    SCU_Port_Code = 0
  Case Else
    MsgBox WrongCommSCU$, 16   'invalid CommSCU (port number for SCU)
  End
End Select
End Sub

```

```

Function ReadPresPsn ()

```

```

'Returns present position of the dye laser

```

```

ReadPresPsn = Format$(Right$(TalkSCU("0"), 8), ".00")
End Function

```

```

Function ReadSCU () As String

```

```

'This function returns a String read from Comm1 or Comm2. Specific port is defined by
'CommSCU (see declarations)

```

```

Dim temp$
Dim Result$      'stores a string to be returned
Result = ""
'read characters until the end of a word :<CR>
Do
  temp = Peak()
  If temp <> Chr$(0) Then
    Result = Result + temp
  End If
Loop Until temp = Chr$(13)
ReadSCU = Result
End Function

```

```

Sub SlewSCU (Position$)

```

```

'Slew Lumonics to the specified position

```

```

Dim Dummy$
Dummy$ = TalkSCU("9:" + Position)
End Sub

```

```

Function StatusSCU$ ()

```

'This function returns the status character from SCU
'respond. See Lumonics manual p. 5-36

```
StatusSCU = Left$(TalkSCU("0"), 1)
End Function
```

```
Sub StepSCU ()
```

'This sub performs one step of Lumonics. Step size in current units is determined by
'parameter 3 "increment" (stored in SCU). Note: "N" command is enabled only if
'"LoopBack" flag is set to "0" ("908:0") - see InitializeSCU in current SCU_PROC.BAS

```
Dim Result$
```

```
'Issue "Next Position" command to SCU
```

```
Result = TalkSCU("N")
```

```
'Wait until step is done or scan is stopped.
```

```
'The first letter of SCU respond "@" means step is done
```

```
'The first letter of SCU respond "S" means scan is stopped
```

```
Do
```

```
    Result = Left$(TalkSCU("0"), 1)
```

```
Loop Until Result = "@" Or Result = "S"
```

```
End Sub
```

```
Sub StopSCU ()
```

```
'Stop the scan in progress
```

```
Do: Loop Until Left$(TalkSCU("S"), 1) = "S"
```

```
End Sub
```

```
Function TalkSCU$ (c$)
```

'This function sends Strng\$ to SCU via Comm port specified by CommSCU, returns a
'respond from SCU and checks if error occurred and if message was "distorted" in the
'course of communication

```
Dim Result$, temp$
```

```
On Error Resume Next
```

```
'keep requesting until no error and no "distortion" occurs
```

```
Do
```

```
    temp = c
```

```
    WriteSCU temp          'send command to SCU
```

```
    Result = ReadSCU()     'get respond
```

```

'Check if Checksum is correct and no error occurred
'return informative respond by exiting function
If CheckSum(Result) = 1 And Left$(Result, 2) <> "EE" Then
    TalkSCU = Left$(Result, Len(Result) - 3)
    Exit Do
End If
Loop                               'otherwise repeat command
End Function

Sub WriteSCU (Strng$)
'


---


'This procedure sends Strng$ to Comm1 or Comm2
'Specific port is defined by CommSCU (see declarations)
'


---


Dim CheckSum%, i%
'Chr$(5) means that SCU is ready to get a word from PC
Do: Loop Until Peak() = Chr$(5)
'Calculate CHECKSUM of the String$
CheckSum = 0
For i = 1 To Len(Strng)
    CheckSum = CheckSum + Asc(Mid$(Strng, i, 1))
Next i
'Compose message by appending CHECKSUM letter code and <CR> to Strng$
Strng = Strng + Chr$((CheckSum And 15) + 96) + Chr$((Int(CheckSum / 16) And 15) +
96) + Chr$(13)
'send composed message to SCU characterwise
For i = 1 To Len(Strng)
    Poke Mid$(Strng, i, 1)
Next i
End Sub
*****
*****

```

APPENDIX C. MULTIPLE LINEAR REGRESSION ANALYSIS USING MICROSOFT EXCEL

C.1. Introduction

This section is devoted to the regression tool of Microsoft Excel 7.0, which was used in some of the fitting of our experimental data. The section is based on a student's guide on multiple linear regression analysis written by M. L. Orlov (1996).

In modern science, regression analysis is a necessary part of virtually almost any data reduction process. Popular spreadsheet programs, such as Quattro Pro, Microsoft Excel, and Lotus 1-2-3 provide comprehensive statistical program packages, which include a regression tool among many others. Usually, the regression module is explained clearly enough in on-line help and spreadsheet documentation (i.e. items in the regression input dialog boxes). However, the description of the output is minimal and is often a mystery for the user who is unfamiliar with certain statistical concepts. The objective of this section is to give a more detailed description of the output of the regression tool and to touch upon related statistical topics.

C.2. Classification of regression models

In a regression analysis we study the relationship, called the regression function, between one variable y , called the dependent variable, and several others x_i , called the independent variables. Regression function also involves a set of unknown parameters b_i . If a regression function is linear in the parameters (but not necessarily in the independent variables !) we term it a linear regression model. Otherwise, the model is called non-linear. Linear regression models with more than one independent variable are referred to as multiple linear models, as opposed to simple linear models with one independent variable.

The following notation is used in this section:

y	- dependent variable (predicted by a regression model)
y^*	- dependent variable (experimental value)
p	- number of independent variables (number of coefficients)
x_i ($i=1,2, \dots p$)	- i th independent variable from total set of p variables
b_i ($i=1,2, \dots p$)	- i th coefficient corresponding to x_i
b_0	- intercept (or constant)
$k=p+1$	- total number of parameters including intercept (constant)
n	- number of observations (experimental data points)
$i=1,2 \dots p$	- independent variables' index
$j=1,2, \dots n$	- data points' index

C.3. Main objectives of multiple linear regression analysis

The primary goal of a regression analysis is to determine the best set of parameters b_i , such that the model predicts experimental values of the dependent variable as accurately as possible (i.e. calculated values y_j should be close to experimental values y_j^*).

We also wish to judge whether our model itself is adequate to fit the observed experimental data (i.e. the correct mathematical form of it was chosen), and whether all terms in our model are significant (i.e. the improvement in "goodness" of fit due to the addition of a certain term to the model is bigger than the noise in experimental data).

The standard regression output of spreadsheet programs provides information to reach these objectives. Two outputs, ANOVA and Regression statistics, are described below.

C.4. ANOVA output and its analysis

There are two tables in ANOVA (Analysis of Variance), which are shown in Table C-1 and Table C-2. Description of the entries of the tables along with related statistical concepts and parameters constitutes this section.

C.4.1. Coefficients

The regression program determines the best set of parameters \mathbf{b} ($b_0, b_1, b_2, \dots, b_p$) in the model

$$y_j = b_0 + b_1 x_{1j} + b_2 x_{2j} + \dots + b_p x_{pj} \quad (\text{C.1})$$

by minimizing the *error sum of squares* SS_E (discussed later). Coefficients are listed in the second table of ANOVA (see Table C-2). These coefficients allow the program to calculate *predicted* values of the dependent variable \mathbf{y} (y_1, y_2, \dots, y_n).

Table C-1. MS Excel ANOVA output (part I)^a.

	df	SS	MS	F	Significance F
Regression	(df _R)	(SS _R)	(MS _R)	(F _R)	(P _R)
Residual (error)	(df _E)	(SS _E)	(MS _E)		
Total	(df _T)	(SS _T)	N/A (MS _T)		

^a The following notation is used: df - the number of degrees of freedom, SS - sum of squares, MS - mean sum of squares, F - F-number; subscript signifies particular type of the quantity (R - for regression, E - for residual (error), T - total); N/A means that the quantity is not available in the Excel output. Notation specific for this section and standard Excel notation are given in parenthesis and without them, respectively. Meaning of each item of the table is described in text.

Table C-2. MS Excel ANOVA output (part II)^a.

	Coefficients (b _i)	Standard Error (se (b _i))	t Stat (t _i)	P-value (P _i)	Lower 95% (b _{L,(1-P_i)})	Upper 95% (b _{U,(1-P_i)})
Intercept (b ₀)	0.52292226	1.7798	0.2938	0.7881	-5.1413318	6.1871763
X Variable 1 (x ₁)	2.91437225	0.7303	3.9901	0.0282	0.58992443	5.2388201
X Variable 2 (x ₂)	2.02376459	0.0731	27.651	0.0001	1.79084949	2.2566797
X Variable 3 (x ₃)	-0.0009602	0.0020	-0.4657	0.6731	-0.0075216	0.0056011

^a Numbers in the table are arbitrary and shown for illustrative purpose only. Notation specific for this section and standard Excel notation are given in parenthesis and without them, respectively. Meaning of each item of the table is described in text.

C.4.2. Sum of squares.

In general, the sum of squares of some arbitrary variable q is determined as:

$$SS_q = \sum_j^n (q_j - q_{avg})^2, \quad (C.2)$$

with q_j and q_{avg} being j th observation of quantity q out of n total and average value of q , respectively. In the ANOVA regression output one will find three types of sum of squares (see Table C-1).

Total sum of squares SS_T

$$SS_T = \sum_j^n (y_j^* - y_{avg}^*)^2 \text{ with} \quad (C.3)$$

$$y_{avg}^* = \frac{\sum_j^n y_j^*}{n}. \quad (C.4)$$

It is obvious that SS_T is the sum of squares of deviations of the experimental values of dependent variable y^* from its average value. SS_T could be interpreted as the sum of deviations of y^* from the simplest possible model (y is constant and does not depend on any variable x):

$$y = b_0 \text{ with } b_0 = y_{avg}. \quad (C.5)$$

SS_T has two contributors: residual (error) sum of squares (SS_E) and regression sum of squares (SS_R):

$$SS_T = SS_E + SS_R. \quad (C.6)$$

Residual (or error) sum of squares SS_E :

$$SS_E = \sum_j^n (r_j - r_{avg})^2 \quad (C.7)$$

Since in the underlying theory the *expected* value of residuals r_{avg} is assumed to be zero, the expression simplifies to

$$SS_E = \sum_j^n (r_j)^2 \quad (C.8)$$

The significance of this quantity is that by the minimization of SS_E the spreadsheet regression tool determines the best set of parameters $\mathbf{b} = b_0, b_1, b_2, \dots, b_p$ for a given regression model. SS_E could be also viewed as the due-to-random-scattering-of $-y^*$ -about-predicted-line contributor to the total sum of squares SS_T . This is the reason for calling the quantity (SS_E) “due to *error (residual)* sum of squares”.

Regression sum of squares SS_R

$$SS_R = \sum_j^n (y_j - y_{avg}^*)^2 \quad (C.9)$$

SS_R is the sum of squares of deviations of the *predicted-by-regression-model* values of dependent variable y from its average *experimental* value y_{avg}^* . It accounts for addition of p variables (x_1, x_2, \dots, x_p) to the simplest possible model of equation (C.5) (variable y is just a constant and does not depend on variables \mathbf{x}), i.e. $y = b_0$ vs. $y = b_0 + b_1x_1 + b_2x_2 + \dots + b_px_p$. Since this is a transformation from the “*non-regression* model” to the true *regression* model, SS_R is called the “due to *regression* sum of squares”.

The definition of SS_R in the form (C.9) is not always given in the literature. One can find different expressions in books on statistics [1, 2] :

$$SS_R = \sum_j^p b_i \sum_j^n (x_{ij} - x_{avg}) y_i, \quad (C.10)$$

or

$$SS_R = \sum_j^p b_i \sum_j^n x_{ij} y_j^* - \frac{\left(\sum_j^n y_j^* \right)^2}{n}. \quad (C.11)$$

Relationships (C.10) and (C.11) give the same numerical result as (C.9), however, it is difficult to see the physical meaning of SS_R from the two former equations.

C.4.3. Mean square (variance) and degrees of freedom

The general expression for the mean square of an arbitrary quantity q is:

$$MS_q = SS_q / df. \quad (C.12)$$

SS_q is defined by equation (C.2) and df is the **number of degrees of freedom** associated with quantity SS_q . Quantity MS is also often referred to as the **variance**. The number of degrees of freedom could be viewed as the difference between the number of observations n and the number of constraints (fixed parameters associated with the corresponding sum of squares SS_q).

Total mean square MS_T (total variance)

$$MS_T = SS_T / (n - 1). \quad (C.13)$$

SS_T is associated with the model (C.5), which has only one constraint (parameter b_0), therefore the number of degrees of freedom in this case is:

$$df_T = n - 1. \quad (C.14)$$

Residual (error) mean square MS_E (error variance)

$$MS_E = SS_E / (n - k). \quad (C.15)$$

SS_E is associated with the random error around the regression model (C.1), which has $k=p+1$ parameters (one per each variable out of p variables total plus intercept). It means there are k constraints and the number of degrees of freedom is :

$$df_E = n - k. \quad (C.16)$$

Regression mean square MS_R (regression variance)

$$MS_R = SS_R / (k - 1). \quad (C.17)$$

The number of degrees of freedom in this case can be viewed as the difference between the total number of degrees of freedom df_T (C.14) and the number of degrees of freedom for residuals df_E (C.16) :

$$df_R = df_T - df_E = (n - 1) - (n - k) \quad (C.18)$$

$$df_R = k - 1 = p$$

C.4.4. Tests of significance and F-numbers

The F-number is the quantity which can be used to test for the statistical difference between two variances. For example, if we have two random variables q and v , the corresponding F- number is:

$$F_{q,v} = MS_q / MS_v \quad (C.19)$$

The variances MS_q and MS_v are defined by an expression of type (C.12). In order to tell whether two variances are statistically different, the corresponding probability P is determined from F-distribution function:

$$P = P(F_{q,v}, df_q, df_v). \quad (C.20)$$

The quantities df_q , df_v - degrees of freedom for numerator and denominator - are parameters of this function. Tabulated numerical values of P for the F-distribution can be found in various texts on statistics or simply determined in a spreadsheet directly by using the corresponding statistical function (e.g. in Microsoft Excel one would use $FDIST(F_{q,v}, df_q, df_v)$ to return the numerical value of P). An analytical form of $P = P(F_{q,v}, df_q, df_v)$ can be found in the literature (e.g. [1, p.383]).

The probability P given by (C.20) is a probability that the variances MS_q and MS_v are statistically *indistinguishable*. On the other hand, $1-P$ is the probability that they are *different* and is often called **confidence level**. Conventionally, a reasonable confidence level is 0.95 or higher. If it turns out that $1-P < 0.95$, we say that MS_q and MS_v are

statistically the same. If $1-P > 0.95$, we say that at least with the 0.95 (or 95%) confidence MS_q and MS_v are different. The procedure just described is called the F-test.

There are several F-tests related to regression analysis. We will discuss the three most common ones. They deal with significance of parameters in the regression model. The first and the last of them are performed by spreadsheet regression tool automatically, whereas the second one is not for the reason discussed below.

Significance test of all coefficients in the regression model

The question being answered in this case is "With what level of confidence can we state that AT LEAST ONE of the *coefficients* \mathbf{b} (b_1, b_2, \dots, b_p) in the regression model is significantly different from zero?". The first step is to calculate the F-number for the whole regression (part of the regression output (see Table C-1)):

$$F_R = MS_R / MS_E. \quad (C.21)$$

The second step is to determine the numerical value of the corresponding probability P_R (also part of the regression output (see Table C-1)) :

$$P_R = FDIST(F_R, df_R, df_E). \quad (C.22)$$

Taking into account expressions (C.16) and (C.18) we obtain

$$P_R = FDIST(F_R, k - 1, n - k). \quad (C.23)$$

Finally we can determine the confidence level $1 - P_R$. At this level of confidence, the variance "due to regression" MS_R is statistically different from the variance "due to error" MS_E . In its turn it means that the addition of p variables (x_1, x_2, \dots, x_p) to the simplest model (C.5) (dependent variable y is just a constant) is a statistically significant improvement of the fit. Thus, at the confidence level not less than $1 - P_R$ we can say: "*At least ONE of coefficients in the model is significant*". In practice F_R is more often used to compare two models describing the same experimental data: the higher F_R the more adequate the corresponding model.

Significance test of subset of coefficients in the regression model

This tests answers the following question: "With what level of confidence can one be sure that at least ONE of the coefficients in a selected subset of all the coefficients is significant?". Let us take a subset of the last m coefficients in the model with a total of p coefficients (b_1, b_2, \dots, b_p). Here we need to consider two models:

$$y_j = b_0 + b_1 x_{1j} + b_2 x_{2j} + \dots + b_p x_{pj} \quad (\text{unrestricted}) \quad (\text{C.24})$$

and

$$y_j = b'_0 + b'_1 x_{1j} + b'_2 x_{2j} + \dots + b'_{p-m} x_{p-m,j} \quad (\text{restricted}). \quad (\text{C.25})$$

These models are called **unrestricted** (C.24) and **restricted** (C.25), respectively. One needs to perform *two separate* least square regression analyses for each model.

From the regression output (see Table C-1) for each model we obtain the corresponding error sum of squares SS_E and SS'_E as well as variance MS_E for the unrestricted model. The next step is to calculate the F-number for testing a subset of m variables “by hand” (it is not part of Microsoft Excel ANOVA for an obvious reason, i.e. *one* must decide how many variables to include in the subset):

$$F_m = \frac{SS'_E - SS_E}{m} / MS_E. \quad (\text{C.26})$$

F_m could be viewed as an indicator of whether the reduction in the error variance due to the addition of the subset of m variables to the restricted model ($SS'_E - SS_E$) / m is statistically significant with respect to the overall error variance MS_E for the unrestricted model. It is equivalent to testing the hypothesis that at least one of coefficients in the subset is not zero. In the final step, we determine probability P_m (also “by hand”):

$$P_m = FDIST(F_m, m, n - k). \quad (\text{C.27})$$

At the confidence level $1 - P_m$ at least ONE of the coefficients in the subset of m is significant. If $1 - P_m$ is not big enough (less than 0.95) one can state that ALL m coefficients in the subset are insignificant.

Significance test of an individual coefficient in the regression model

Here the question to answer is: “With what confidence level can we state that the i th coefficient b_i in the model is significant?”. The corresponding F-number is:

$$F_i = \frac{b_i^2}{se(b_i)^2}. \quad (\text{C.28})$$

Quantity $se(b_i)$ is the *standard error* in the individual coefficient b_i and is part of the *ANOVA output* (see Table C-2). The corresponding probability

$$P_i = FDIST(F_i, 1, n - k) \quad (C.29)$$

leads us to the confidence level $1 - P_i$ at which we can state that *coefficient b_i is significant*. If this level is lower than desired one, we say that *coefficient b_i is insignificant*. F_i is not part of spreadsheet regression output, but might be calculated by hand if needed. However, there is another statistics for testing individual parameters, which is *part of ANOVA* (see Table C-2):

$$t_i = \frac{b_i}{se(b_i)} \quad (C.30)$$

The t_i -number is the square root of F_i (equation (C.29)). It has a **Student's distribution** (see [1, p. 381] for the analytical form of it). *The corresponding probability is numerically the same as that given by (C.29)*. There is a statistical function in Microsoft Excel which allows one to determine P_i (*part of ANOVA* (see Table C-2)):

$$P_i = TDIST(t_i, n - k, 2) \quad (C.31)$$

Parameters of the function are: the number of degrees of freedom df ($df_E = n - k$) and *form* of test ($TL=2$). If $TL=1$ a result for a *one-tailed* distribution is returned; if $TL=2$ two-tailed distribution result is returned [1]. Analysis of P_i is similar to that previously discussed for the F-test.

In conclusion of the F-test discussion, it should be noted that in case one removes even one insignificant variable from the model, the latter needs to be tested once again, since coefficients which were significant in certain cases **might** become insignificant after removal and *visa versa*. It is a good practice to use a reasonable combination of all three tests in order to achieve the most reliable conclusions.

C.4.5. Confidence interval

In the previous section we were obtaining confidence levels given F-numbers or t-numbers. One can go in an opposite direction: given a desired minimal confidence level $1 - P$ (e.g. 0.95) calculate the related F- or t-number. Microsoft Excel provides two statistical functions for that purpose:

$$F_{(1-P)} = FINV(P, df_q, df_v) \quad (C.32)$$

and

$$t_{(1-P)} = TINV(P, df), \quad (C.33)$$

in which df_q , df_v are degrees of freedom of numerator and denominator, respectively (see equation (C.19)), and df is degree of freedom associated with a given t-test (varies from test to test). In expression (C.33) P is the probability associated with “two-tailed” Student’s distribution. Values of F-numbers and t-numbers for various probabilities and degrees of freedom are tabulated and can be found in any text on statistics [1,2,3,4]. Usually the “one-tailed” Student’s distribution is presented.

Knowing the **t-number** for a coefficient b_i we can calculate the numerical interval which contains the coefficient b_i with the desired probability $1-P_i$:

$$t_{(1-P_i)} = TINV(P_i, n - k) \quad (C.34)$$

$$b_{L, (1-P_i)} = b_i - se(b_i) \cdot t_{(1-P_i)} \quad (\text{lower limit}) \quad (C.35)$$

$$b_{U, (1-P_i)} = b_i + se(b_i) \cdot t_{(1-P_i)} \quad (\text{upper limit}) \quad (C.36)$$

The standard errors for individual parameters $se(b_i)$ are part of ANOVA (Table C-2). The interval $[b_{L, (1-P_i)}; b_{U, (1-P_i)}]$ is called the **confidence interval** of parameter b_i with the $1-P_i$ *confidence level*. The upper and lower limits of this interval at a 95% *confidence* are listed in the ANOVA output by default (Table C-2; columns “Lower 95%” and “Upper 95%”). The limits for different levels also can be obtained.

C.5. Regression statistics output

The information contained in the “*Regression statistics*” output characterizes the “goodness” of the model as a whole. In a sense it duplicates F-test of all coefficients previously discussed: quantities listed in this output can be expressed in terms of the regression F-number F_R (Table C-1). The form of this output is presented in Table C-3 and described below.

Standard error (S_y):

$$S_y = \sqrt{MS_E} \quad (C.37)$$

MS_E is an error variance (see expression (C.15)). Quantity S_y is an estimate of the *standard error (deviation)* of experimental values of the dependent variable y^* with respect to those predicted by the regression model.

Table C-3. Regression statistics output of MS Excel^a.

Multiple R	0.99999882
R Square (R ²)	0.99999765
Adjusted R Square (R ² _{adj})	0.9999953
Standard Error (S _y)	0.75291216
Observations (n)	7

^a Numbers in the table are arbitrary and shown for illustrative purpose only. Notation specific for this section and standard Excel notation are given in parenthesis and without them, respectively. Meaning of each item of the table is described in text.

Coefficient of determination R² (or R Square):

$$R^2 = SS_R / SS_T = 1 - SS_E / SS_T \quad (C.38)$$

The *coefficient of determination* is a measure of entire regression model. The closer R² is to unity, the better the model (C.1) describes the data. In the case of a perfect fit R²=1.

Adjusted coefficient of determination R² (or Adjusted R Square):

$$R_{adj}^2 = 1 - \frac{SS_E / (n - k)}{SS_T / (n - 1)} \quad (C.39)$$

The significance of R²_{adj} is basically the same as that of R² (the closer to unity the better). Strictly speaking R²_{adj} should be used as an indicator of an adequacy of the model, since it takes in to account not only deviations but also numbers of degrees of freedom.

Multiple correlation coefficient R:

$$R = \sqrt{SS_R / SS_T} \quad (C.40)$$

This quantity is just the square root of *coefficient of determination*.

Coefficients R, R² and R²_{adj} are normally used for relative comparison of several models rather than for absolute judgment on adequacy for an individual one.

C.6. References

1. Afifi A. A., Azen S. P. "Statistical analysis. Computer oriented approach", Academic press, New York (1979).
2. Natrella M. G. "Experimental Statistics", National Bureau of Standards, Washington DC (1963).
3. Neter J., Wasserman W. "Applied linear statistical models", R. D. Irwin Inc., Homewood, Illinois (1974).
4. Gunst R. F., Mason R. L. "Regression analysis and its application", Marcel Dekker Inc., New York (1980).
5. Shoemaker D. P., Garland C. W., Nibler J. W. "Experiments in Physical Chemistry", The McGraw-Hill Companies Inc. (1996).